Development of sustainable bioenergy system by integrating hydrothermal carbonization and anaerobic digestion processes

（水熱炭化と嫌気性消化プロセスの統合による持続可能なバイオエネルギーシステムの開発）

Hokkaido University Graduate School of Agriculture

Frontiers in Production Science　Doctor Course.

MOHAMMED Ibrahim Shaba

Development of sustainable bioenergy system by integrating hydrothermal carbonization and anaerobic digestion processes

Thesis submitted to the Graduate School of Agriculture
Hokkaido University, Sapporo, Japan in partial fulfilment of the requirements for the award of the degree of Doctor of Philosophy (PhD) in Bioresources and Environmental Engineering (Laboratory of Agricultural Biosystem Engineering)

MOHAMMED Ibrahim Shaba

March 2022

DECLARATION

I hereby declare that this Thesis titled: “Development of Sustainable Bioenergy System by Integrating Hydrothermal Carbonization and Anaerobic Digestion Processes” is a collection of my original research work, and it has not been presented for any other qualification anywhere. Information from other sources (published or unpublished) has been duly acknowledged.

MOHAMMED Ibrahim Shaba
Student number: 32195011
GRADUATE SCHOOL OF AGRICULTURE
HOKKAIDO UNIVERSITY, SAPPORO, JAPAN.

SIGNATURE/ DATE

DEDICATION

This thesis is dedicated to Almighty Allah, my beloved wife, parents, lovely sons, daughter, siblings, and friends.

ACKNOWLEDGEMENTS

I will forever be grateful to my supervisor Associate Professor Shimizu Naoto for his constructive criticism, fatherly advice, and guidance throughout the period of my research work. I sincerely appreciate his effort, patient, motivation, and immense knowledge. His guidance helped me during the period of my research and writing of this thesis. I couldn't have imagined having better advisor and mentor for my PhD study. I sincerely appreciate Professor Kazunori Iwabuchi in the Laboratory of Agricultural Biosystem Engineering and Distinguished Professor Noboru Noguchi in the Laboratory of Vehicle Robotics for their carefully review of my thesis.

My acknowledgement will not be complete without appreciating my colleagues and friends in the laboratory of Agricultural and Biosystem Engineering, Hokkaido University, Sapporo, Japan for their cooperation throughout the program.

I also acknowledge the effort of my current Head of Department Engr. Dr. S. M. Dauda, the former Head of Department Engr. Prof. B. A. Adejumo, the former and present Deans of School of Infrastructure, Process Engineering and Technology (SIPET), Engr. Prof. O. K. Abubakre and Engr. Prof. Z. D. Osunde. I also acknowledge all my senior colleagues and my colleagues in the Department of Agricultural and Bioresources Engineering, Federal University of Technology, Minna for their unrelenting effort in the Department.

I also acknowledge and register my profound appreciation to the Tertiary Education Trust Fund (TETFund) of Nigeria and Hokkaido University DX Doctoral followship, Japan.

Finally, my sincere gratitude goes to the Almighty Allah for sparing my life and giving me the wisdom and capability to be able to carry out this research work. I hereby say "Praise be to Allah, the lord of the Universe"

ABSTRACT

The application of lignocellulose biomass as a sustainable resource has gained traction to achieve a reduction in greenhouse gas emissions. Valorization via hydrothermal carbonization (HTC) of lignocellulosic biomass is necessary to convert high moisture biomass to solid fuel with a reduced inorganic content and to improve it biodegradability through hydrolysis of the recalcitrant in lignocellulose biomass that would enhance the production of biogas in anaerobic digestion process. Utilization of anaerobic digestion (AD) process for energy demand and supply regulation are still rare at the industrial scale, probably because they are unstable under some circumstances, such as variation of process conditions. This drawback can be overcome by developing an adaptive identifier system that will enhance the stable performance of the online biogas production.

This investigation has focused on the effect of processing parameters on the products of HTC namely solid fuel or hydrochar, liquid and gas fractions, and utilizing the produced corn stover hydrochar in AD process to increase biogas production. HTC was conducted in a temperature-controlled batch reactor with corn stover and deionized water under oxygen-free conditions obtained by pressurizing the reactor headspace with nitrogen gas. The properties of the hydrochar and liquid and gas fractions were evaluated as a function of the process temperature (250–350 °C), residence time (30–60 min) and biomass/water ratio (0.09–0.14). Central composite design (CCD) modules in a response surface methodology (RSM) were used to optimize processing parameters. The maximum mass yield, energy yield and high heating value (HHV) of the hydrochar produced were 29.91% dry weight (dw), 42.38% dw and 26.03 MJ/kg, respectively. corn stover hydrochar produced at high temperature decreased biogas production while corn stover hydrochar produced at low temperature increased biogas production. Concentrations of acetic acid and hydrogen gas were 6.93 g/L and 0.25 v/v%, respectively. Experimental results after process optimization were in satisfactory agreement with the predicted HHV. The optimal HTC process parameters were

determined to be 305 °C with a 60 min residence time and a biomass/water ratio of 0.114, yielding hydrochar with a HHV of 25.42 MJ/kg.

The corn stover hydrochar obtained from hydrothermal carbonization at a temperature, residential time, and biomass/water ratio of 215 ^{o}C, 45 min and 0.115 respectively was added to the bioreactor as a substrate inoculated with food waste and cow dung to generate biogas. A state–space AD model containing one algebraic equation and two differential equations was constructed. All the parameters used in the model were dependent on the AD process conditions. An adaptive identifier system was developed to automatically estimate parameter values from input and output data. This made it possible to operate the system under different conditions. Daily cumulative biogas production was predicted using the model, and goodness-of-fit analysis indicated that the predicted biogas production values had accuracies of >90% during both model construction and validation.

In conclusion, this study demonstrates that corn stover can be converted to solid fuel through HTC. The corn stover hydrochar produced was compared with pulverized coal utilized in power plant. Using the adaptive identifier system indicated that data for at least 20 and 140 h were required to estimate stable parameters related to bacterial and substrate inputs, respectively. It is recommended to produced corn stover hydrochar at low temperature (100 – 200 ^{o}C) and residential time (10 – 30 min) to prevent inhibitor of methanogenesis, for increase production of biogas and utilize the hydrothermal process water in AD process.

TABLE OF CONTENT

Table of Contents

LIST OF TABLES

List of Tables

LIST OF FIGURES

List of Figures

NOMENCLATURE

AD: $Anaerobic\ Digestion$

HTC: $Hydrothermal\ Carbonization$

HTL: $Hydrothermal\ Liquefaction$

HTG: $Hydrothermal\ Gasification\ HTG$

CED: $Classical\ Experimental\ Design$

HHV: $High\ Heating\ Value$

RSM: $Response\ Surface\ Methodology$

SCW: $Supercritical\ Water$

CCD: $Central\ Composite\ Design$

$\frac{C}{N}$: $\frac{Carbon}{Nitrogen}\ Ratio$

$z(t)$: $Bacteria\ Concentration\ [kgm^{-3}]$

$X(t)$: $State\ Vector$

$m(t)$: $Substrate\ Concentration\ [kgm^{-3}]$

$U(t)$: $Input\ Vector$

$\mu(m)$: $Specific\ growth\ rate\ \ [h^{-1}]$

$h(q^{-1})$: $Impulse\ response$

z_{max}: $Maximum\ Bacteria\ Concentration\ [kgm^{-3}]$

q^{-1}: $Shift\ operator$

$u_z(t)$: $bacterial\ input\ (kgm^{-3})$

$u_m(t)$: $substrate\ input\ (kgm^{-3})$

$Q(t)$: $biogas\ flow\ rate\ (m^3h^{-1})$)

$Lq_1 and\ Lq_2$: $are\ gas\ generation\ coefficients$

v: $is\ the\ sludge\ volume\ \ (m^3)$,

K_s: $is\ the\ dissociation\ constant\ (kg/m^3)$

b : $is\ the\ inhibition\ coefficient$,

w : $is\ the\ bacterial\ cell\ yield$

$\zeta_{11}, \zeta_{12}, \zeta_{21}, \zeta_{22}, \zeta_3, and\ \zeta_4$: $are\ control\ signals$

$h(q^{-1})$: $\ is\ the\ filter$,

$a_1, a_2\ and\ b_1, b_2, b_3, b_4$: $are\ parameters$,

$\lambda\ \ and\ \omega$: $are\ control\ system\ design\ constants$

K_{AI}: $is\ the\ coefficient\ for\ the\ least-squares\ method$

$\hat{\varphi}$: $\ is\ an\ estimated\ parameter$.

CHAPTER 1

1. General Introduction

1.1 Corn stover for Bioenergy production

Corn stover consists of the leaves, stalks, and cobs of maize (corn) (*Zea mays ssp. mays L.*) plants left in a field after harvest. Such stover makes up about half of the yield of a corn crop. It is a potential feedstock for bioenergy production that could reduce over dependence on fossil fuel oil. Recent attention has been focused on second-generation biofuels, which are not generated from food sources. Sources of second-generation biofuels include crop residues and crops that are grown solely for energy production, called dedicated energy crops. Examples of dedicated energy crops are Miscanthus and switchgrass. By requiring fewer reallocations of resources in comparison to biofuels created from food sources, second generation biofuels may have less impact on agricultural commodity markets. We focus on the use of corn stover, the non-grain portion of the corn crop, as a feedstock for bioenergy production. Corn stover could serve as a feedstock for biofuels, as a substitute for coal in producing electric power, or both. In addition to meeting renewable energy goals, use of corn stover for energy production may provide a new source of income for corn growers. It is also lignocellulose biomass that mainly composed of cellulose (~ 35% w/w), hemicellulose (~ 20% w/w), and lignin (~ 12% w/w).

1.2 Lignocellulosic Biomass

Virtually all biological materials could be converted to biogas, organic acids, alcohol, and other products of biotechnological interest, but chemical composition plays a critical role in the biomass selection and is directly related to products yield and overall process efficiency. For example, lignocellulosics biomass with higher lignin content tends to produce lower methane(Li et al., 2013). To obtain desired results and optimum pre-treatment efficiency, it is important to get a clear picture

of the lignocellulosic composition to visualize what is going on with lignocellulosic components during pre-treatment. ^{31}P NMR (phosphorus 31 – Nuclear Magnetic Resonance) is a direct analysis tool to quantify hydroxyl groups in lignin. Real-time monitoring of lignocellulosic components during pre-treatment may pave the way to understand pre-treatment impact better and to optimize maximum sugar recovery. Physical properties of the lignocellulosic material; water-holding capacity, specific porosity, specific surface area and crystallinity index change with each kind of pre-treatment applied but to a different extent depending on pre-treatment type, severity, and lignocellulosic composition.

1.3 Lignocellulosic Biomass Chemical Composition

Lignocellulosic biomass irrespective of their physical appearance shares the same chemical make-ups; cellulose (30–70%), hemicellulose (15–30%), and lignin (10–25%), and extractives(Monlau et al., 2013).

1.3.1 Cellulose

Cellulose, [$C_{6n}H_{10n+2}O_{5n+1}$, n –degree of polymerization of glucose] the most abundant polysaccharide, is a constituent of anhydro-glucan units linked together by β, 1–4 glycosidic linkages in a linear fashion(Fengel, 1992). The hydrogen bonds between glucan units determine cellulose crystallinity. Furthermore, some chains are irregularly arrayed rendering amorphous regions intertwined with crystalline cellulose(Taherzadeh & Karimi, 2008). Chain length is inversely proportional to hydrolysis efficiency(Karimi & Taherzadeh, 2016). It is insoluble in water and dilute acid and alkaline solutions at room temperature. Cellulose in its amorphous form is most susceptible to microbial degradation(Monlau et al., 2013).

1.3.2 Hemicellulose

Hemicellulose $(C_5H_8O_4)_n$ is a linear and highly branched-heteropolymer composed primarily of D-xylose, L-arabinose (members of C_5 sugar family), D glucose, D-mannose, D-galacturonic acid, D-galactose, and glucuronic acid (members of C_6 sugar family) and C_7 sugar 4-Omethyl glucuronic acid (Soccol et al., 2019). Individual sugars may be methylated or acylated. This group contains three pentoses (D-xylose, L-arabinose, and D-ribose) and two pentitols (D-arabitol, and ribitol). The composition is heavily dependent upon the source whether it is derived from angiosperm (hardwood) or gymnosperm (softwood). Xylose is the principal sugar for angiosperms and agricultural wastes while glucomannan for softwood. Hemicelluloses have lower molecular weight, lower DP (degree of polymerization), and less crystallinity with random amorphous structure compared to highly packed cellulose rendering it more susceptible to hydrolysis than cellulose(Yoshida et al., 2008).

1.3.3 Lignin

Lignin, the most abundant highly branched natural non-carbohydrate polymer next to cellulose and hemicellulose; 40% of dry biomass weight (Effendi et al., 2008), is an important component in plant cell wall providing structural strength. Moreover, to counter it from biotic and abiotic stresses(Weng & Chapple, 2010). It is composed of phenylpropane alcohols; coniferyl, sinapyl, and to a lesser extent p-coumaryl which form guaiacyl (G), sinapyl (S), and p hydroxyphenyl units linked through the (β-O-4) β-aryl ether and 5-O-4 (biphenyl ether). C-C ("condensed") bonds such as 5–5 (biphenyl) linkages or a combination of C-C and ether linkages(Rowel RM, 2005). Furthermore, lignin frequently forms a covalent bond with the surrounding carbohydrate mainly hemicellulose (Wörmeyer et al., 2011). The relative portion of each component varies by plant species. Coniferyl alcohol is the principal monomer in softwood lignin. Both sinapyl and coniferyl

monomers are the building blocks for hardwood lignin. Other "noncanonical" aromatic monomers also known to be incorporated into lignin framework(Bonawitz & Chapple, 2010). It provides the protective cover around the cellulose and hemicellulose as a hydrophobic sheet and has high significance for AD since lignin concentration varies inversely to methane production(Ahring et al., 2015).

1.3.4 Extractives

Lignocellulosic biomass may also contain a broad range of extractives based on origin. Extractives are not accounted for integral parts of the biomass structure(Qian EW, 2013). Extractives could be divided into two broad categories based on their solubility: hydrophilic (water soluble) and lipophilic (soluble in non-polar solvents). However, some phenols are on the borderline of the two said groups(Theander, 1985). Hydrophilic extractives include simple sugars, simple phenolics, stilbenes, lignans, flavonoids, and tannins. While waxes, fats, fatty alcohols, terpenes, sterols and steryl esters are the examples of lipophilic extractives. Extractives serve as metabolites, energy reserves, and protective agents against the microbial enzymic action.

1.4 Hydrothermal Process

Promising technologies for the conversion of lignocellulose waste biomass into bio-based chemicals and biofuels are hydrothermal (HT) processes, which use sub- and supercritical water as processing media in Figure 2.1, presents phase diagram of water. Subcritical water is pressurized water at temperatures above its boiling point at ambient pressure and below the critical point (343 ^{o}C, 22.1 MPa).

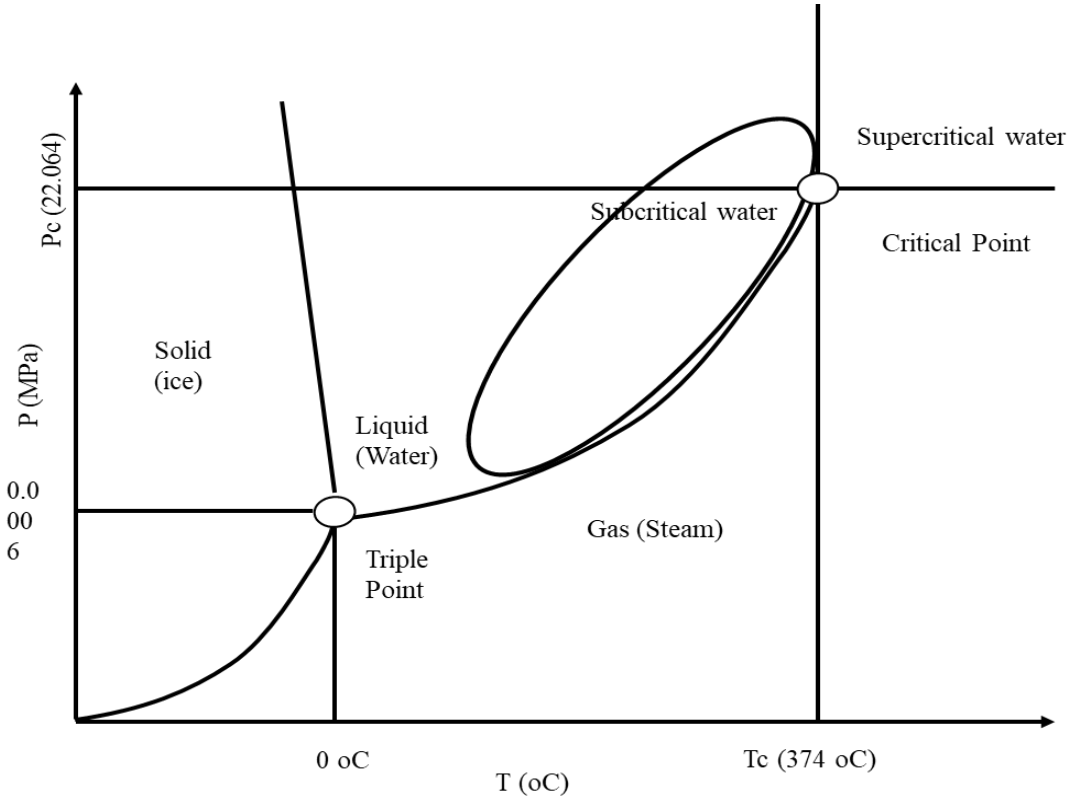

Figure 1.1: Phase diagram of water with area of application for hydrothermal treatment; (T_c – critical temperature, P_c – critical pressure).

Within a region close to the critical conditions, system properties become more sensitive to pressure and temperature changes. By increasing temperature, the density of the liquid phase decreases, the density of the vapor increases and becomes more similar and finely identical at critical point. Water above the critical point is named supercritical water and has properties between liquid-like and gas-like phase(Pavlovič et al., 2013). Generally, HT processes could be divided into four main processes.

1.4.1 Hydrothermal carbonization (HTC)

The first step of HTC reaction of biomass is hydrolysis, where water reacts with extractives, hemicellulose, or cellulose and breaks ester and ether bonds (mainly β-(1-4) glycosidic bonds), resulting in a wide range of products, including soluble oligomers like (oligo-) saccharides from

cellulose and hemicelluloses(Erlach et al., 2012). Hydrochar yield as a function of carbonization temperature and residence time.Gao et al. (2016) report that during the process of hydrothermal carbonization to convert eucalyptus bark into hydrochar carbonization temperature played an important role in the yield, physicochemical properties, and thermal behavior of the hydrochar. Effect of residence time was marginal. Higher temperature enhanced the hydrothermal conversion of raw material, resulting in lower yield, higher fixed carbon content, higher fuel ratio, higher heating value, lower O-containing functional groups (i.e., O-H and C-O groups) and a higher thermal stability of hydrochar. The hydrochar yield decreased with an elevation of carbonization temperature. Generally, the process usually takes place at moderate conditions (250 ^{o}C and 2 MPa) where carbonaceous bio solid product named "hydro char" is obtained. The same product can be generated at even higher temperatures (250-800 ^{o}C) based on wet pyrolysis. In both cases reactions normally need several hours \for conversion and has been tested with substantial types of biomasses(Liu et al., 2013).

1.4.2 Hydrothermal liquefaction (HTL)

Hydrothermal liquefaction (HTL) is one of the most investigated HT process for converting waste biomass into chemicals and biofuels, where the reaction is performed under medium temperature and high pressure (280-370 ^{o}C, 10-25 MPa) sufficient to keep the water in a liquid state. The main product is water-insoluble bio-oil (also called bio-crude) with small quantities of water-soluble products like char (solid residue) and light gases (e.g., H_2, CO, CO_2, CH_4). Bio oil is a mixture of several oxygenated compounds with an oxygen value of 10 - 20 wt% (Pavlovič et al., 2013). In hydrothermal processes usually dehydration occurs and results in removing of biomass oxygen from 40 wt% up to 10 wt%. Therefore, HTL products have lower oxygen content and higher heating values compared to those from pyrolysis and can be directly used for combustion in coal-

and oil-fired power stations. Since oxygen content of high-quality transportation fuels is less than 1 wt%, bio-oils need to be sufficiently improved to be use instead of gasoline or diesel. This includes possessing additional physical characteristics like high energy content, a good combustibility high energy content with a good combustibility, lower viscosity, and the ability to conventionally store in an effective manner (Tekin et al., 2014).

1.4.3 Hydrothermal Gasification (HTG)

Hydrothermal gasification (HTG) is a process in which biomass waste without pre-drying reacts with water that acts not only as a solvent but also as a reactant under sub- and supercritical conditions to produce gaseous products, mainly CH_4, H_2, CO_2 and C_1-C_4 carbon gases. As side products when applying lower temperatures, also some bio-oil, char, and tar are formed, which decreases the yield of gases. Depending on the temperature the range process can be divided into three main types: supercritical water gasification, catalyzed near-critical gasification to methane and aqueous phase reforming.

1.5 Anaerobic Digestion

Anaerobic digestion is a process for biological treatment of organic wastes with production of methane gas. Four metabolic paths can be identified in this process: two for acidogenesis and two for methanization (Figure 2.2). In the first acidogenic path (Path 1), glucose is decomposed into fatty volatile acids (acetate, propionate), hydrogen and inorganic carbon by acidogenic bacteria. In the second acidogenic path (Path 2), OHPA (Obligate Hydrogen Producing Acetogens) decompose propionate into acetate, hydrogen, and inorganic carbon. In a first methanization path (Path 3), acetate is transformed into methane and inorganic carbon by acetoclastic methanogenic bacteria. While in the second methanization path (Path 4), hydrogen combines with inorganic carbon to produce methane under the action of hydrogenophilic methanogenic bacteria.

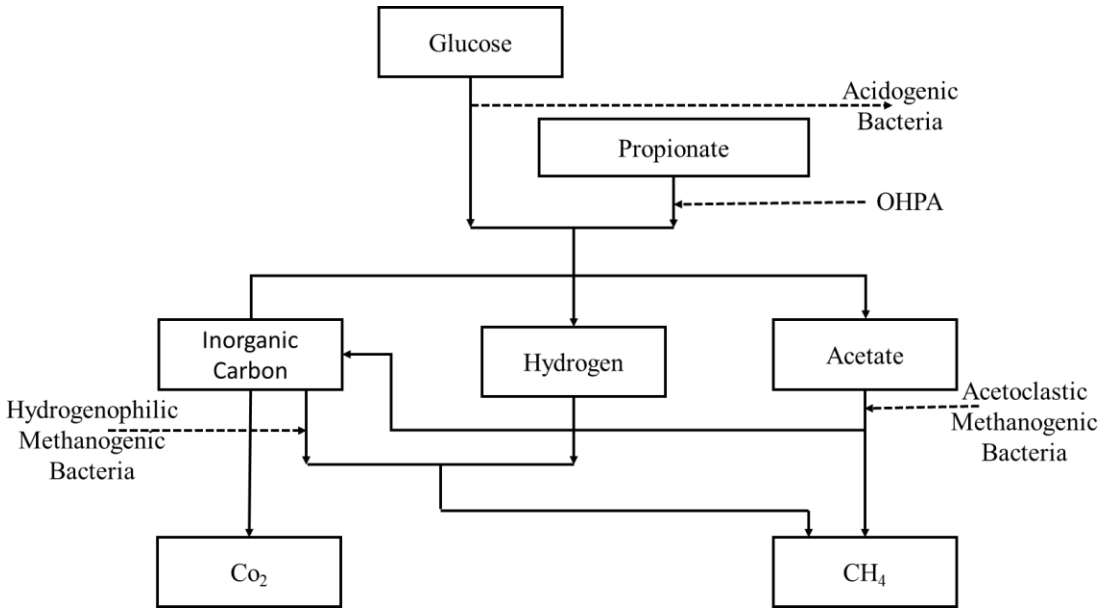

Figure 1.2: Reaction Scheme of Anaerobic Digestion.

1.6 The Integration of Hydrothermal Carbonization and Anaerobic Digestion.

Integration of hydrothermal processing with anaerobic digestion is gaining interest to maximize the energetic output from different feedstocks. However, despite numerous reports in the literature, it is still uncertain which integration strategy is the most effective approach for maximizing energy recovery. Separation of hydrochars and process waters after hydrothermal treatment for different applications is one method to integrate HTC and AD. Few studies have investigated the biomethane generation from hydrochars due to their high recalcitrance to microbial digestion. Despite this, Luz et al. (2018) found significant yields of biomethane from spent coffee ground hydrochar, however, the biomethane yields were not compared to untreated coffee grounds. This approach would require an alternative application for the process water, such as recirculation into HTC ((Catalkopru et al., 2017) or as a nutrient-rich fertilizer (Chen et al., 2017)).

A more common approach is to separate the hydrochar for use as a solid combustion fuel and subsequent anaerobic digestion of the process waters (Marin-Batista et al., 2019). However, there

is only limited data on the properties of seaweed derived process waters and the most extensive studies are based on predictive yields (Smith & Ross, 2016). Wang et al. (2019) investigated the influence of process water recirculation on the HTC of a *Laminaria species*, including biomethane generation from process water digestion. However, this was only conducted at a single HTC temperature; 220 °C. Anaerobic digestion of process waters bypass the hydrolysis stage, which is often regarded as the rate limiting step (Monlau et al., 2013), therefore faster degradation rates can be assumed. However, severe pre-treatments cause the formation of inhibitory by-products, including furfural, furfuryl alcohol, 5-HMF, formic acid, acetic acid and propionic acid (Nakason et al., 2018b). The formation of these compounds reduce biomethane yields (Marin-Batista et al., 2019). Despite this, Heidari et al. (2020) recently simulated the energetic output of combustion compared to HTC-AD; suggesting HTC-AD is a more suitable conversion option for feedstocks with high moisture and initial low HHV values. Another approach is to hydrothermally pre-treat feedstocks at lower HTC temperatures; between 100 °C −200 °C (Ding et al., 2020) and generate biomethane from the slurry (mixed hydrochar and process water). (Ding et al., 2020) found low temperature (140 °C) hydrothermal treatment to be the optimal pretreatment for two-stage digestion of the macroalgae *Laminaria digitata* when compared with a range of pre-treatments, such as dilute acid pretreatment and enzymatic hydrolysis. An optimal pre-treatment temperature of 140 °C was found for both food waste (Ding et al., 2017) and seaweed species *S. latissima* (Lin et al., 2019), to produce enhanced biomethane yields from a two-stage process, linked to optimal carbohydrate solubilization. Increasing the temperatures above 140 °C reduced biomethane yields due to inhibitory Malliard reactions with food waste and inhibitory by-product formation from *S. latissima.* Wang et al. (2019) found hydrothermally treating rice straw at 210 °C significantly reduced biogas yields by 30%, probably due to the inhibitory nature of the hydrochar. Typically,

hydrothermal slurries generated at higher temperatures are not recommended for anaerobic digestion. Zhao et al. (2018) investigated the integration strategies of HTC and AD; digesting food waste hydrochar, process water and a mixed slurry. The addition of hydrochar to the process water improved biomethane yields by 153% compared to digestion of the process water alone, due to the hydrochar acting as a surface for microbial interaction. However, these results were not compared to biomethane yields from the untreated food waste.

1.7 Modelling of Anaerobic Digestion process

It has long been known that organic compounds can be metabolized in anaerobiosis down to a mixture of methane and carbon dioxide (Renard et al., 1988). It is commonly considered as a two-step biological process: fermentation (or acidogenesis) and methanogenesis. In the first step, organic compounds are fermented usually to volatile fatty acids by a group of acidogenic bacteria. In the second step, the methanogenic archae-bacteria convert the products of acidogenesis, into methane, CH_4, and carbon dioxide, CO_2. Recently, the biological process has appeared more complicated. However, the two-step picture will suffice for this purpose. If, as it is often assumed, the methanogenic step is rate-limiting, the following state space representation based on mass balances can be used to describe the dynamical behavior of a continuously fed, completely mixed anaerobic digestion reactor. The net accumulation of active biomass in the reactor is

$$\frac{dX(t)}{dt} = \mu(t)X(t) - D(t)X(t) \qquad Eq\ 1.1$$

The net accumulation of substrate biomass in the reactor is

$$\frac{dS(t)}{dt} = -K_1\mu(t)X(t) - D(t)S_{in}(t) - D(t)S(t) \qquad Eq\ 1.2$$

The rate of methane gas (product) production is

$$Q(t) = K_1\,\mu(t)X(t) \qquad Eq\ 1.3$$

where

$X(t)$ is the methanogenic bacterial (active biomass) concentration; $S(t)$ is the substrate biomass concentration in the effluent (g COD/L); $S_{in}(t)$ is the substrate biomass concentration in the influent (g COD/L); $Q(t)$ is the methane gas (product) production rate (L CH_4/h). $D(t)$ is the dilution rate (day^{-1}). $\mu(t)$ is the specific growth rate (day^{-1}); and K_1 and K_2 are the yield coefficients.

The specific growth rate, $\mu(t)$, is known to be a complex function of many physicochemical and biological environmental factors, such as the substrate biomass concentration, *S*, the active biomass concentration, *X*, and the pH or the temperature, and many different analytical expressions have been suggested to account for these factors in anaerobic waste treatment processes (Sinechal et al., 1979).

1.8 Problem Identification

As global energy demand is increasing at a rate of 2.3%/year. There is a strong need to increase bioenergy production because of the rising in energy cost and risk of global warming caused by fossil combustion. Bioenergy, being carbon-neutral and energy sources are important alternative to fossil fuel. Lignocellulose biomass are potential feedstocks to produce chemical and fuels. Corn stover is an important source of lignocellulosic biomass in Nigeria, with total production of approximately 200 million tons per year. Because of its carbonaceous nature, corn stover has excellent potential to converted to bioenergy. However, the use of corn stover as a solid fuel feedstock is limited by its low energy density, structural heterogeneity, low heating values and high moisture content. With only scant amounts used to feed livestock and in the pulp/paper industries, a huge amount of Nigeria's corn stover is being discarded or combusted, which causes pollution of both the air and the landscape.

Various researchers have made conclusions about improvement of the combustible properties of lignocellulose biomass such as their moisture content, combustion efficiency, energy density, heating value and hydrophobic nature. Torrefaction greatly improves the combustible properties of lignocellulose biomass materials in terms of their moisture content, combustion efficiency, energy density, heating value and hydrophobic nature. But a degree of uncertainty exists in torrefaction, especially in the areas of reduction in alkali content from agricultural biomass and degradation of mill performance in the grinding of torrefied biomass. These challenges result in agglomeration, corrosion, and a reduction in combustion efficiency due to a higher percentage of unburned carbon in fly ash. Lignocellulosic biomass contains complex three-dimensional polysaccharide structures restrict enzymatic degradation by anaerobic microbes during AD. Therefore, pretreatment of lignocellulosic biomass is necessary to improve its biodegradability through hydrolysis of the recalcitrant components in lignocellulose biomass.

The need for computer control in biotechnological processes to improve product quality or to optimize production efficiency is becoming more and more obvious. For the last two decades, it has been the subject of much research work and has resulted in numerous scientific publications. The computer control of variables such as temperature or pH has become a routine. But real-life control applications of the biological variables such as biomass substrate, S**,** active biomass, X, or product, P**,** are developing slowly. There are two main reasons for this. First, basic biological processes underlying biotechnologies, and their dynamics, only begin to be well understood. They involve living organisms, the dynamical behavior of which is strongly nonlinear and nonstationary. Secondly, there is a lack, in most cases, of cheap sensors capable of providing reliable on-line measurements of the biological and biochemical parameters required to implement high performances computer control strategies.

CHAPTER 2

Investigating the effect of processing parameters on the products of hydrothermal carbonization of corn stover.

2.1 Introduction

Biomass is the waste and residual biological material of plants and animals (Chew & Doshi, 2011). The application of lignocellulose biomass as a sustainable resource has gained traction to achieve a reduction in greenhouse gas emissions (Hastings et al., 2009). Near-zero greenhouse gas emissions can be accomplished by balancing plant biomass production and use in the future (Akhtar & Amin, 2011). Bioenergy is a potential renewable energy and low-emissions resource, and is sustainable if its social impact, economics, and environment are well managed (Mohammed, Aliyu, et al., 2020). Lignocellulose biomass is recognized as an essential source of renewable energy because of its universal availability, low cost, flexible application (energy or heat production) and carbon neutrality (Anca-Couce, 2016). However, the capital costs and labor-intensive pretreatment and processing requirements associated with utilizing lignocellulose biomass must be addressed before any technique can become widely adopted (Himmel et al., 2007).

Numerous literatures have made conclusions regarding the upgrade of biomass combustion properties such as their hydrophobic nature, combustion efficiencies, heating values, moisture content and energy density. Torrefaction significantly improves the combustion properties of lignocellulose biomass with respect to the aforementioned properties, but a degree of uncertainty exists in torrefaction, particularly involving a decrease in alkali contents from agricultural residuals (Paul et al., 2018) and a gradual breakdown of mill performances in the grinding of torrefied biomass. These challenges result in corrosion, agglomerations and a reduction in combustion efficiencies due to high percentages of unburned carbon in fly ash. Valorization via hydrothermal

carbonization (HTC) is particularly suitable for biomass residues with high proportions of inorganic elements (a high mass fraction of ash content). The benefit of hydrothermal biomass conversion techniques is that they do not demand drying of biomass, which reduces energy requirements and process expenditure. The hydrothermal conversion process itself is cost-effective when compared to other conventional thermal drying techniques (Zhao et al., 2014). HTC has received significant attention for converting high moisture biomass to coal-like materials (solid fuel) with a reduced inorganic content. For example, HTC has been applied in the production of solid fuels with high energy contents using wine industry waste (Pala et al., 2014), wheat straw (Reza et al., 2015)tobacco stalks (Cai et al., 2016), olive mill industry residual biomasses (Volpe & Fiori, 2017), citrus wastes (Erdogan et al., 2015) and pulp mill waste (Wikberg et al., 2016).

Corn stover is an important source of lignocellulosic biomass in Nigeria, with total production of approximately 200 million tons per year. Because of its carbonaceous nature, corn stover has excellent potential to serve as a raw material to produce coal-like materials (Deng et al., 2016). However, the use of corn stover as a solid fuel feedstock is limited by its low energy density, structural heterogeneity, low heating values and high moisture content. With only scant amounts used to feed livestock and in the pulp/paper industries, a huge amount of Nigeria's corn stover is being discarded or combusted, which causes pollution of both the air and the landscape. HTC is a process of lignocellulose biomass transformation in subcritical or supercritical water under high pressure and temperature in the absence of oxygen, also known as wet pyrolysis. It can be divided into three main stages, namely, gasification, carbonization and liquefaction, which vary based on the processing temperature and residence time. In HTC, a sequence of reactions occurs during lignocellulosic biomass disintegration, including dehydration, hydrolysis, condensation, decarboxylation, aromatization and polymerization (Gao et al., 2012). Solid, liquid and gas

products are derived from this sequence of reactions. The solid is the main product; it has higher carbon content and increased hydrophobicity relative to the feedstock. The applications of HTC solids include energy storage (Funke & Ziegler, 2010), carbon-based catalysis (Hu et al., 2010), soil amendment (Kang et al., 2013), adsorbent (Steinbeiss et al., 2009) and fuel source (Kruse et al., 2013). The liquid comprises valuable organic chemicals such as acetic acid, glycolic acid, lactic acid, levulinic acid, formic acid, furfural, succinic acid, hydroxymethyl-furfural, furfuryl alcohol and propionic acid. The gas fraction mainly comprises hydrogen, carbon dioxide, methane and carbon monoxide.

Table 2.1 summarizes previous works of HTC process parameters using a classical experimental design (CED) and responses surface methodology (RSM), as well as solid fuel obtained at supercritical water (SCW) conditions. However, there are limited studies on the production of solid fuel at SCW conditions. Table 2.1 shows that previous studies utilized CEDs that change one variable at a time and does not reveal the effects of interaction and pure squares between process variables due to a large number of experimental trials, making this approach time consuming. Thus, based on a previous report of compound models, the optimization of solid fuel yield obtained by reducing the number of experimental trials has received insignificant attention in this area of research (Mohammed et al., 2019). In this research, a novel approach to HTC process has been employed to produce a solid fuel with high yields; this fuel is usually examined by optimizing the HTC process parameters mentioned in Table 2.1. In addition, effects of individual variables, pure squares and their interactions have been estimated by using RSM.

Table 2.1 Literature review on hydrothermal carbonization (HTC) parameters by using classical experimental design (CED) and responses surface methodology (RSM), solid fuel produced at supercritical water (SCW) conditions made from corn stover.

Previous Work	HTC Parameters using CED	HTC Parameters by RSM	Solid fuel Produced under SCW Conditions from Corn Stover
(Zhu et al., 2016)	Temperature (190–320 °C) and hydrothermal treatment severity (4.17–8.28 min)	NA	NA
(Machado et al., 2018)	Temperature (175–250 °C)	NA	NA
(Mosier et al., 2005)	Temperature (170–200 °C) and residence time (5–20 min)	NA	NA
(Fuertes et al., 2010)	Temperature (250 °C)	NA	NA
(Xiao et al., 2012)	Temperature (250 °C),	NA	NA
(Volpe et al., 2018)	Temperature (180–250 °C), residence time (0.5–3 h) and biomass/water ratio (0.07–0.30).	NA	NA
(Kang et al., 2019)	NA	Temperature (122.7–257.3 °C), residence time (4.8–55.2 min) and biomass (0.98–6.02 g/50 mL H_2O)	NA
This Study	NA	Temperature (215.91–384.09 °C), residence time (19.8–77 min) and Biomass/water ratio (0.073–0.157)	Solid fuel was produced at SCW conditions

NA: Not Applicable;

RSM is a flexible mathematical method employed in optimization, modeling and experimental design. It is an empirical modeling method that relates one or more responses to independent parameters. It gives statistical indications on individual model terms and interactions (Mohammed et al., 2019). To develop a complete biosystem for the solid fuel, liquid and gas fractions from corn stover must also serve as a pathway to sustainable bioenergy generation. Information regarding

the optimization of HTC process parameters by using RSM is limited to the best of our knowledge. Therefore, the aims of this investigation are (1) to optimize conditions and determine the effect of process parameters (the biomass/water ratio, residence time and temperature) on the properties of the hydrochar, (2) to gain insight into the underlying mechanism during HTC, as well as the thermal and structural properties of the hydrochar, and (3) to determine the yield and composition of the liquid and gas fractions, and to assess the feasibility of utilizing them in anaerobic digestion in future work.

2.2 Materials and Methods

2.2.1 Material Used in this study

The corn stover (New Dent, 105 days) used in this study was harvested from Hokkaido University Farm. The moisture contents as received were 80 wt%. The collected corn stover was pulverized into a 10 mm square and dried in a ventilated oven at 105 °C for 24 h. This pretreatment was conducted to avoid degradation and begin with a dry reference point. Samples were further milled and sieved to particle sizes of 500 and 800 μm.

2.3. Hydrothermal Experimental Setup of Corn Stover

HTC was conducted in a temperature-controlled batch reactor (Model: 122841, SUS 316 Tsukuba, Japan) at volumes between 160 and 190 mL. For each experiment, the reactor was charged with 1.09 to 2.36 ± 0.002 g of dried sample (corn stover) and 12.64 to 13.91 ± 0.03 g of deionized water to obtain the desired biomass/water ratio. The experimental layout is detailed in Table 2.2. Deionized water and corn stover were placed in the batch reactor. Oxygen-free conditions were obtained by pressurizing nitrogen gas to an initial pressure of 4 MPa in the reactor headspace; this also kept the water boiling during the hydrothermal process (Ushiyama & Shimizu, 2018). Gases were

obtained by gas trap bag after the reactor was cooled down. Liquid and solid phases of the reaction solution were separated by vacuum filtration. The liquid fraction, which is rich in acetic acid, will be used for biogas production in anaerobic fermentation in future work.

Table 2.2. Variables that were in the Central Composite Design for the Hydrothermal Hydrochar Process.

Factors	Unit	Code Factor Level				
		(-α)	**(-1)**	**(0)**	**(+1)**	**(+α)**
Temperature	^{o}C	215.91	250	300	350	384.09
Residential Time	h	0.33	0.5	0.75	1	1.17
Biomass/water Ratio	%	0.073	0.09	0.115	0.14	0.157

2.4. Characterization of Raw Corn Stover and Products of HTC

The proximate analysis of raw corn stover and solid fuel was conducted using the ASTM 1762–84 and 3173–87 method. CHN analysis (CE440, Exeter Analytical, Inc, Coventry, UK) was performed to determine the carbon, nitrogen, oxygen, and hydrogen content. The high heating value (HHV) of the solid fuels were determined using a digital calorimeter (Model DCS-196, Shinjuku Tokyo, Japan). The thermogravimetric analysis (TGA) of corn stover and the hydrochar were conducted on a Thermo plus EVO II TG 8120 instrument (Rigaku, Tokyo, Japan). A sample (10–15 mg) was heated from ambient temperature to 600 °C at a constant ramp rate of 10 °C min−1 under a nitrogen flow rate of 50 mL min−1. The difference in weight after devolatilization and controlled heating was estimated as the weight loss. Surface morphological characteristics of the samples were investigated using a scanning electron microscope (SEM) JSM-6301F system (JEOL, Tokyo, Japan). Samples were place on aluminium stub coated with gold palladium alloys and equal sided carbon tape employing an ion sputtering device (e101 Ion Sputter, Hitachi, Ltd, Tokyo, Japan) before SEM investigation. Investigation was done under high vacuum conditions, <1.0 ×

10−3 Pa, at a voltage of 10 kV (Shimizu et al., 2020). The liquid fractions were analysed using the high-performance liquid chromatography-refraction index (HPLC-RI) 1200 Infinity series with Shodex KS-802 column (Showa Denko, K.K, Tokyo, Japan). Ultrapure water was employed as the mobile phase. The column temperature and flow rate were set to 60 °C and 0.6 mL/min. A solution of 0.3% pullulan standard was used to perform for an alignment peak. The injected volume was 100 μL (Shimizu et al., 2020). Gas chromatography (GC-4000, GL Science, Tokyo, Japan) was used to analyse the gas fraction. CH_4, CO and CO_2 were detected using a GC-FID-TCD interphase (GC with a flame ionization detector and thermal conductivity detector) with hydrogen as the carrier gas. H_2 was detected by GC-TCD (Athika Chuntanapum et al., 2008). Each of these analyses was replicated three (3) times to minimize errors. The HHV was calculated using the modified Dulong's formula shown below as Eq. (2.1), according to previously published work by (Theegala & Midgett, 2012). Nitrogen, carbon, hydrogen, and oxygen were determined using elemental analysis (although the percentage content of nitrogen is not used in this formula). The mass and energy yield of the hydrochar was obtained from Eq. (2.2) and (2.3).

$$HHV\ \left[\frac{MJ}{kg}\right] = \frac{33.5\ \times\ wt.\%C}{100} + \frac{142.3\ \times\ wt.\%H}{100} - \frac{15.4\ \times\ wt.\%\ O}{100} \qquad Eq\ 2.1$$

$$Mass\ Yield = \frac{Mass\ of\ Produced\ Hydrochar}{Mass\ of\ Raw\ Corn\ Stover} \times 100 \qquad Eq\ 2.2$$

$$Energy\ Yield = Mass\ Yield\ X \frac{HHV\ of\ Produced\ Hydrochar}{HHV\ of\ Raw\ Corn\ Stover}\ \times\ 100 \qquad Eq\ 2.3$$

2.5. Experimental Design, Response Surface Methodology Development and Hydrothermal Process Optimization.

In this work, process variables (temperature, residence time and biomass/water ratios) that influence the yield of hydrochar were examined using a response surface methodology (RSM). To avoid laying-off (unnecessary repetition of experiments), a central composite design (CCD) was employed to gives 20 experimental trials to study the influence of 3 chosen variables on the solid fuel yield (Table 4.3). The range of parameters that were examined are shown in Table 2.5. Process temperature was assessed in a range from 250 to 350 °C, the biomass/water ratio varied from 0.09 to 0.14 and the residence time varied from 0.5 to 1 h. Three input parameters were investigated at low (−1), medium (0) and high (+1) levels, and axial points were added (axial distances; ± α = 1.68) for design orthogonality. Six center points were utilized to appraise the lack of fits and pure errors of the proposed model. Each of these processes was repeated three times. Multiple regression was employed to fits the coefficients of quadratic model of the response. Quality of the fitted quadratic model was evaluated by using the significances test and analysis of variances (ANOVA). The fitted model is shown in $Eq.(2.4)$.

$$Y = \eta_0 + \eta_1 x_1 + \eta_2 x_2 + \eta_3 x_3 + \eta_4 x_1 x_2 + \eta_5 x_1 x_3 + \eta_6 x_2 x_3 + \eta_7 x_1^2 + \eta_8 x_2^2 + \eta_9 x_3^2 \qquad Eq\ 2.4$$

Here, Y is the dependent variable (HHV in MJ/kg), η_0 is the intercept value,η_1, η_2 and η_3 are the first order coefficients, η_4, η_5 and η_6 are the interaction coefficients,η_7, η_8 and η_9 represent the quadratic coefficients and x_1, x_2 and x_3 represents the independent parameters. Local optimization of RSM was utilized to determine the optimum sets of 3 process input variables to maximize HHV. The HHV was set at maximum while the inputs variable was set in the range examined in this study. A desirability function in the RSM module was utilized to search for

optimal values which gave the maximum HHV. Predicted optimal value was validated by performing experiments in triplicate using the same conditions as those predicted by RSM. Mean experimental values were compared with the predicted values to assess the precision of prediction(Mohammed et al., 2019).

2.6 Results and Discussions

2.6.0 Characterization of Solid Fuel, Liquid and Gas Fraction from Corn Stover

2.6.1 Solid Fuel

The composition and energy properties of the raw corn stover and its hydrochar are presented as a function of the processing temperature, residence time and biomass/water ratio in Table 2.3. For comparison, other feedstocks (corn stalk and Opuntia ficus-indica cladodes (OC)) are also included in Table 2.3. The ash content of the hydrochars increased relative to raw corn stover. This observation is contrary to published works on HTC of corn stalk(Kang et al., 2019) and Miscanthus(Kambo & Dutta, 2015) but in agreement with the study of Opuntia ficus-indica cladodes(Volpe et al., 2018). The ash content of the corn stover hydrochar increases from 18 wt.% of 250 °C, 45 min, to 18.95 wt.% of 300 °C, 77 min, to 25.87 wt.% of 350 °C, 60 min at constant biomass/water ratios of 0. 115.The increase in ash content may be caused by reprecipitation of some inorganic material on the solid fuel after a long residence time at high temperatures, as suggested by Nakason et al. (2018a).

The volatile matter (VM) of the raw corn stover obtained was 71.34%, comparable to corn stalk(Kang et al., 2019) and higher than OC(Volpe et al., 2018). The VM of the raw corn stover was higher than all the hydrochars produced. The VM in the hydrochar decreased significantly with the increasing processing temperature (250 to 350 °C) at a constant residence time of 60 min

and biomass/water ratios of 0.14. This decrease in VM may be attributable to the decomposition of celluloses and hemicelluloses during hydrothermal treatment.

The highest percentage of fixed carbon obtained in the corn stover hydrochar was 31.30% at the processing temperature of 350 °C, residence time of 60 min and biomass/water ratio of 0.14, substantially more than in the hydrochars reported by Cai et al. (2016) and Hoekman et al. (2011). High fixed carbon and low volatile matter are more highly desirable characteristics for solid biofuels than raw biomass, which often ignites easily at low temperatures (~250 °C), resulting in rapid maximum weight loss(Hoekman et al., 2011). The increase in temperature (215.9, 300 and 384.09) and residence time (45 and 77 min) at a constant biomass/water ratio of 0.115 enhances the carbon content and decreases the percentages of oxygen and hydrogen. This is a result of decarboxylation and dehydration reactions that take place during HTC, which lead to a decrease in the ratios of O/C and H/C. The ultimate analysis shows that the content of carbon increases gradually with the extension of processing temperature (250 and 350 °C) at a constant residence time and biomass/water ratio of 60 min and 0.14, respectively. This changed of carbon content trend in hydrochar is consistent with a report developed by Zhu et al. (2016)

Table 2.3: Comparison of Average Values of Proximate Analysis, Ultimate Analysis and Energy Properties of Raw Corn Stover Hydrochar with other Types of Biomass Hydrochars.

Properties	Raw Corn Stover [This Study]	Hydrochars						
		215.9 °C, 0.115, 45 min	250 °C, 0.14, 60 min	300 °C, 0.115, 77 min	350 °C, 0.14 60 min	384.09 °C, 0.115, 45 min	CS(Kang et al., 2019)	OC(Volpe et al., 2018)
Proximate Analysis (SD ≤ 1.25)								
Volatile Matter (%)	71.34	57.28	60.72	54.47	42.83	40	74.32	56.88
Fixed Carbon (%)	17.67	24.72	19.52	26.58	31.30	30.89	18	28.17
Ash Content (%)	11.05	18	19.75	18.95	25.87	29.11	3.54	14.95
Ultimate Analysis (SD ≤ 1.09)								
Carbon (%)	40.83	52.39	56.67	62.07	57.60	54.18	53.44	50.48
Hydrogen (%)	5.21	4.8	4.76	4.93	4.33	3.7	5.67	4.83
Oxygen (%)	41.38	22.86	16.62	11.52	9.95	10.85	39.64	28.94
Nitrogen (%)	1.54	1.95	2.2	2.53	2.25	2.16	1.12	0.81
O/C	1.01	0.44	0.29	0.19	0.17	0.2	0.74	0.57
H/C	1.28	0.92	0.84	0.79	0.75	0.68	0.106	0.095
Energy Properties (SD ≤ 1.67)								
HHV (MJ/kg)	16.16	22.30	24.20	27.47	25.37	23.75	22.82	22.39
HHV (MJ/kg) [a]	14.72	20.86	23.20	26.03	23.93	21.75		
Energy Yield (%)	1	42.38	22.88	40.90	32.97	29.88	55.70	83

HHV (MJ/kg) [a]: Calculation by formula; CS: Corn Stalk. SD: Standard deviation. OC: Opuntia Ficus-Indica Cladodes.

The atomic ratios quantitative index is an essential standard for assessing the aromatic contents and degree of deoxygenation, during HTC of lignocellulose biomass. The H/C and O/C atomic

ratio provide clues about the aromatic contents; a lower ratio of H/C indicates that the aromatic contents of the hydrochar is high. The atomic H/C and O/C ratio of corn stover and its hydrochar are shown in Figure 2.1. Anthracite, coal, lignite and peat are also presented in the same figure for a coalification comparison. The H/C and O/C ratios of the hydrochar decrease as the residence time and temperature increase. It was obvious that the hydrochar produced at 384.91 °C shows a higher degree of coalification compared to the hydrochars produced at 215.9 °C with a similar residence time and biomass/water ratio, which indicated that demethanation, decarboxylation and dehydration reaction occur during the HTC process, though the rate of reaction of decarboxylation was lower than that of the dehydration. This finding similar to one on the HTC of a high moisture content outlined by Zhu et al. (2016). The hydrochar produced at 300 °C after 77 min with a biomass/water ratio of 0.115 has the highest carbon content of 62.07 wt.% basis; this value is comparable to coal material. Thus, these processing conditions were found to be optimal and would be recommended to produce corn stover hydrochar as a substitute solid fuel for power generation.

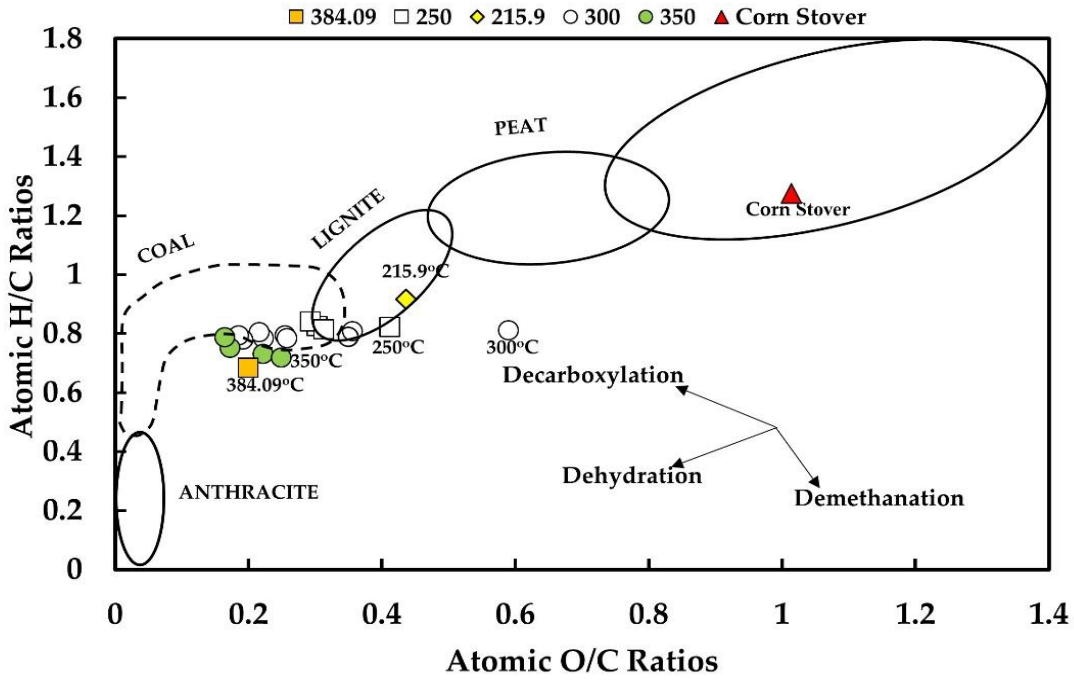

Figure 2.1: Van Krevelen diagram for raw corn stover and hydrochar.

Differential thermogravimetric analysis (DTG) and thermogravimetric analysis (TGA) were conducted to examine the thermal disintegration behaviors of raw corn stover and its hydrochar. As presented in Figure 2.2a, three levels of disintegration were recognized. The first level ranged from 100 to 250 °C and showed gradual weight loss, mostly from the removals of moisture and the release of some volatiles. The second level ranged from 250 to 400 °C and mainly involved the disintegration of cellulose and hemicellulose. At temperatures >450 °C, decomposition was attributed to the slower thermal breakdown of lignin(Volpe et al., 2018). At 600 °C, the final weight loss of solid fuels increased in the following order: 350 °C < 250 °C < 384.09 °C < 215.91 °C < 300 °C < Raw corn stover.

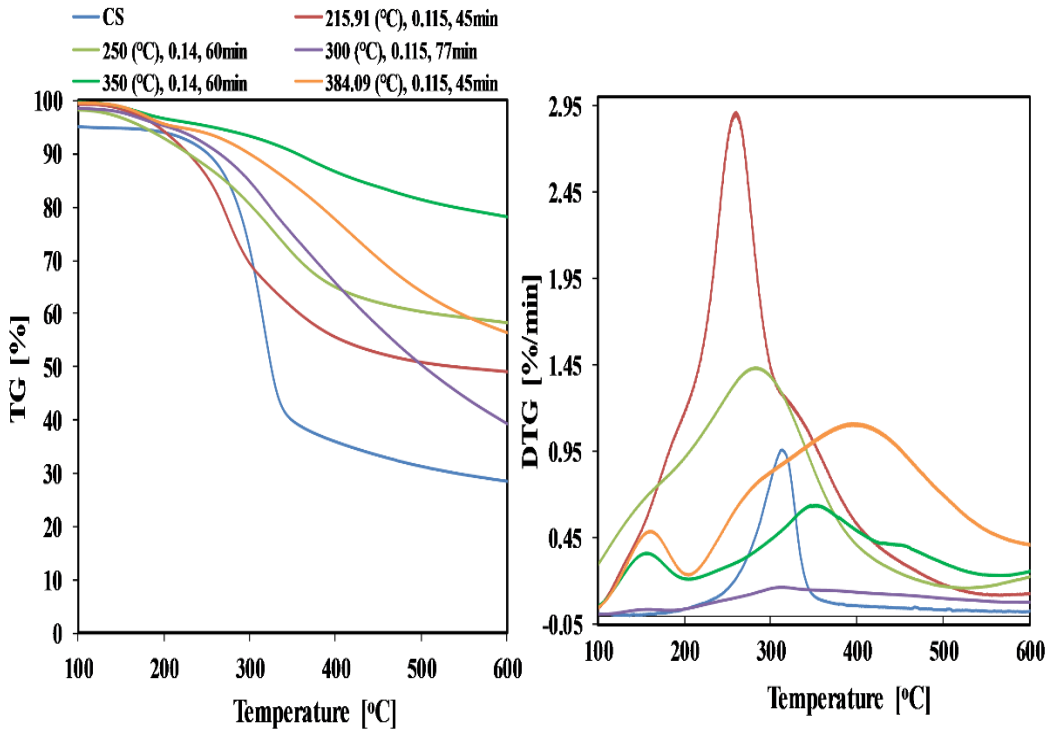

Figure 2.2: TGA (**a**) and DTG (**b**) Curve of Raw Corn Stover and its Hydrochar.

As shown in Figure 2.2b, a sharp DTG peak was observed at 320 °C for raw corn stover, likely because of the high content of volatile matter. The temperature of the DTG peak increased in line with the increasing processing temperature (250 to 350 °C) and residence time (30 to 60 min) employed in the production of hydrochar. Significant weight loss was not observed for the hydrochar produced at 300 °C, which is likely a result of its high carbon content. As the thermal stability of a solid fuel improves, the air pollution it produces is reduced because of complete combustion(Elaigwu & Greenway, 2016),

The corn stover and its hydrochars were examined to determine their microstructures (Figure 2.3) using SEM. The raw corn stover contained a rigid and well-organized fibril structure. The hydrochars processed at 215.91 °C and 250 °C depict a rough surface with many discrete droplets

where the corn stover was slowly degraded. As the processing temperature increased to 300 °C and 350 °C, more discrete droplets appear on the surface of the hydrochar, and the droplets gradually increase in size. Finally, granular, and molten structures were formed in the hydrochar at a processing temperature of 384.09 °C. The highly organized structure of the raw corn stover is attributable to Van der Waals forces, covalent bond and hydrogen bond in the three-dimensional binding of hemicellulose, cellulose and lignin(Cantero et al., 2014). With increasing temperature and residence times, these interactions decrease or disappear as lignin degrades.

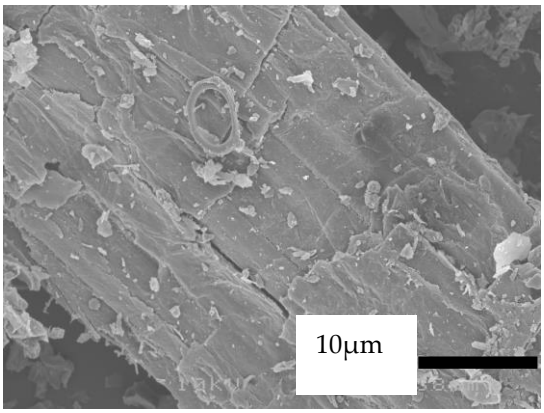

Raw Corn Stover

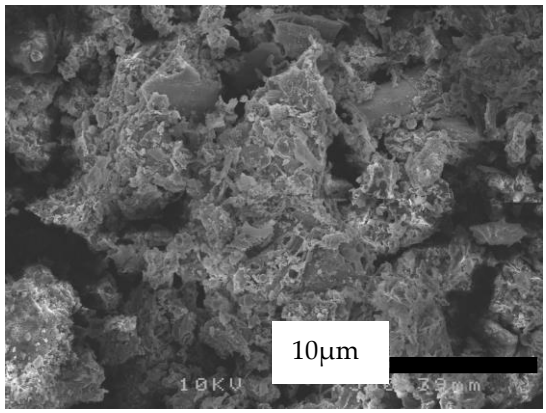

Hydrochar at *215.91 °C, 0.115, 45 min*

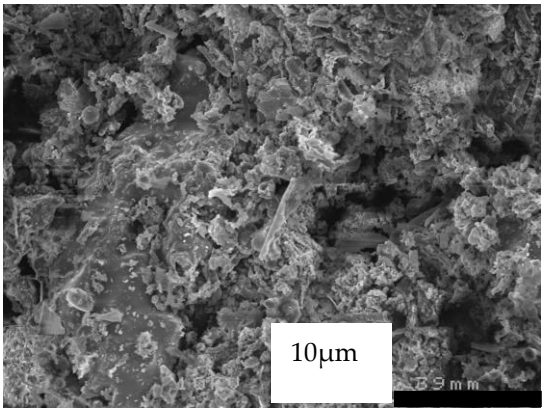

Hydrochar at *250 °C, 0.14, 60 min*

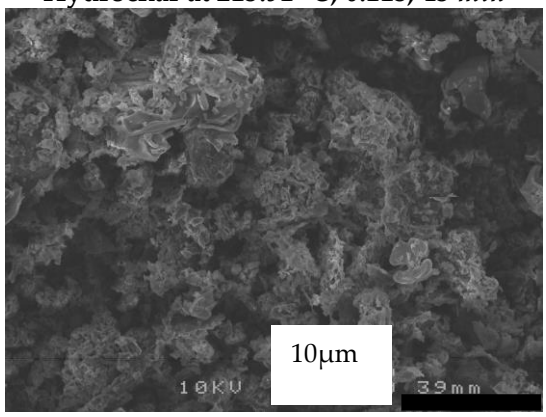

Hydrochar at *300 °C, 0.115, 77 min*

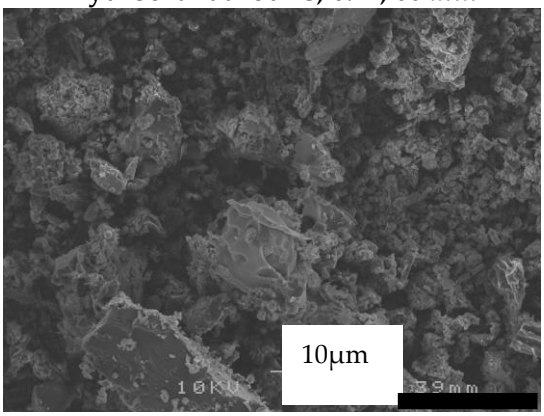

Hydrochar at *350 °C, 0.14, 60 min*

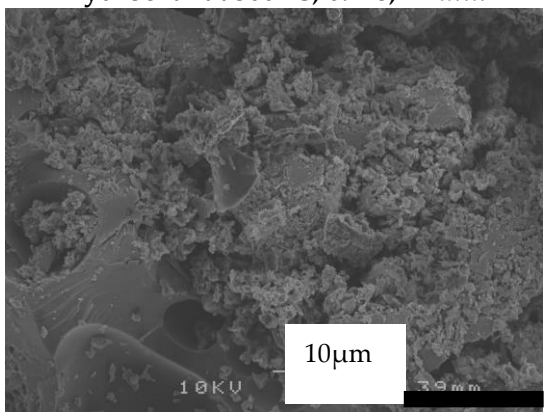

Hydrochar at *384.09 °C, 0.115, 45 min*

Figure 2.3.: Analysis of raw corn stover and solid fuels at 500× magnification.

2.6.2. Liquid Fraction

HPLC-RI analysis indicated that the major components of the liquid fraction were acetic acid, glycolic acid, and ethanol. The concentrations of acetic acid, glycolic acid and ethanol ranged from 4.152 to 6.930 g/L, 1.410 to 5.11 g/L and 0.086 to 0.297 g/L, respectively (see Figure 2.4). The highest concentrations of acetic acid, glycolic acid and ethanol were achieved with a processing temperature of 250 or 350 °C, a constant biomass/water ratio of 0.14 and a residence time of 60 min. The acetic acid concentration increased with higher processing temperatures, while the glycolic acid concentration increased with longer residence times, likely because of the oxidation of glycoladehyde. Hemicellulose and cellulose are hydrolyzed into monosaccharides via the hydrothermal process(Abdullah et al., 2014). These monosaccharides are unstable, and some of them are converted into other products such glycoladehyde, furfural and acetaldehyde, which in turn are converted to acetic acid (at high temperatures) and glycolic acid (at a longer residence time). The optimal processing conditions to produce acetic acid for an AD process is at a temperature of 350 °C, a biomass/water ratio of 0.14 and a residence time of 60 min. These conditions maximize the concentration of acetic acid in the liquid fraction; this result is desirable because acetic acid is the key feedstock for biomethane production via anaerobic digestion(Zhu et al., 2016).

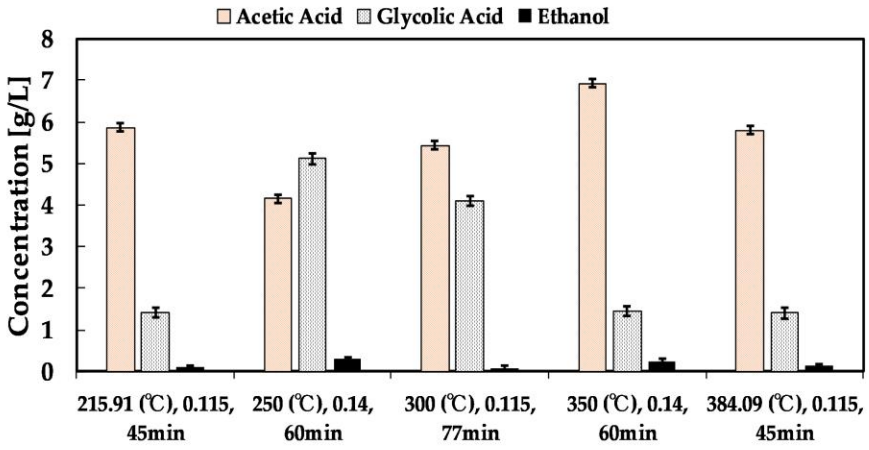

Figure 2.4: Concentration of acetic acid, glycolic acid and ethanol at different temperatures, residential times, and biomass/water ratios. Each bar represents the mean ± standard deviation of results from three replications.

2.6.3. Gas Fraction

Gas yields from the HTC of corn stover as a function of the processing temperature, residence time and biomass/water ratio are presented in Figure 2.5. As the processing temperature was increased from subcritical water conditions to supercritical water conditions (215.91–384.09 °C), H_2 yield increased from 0.02 *v/v*% to 0.25 *v/v*%. The highest concentrations of CH_4 (0.135 *v/v*%) and CO_2 (3.5 *v/v*%) were also obtained with a processing temperature of 384.09 °C, residence time of 45 min and biomass/water ratio of 0.115, while the yield of CO yields was maximized at 250 °C, 60 min and 0.14 (0.085 *v/v*%). This is a result of CO reacting with water vapor in the water–gas shift reaction to liberate CO_2 and H_2 (Kruse, 2008). The water–gas shift reactions are favorable at high temperatures, mainly in supercritical water, and contribute to major yields of H_2 and CO_2(Reddy et al., 2014). Supercritical water exists at a temperature and pressure above its critical point, which reduces its density and impedes ionic product formation. Free radical reactions become more facile

near the critical point of water, therefore gasification (See Equation (2.1)) (steam reforming) and Equation (2.2) (water–gas shift reaction)) are favored to produce hydrogen and methane.

$$CH_4 + H_2O = CO + 3H_2 \quad \Delta H_{298}^{\circ} = -205\ kJ/mol \qquad Eq\ 2.1$$

$$CO + H_2O = H_2 + CO_2 \quad \Delta H_{298}^{\circ} = +42\ \text{kJ}/mol \qquad Eq\ 2.2$$

The formation of hydrogen is endothermic (Equation (2.2)) and the formation of methane is slightly exothermic (Equation (2.2))(Vlieger et al., 2012). Therefore, hydrogen formation dominates over methane formation at supercritical conditions, according to Le Chatlier's principle(Liu et al., 2013). At 250 °C, 60 min and 0.14, the equilibrium position shifts in the exothermic direction, in which more water and carbon monoxide are formed, and hydrogen gas is present only in trace amounts. The CO concentration rises with increasing temperatures of up to 250 °C, and then drastically declines to >250 °C. The CO yield was higher than the yields of hydrogen and methane at processing temperatures between 225 and 280 °C. This result is like the findings of In-Gu Lee et al. (2002), and indicates that a significant amount of cellulose and other substrate in the corn stover was converted to CO over the temperature range 225–280 °C. Some carbon in the cellulose might have been gasified directly to form CO by pyrolysis. According to the report of In-Gu Lee et al. (2002), most of the cellulose in supercritical water is first disintegrated into biocrude (liquid phase) before being transformed into gaseous products. As the temperature is increased above 300 °C, the yields of carbon dioxide (CO_2) and hydrogen (H_2) increase, and the production of CO drops off. These results confirm that the steam reforming and the water–gas shift reaction play a vital role in the production of hydrogen gas and methane.

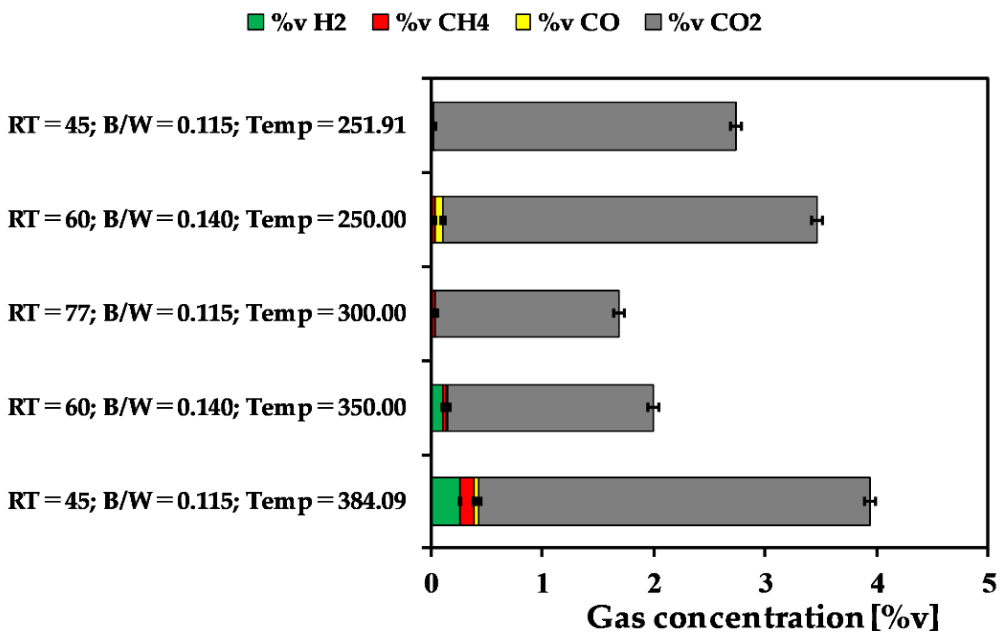

Figure 2.5: Concentration of gas at different temperature (Temp), residential time (RT) and biomass/water ratios (B/W). Each bar represents the mean ± standard deviation of result from three replication.

2.7. Mechanism of Hydrothermal Carbonization

Our results confirm that the hydrothermal carbonization of corn stover induces hydrolysis, dehydration, aromatization, decarboxylation, polymerization, and reforming reactions, as presented in Figure 2.6. The hydrochar is produced via two reaction pathways: (1) the cleavage of hemicellulose and cellulose into smaller compounds, such as pentose, hexose, and polysaccharides, is caused by hydrolysis. The product obtained from hydrolysis undergoes a sequence of dehydration, fragmentation, and isomerization reactions, forming the main intermediate Hydroxymethylfurfural and its derivative product. This intermediate further undergoes condensation and polymerization reactions associated with opposite intermolecular dehydration and aldol condensation(Funke & Ziegler, 2010; Kumar, 2013). The disintegration of this intermediate products also yields organic acid which comprises of formic, glycolic, acetic, propenoic and levulinic acids that reduced the reactions medium pH, and the condition of the solution (liquid

phase) led to a gradual breakdown of the intermediate; in Figure 2.6, the gradual breakdown of hexoses and pentose into furfurals and HMF can be seen(Camillo Falco et al., 2011; Funke & Ziegler, 2010; Hoekman et al., 2011). The conversion process of polymers to solid fuel involves keto-enol tautomerism and intramolecular dehydration because of increased double bonds, which are favored via an aromatization reaction(Akhtar & Amin, 2011). Hence, the aromatic cluster concentration in the liquid phase continues to increase because of an aromatization reaction, which reaches a critical point of saturation to form a burst nucleation(Sevilla & Fuertes, 2009). The outward grows of the nuclei was formed by linkages and a diffusion of chemical compounds present in the liquid phase to the surface of nuclei; these linkages form a reactive functional group including oxygen and other elements such as quinines and ethers(Sevilla & Fuertes, 2009). As the growth stopped, the external solid fuel particle contained a high concentration of reactive oxygen related to the core (Akhtar & Amin, 2011). This solid fuel particle that comprises of a hydrophilic shell and hydrophobic core is in line with the findings of Sevilla & Fuertes, (2009). The furanic and arene proportion is formed at a high temperature and with a residence time. (2) The degradation of lignin to catechol (phenol) is also the result of hydrolysis; this intermediate undergoes cross-linking reactions and is polymerized into hydrochar; the insoluble lignin, which is not totally dissolved at low temperatures, undergoes a solid–solid reaction like pyrolysis, which produced a high condensed hydrochar with a polyaromatic structure(Fang et al., 2008). The reaction in the HTC process favors solid–solid formations due to the small amount of soluble intermediate being used, which results in a low phenolics hydrochar(Akhtar & Amin, 2011). At a temperature and pressure above the critical point of water, steam reforming and water–gas shift reactions occur to produce methane, hydrogen, and carbon dioxide(In-Gu Lee et al., 2002).

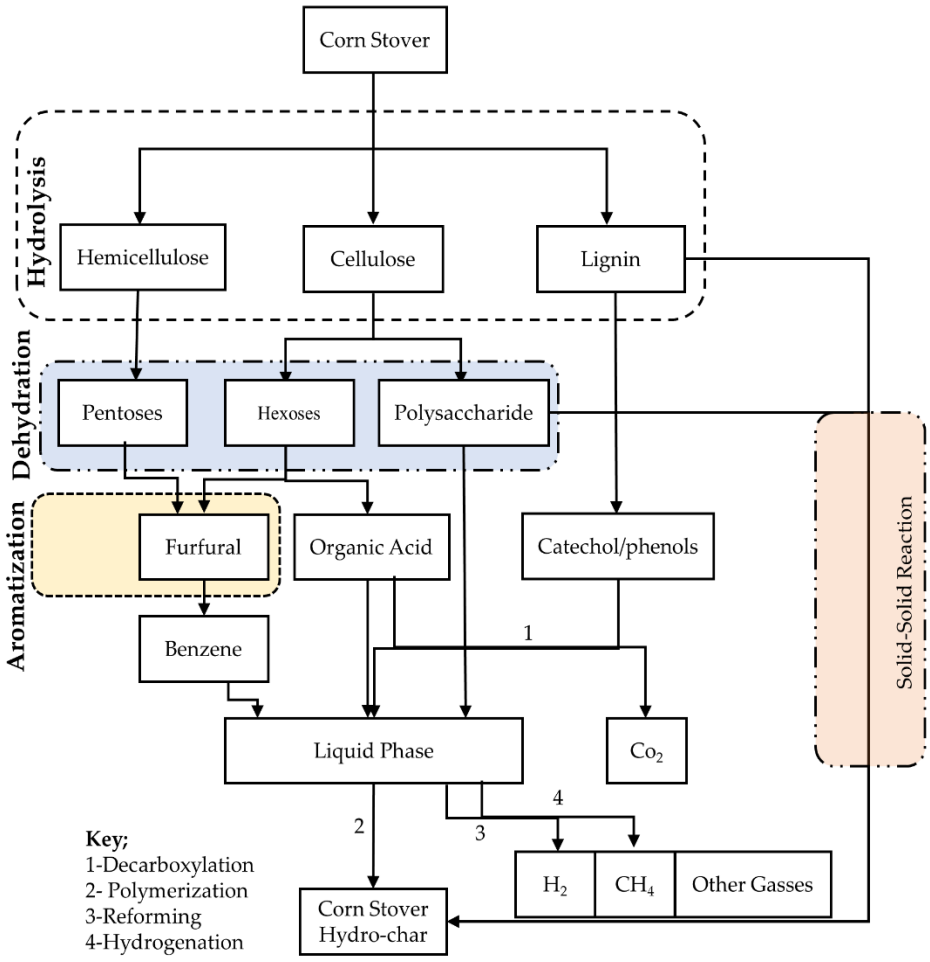

Figure 2.6: Pathways of the corn stover hydrochar formation mechanism [adapted from [(Chew & Doshi, 2011)]].

2.8 Effect of Temperature, Residence time, Biomass/water Ratio on Corn Stover Hydrochar

The combined effects of the three process variables investigated on the properties of the hydrochar are visualized in Figure 2.7a–f. The response surface and contour plots of the interactions of processing temperature and residence time with respect to the HHV of the hydrochar at a fixed biomass/water ratio of 0.115 are presented in Figure 2.7a, b. The combined plots of temperature and residence time show the highest HHV of 26.03 MJ/kg at 300 °C and 77 min, while the minimum HHV of 16.37 MJ/kg is observed at 300 °C and 19 min 8 s. The results of the ANOVA

test are presented in Table 2.4. Temperature and residence time are the most significant variables influencing the HHV(Wang et al., 2018). This may be attributable to the fact that increased temperature and residence time improve the degree of intermediates dissolution and subsequent conversions through polymerization, leading to the formation of secondary char. This is the predominant mechanism of hydrochar formation (Figure 2.6). The HHV of the hydrochar decreases at a lower processing temperature and shorter residence time because low solid loading leads to a slow polymerization rate in the liquid phase, thereby limiting the formation of secondary hydrochar (Fan et al., 2013). At supercritical conditions for water, the HHV (21.75 MJ/kg) of the hydrochar obtained was lower than the HHV of the hydrochar produced at subcritical conditions (26.03 MJ/kg). This may be a result of direct gasification of the corn stover constituents. The HHV of all the hydrochars was higher than raw corn stover; this result agrees with the results of(Kang et al., 2019; Xiao et al., 2012).

Table 2.4: ANOVA for the High Heating Value [MJ/kg] Response Surface Quadratic Model.

Source	Sum of Squares	df	Mean Square	F-value	P-value	
Model	101.72	9	11.30	3.32	0.02	
X_1 -Temperature	5.63	1	5.63	1.65	0.03	
X_2 -Residential Time	54.19	1	54.19	15.91	0.00	
X_3 -Biomass/Water	0.65	1	0.65	0.19	0.02	
X_1X_2	0.49	1	0.49	0.14	0.01	significant
X_1X_3	1.08	1	1.08	0.32	0.05	
X_2X_3	0.10	1	0.10	0.03	0.02	
X_1^2	21.91	1	21.91	6.43	0.03	
X_2^2	18.05	1	18.05	5.30	0.01	
X_3^2	6.66	1	6.66	1.96	0.03	
Residual	34.05	10	3.41			
Lack of Fit	27.86	5	5.57	4.50	0.06	
Pure Error	6.19	5	1.24			
Cor Total	135.78	19				
Std Dev.	1.85	R^2	0.85			
Mean	19.15	AdJ-R^2	0.80			Not
C.V. %	9.63	Pred-R^2	0.70			significant
PRESS	231.49	Adeq-Precision	5.21			
-2Log Likelihood	67.40	BIC	97.36			
		AICc	111.85			

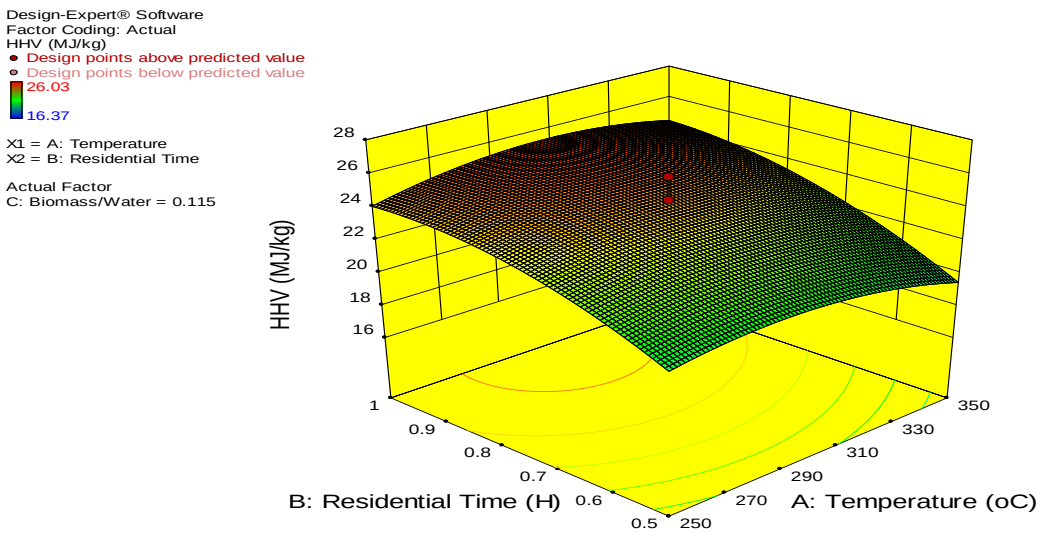
Design-Expert® Software
Factor Coding: Actual
HHV (MJ/kg)
Design points above predicted value
Design points below predicted value
26.03
16.37
X1 = A: Temperature
X2 = B: Residential Time
Actual Factor
C: Biomass/Water = 0.115
HHV (MJ/kg)
28
26
24
22
20
18
16
B: Residential Time (H)
1
0.9
0.8
0.7
0.6
0.5
A: Temperature (oC)
250
270
290
310
330
350

(a)

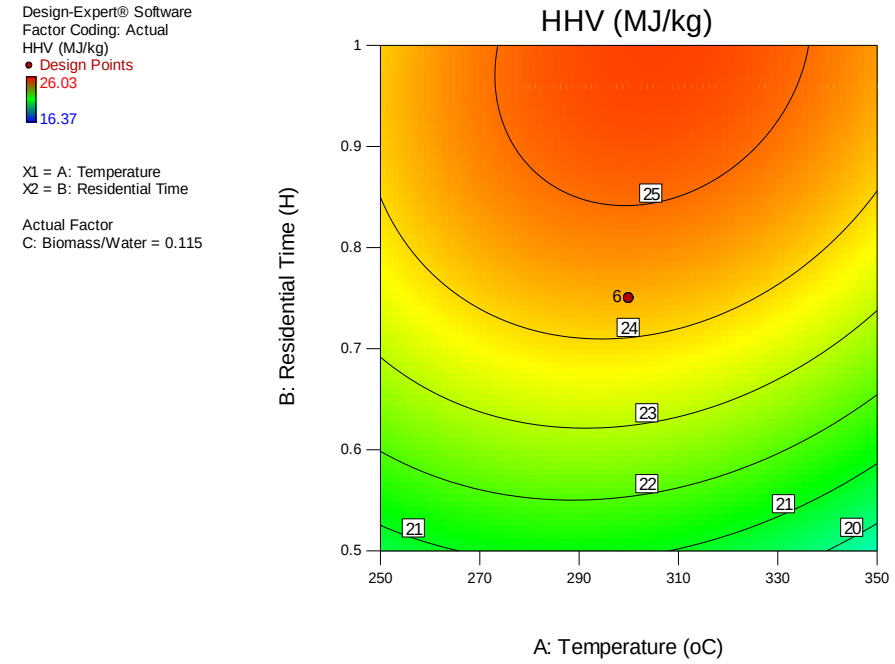
Design-Expert® Software
Factor Coding: Actual
HHV (MJ/kg)
Design Points
26.03
16.37
X1 = A: Temperature
X2 = B: Residential Time
Actual Factor
C: Biomass/Water = 0.115
HHV (MJ/kg)
B: Residential Time (H)
1
0.9
0.8
0.7
0.6
0.5
25
24
23
22
21
20
6
A: Temperature (oC)
250
270
290
310
330
350

(b)

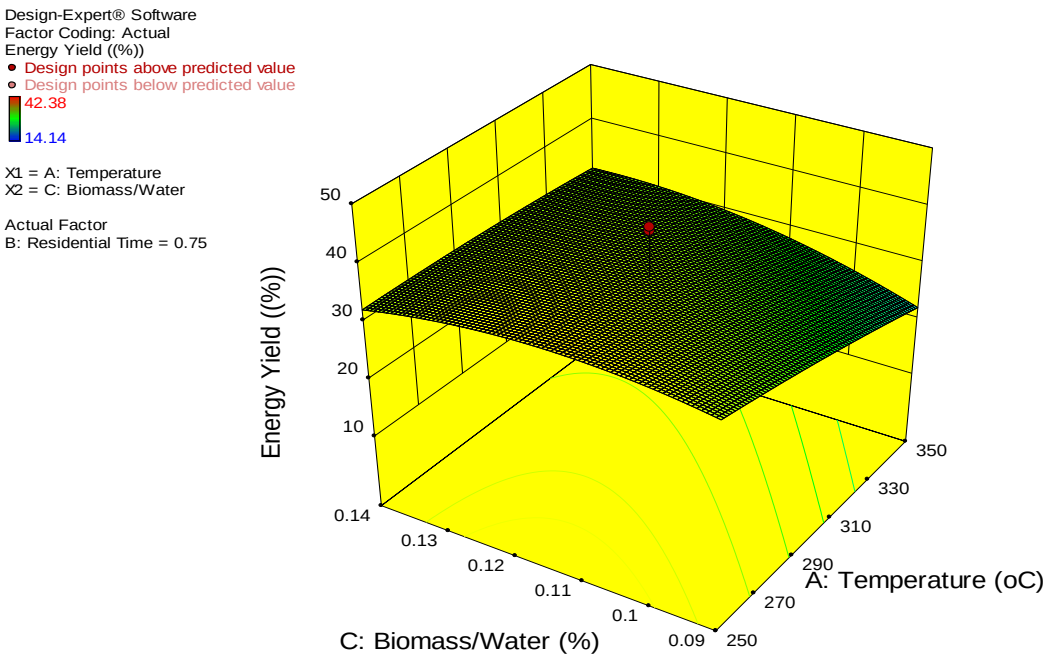
Design-Expert® Software
Factor Coding: Actual
Energy Yield ((%))
Design points above predicted value
Design points below predicted value
42.38
14.14
X1 = A: Temperature
X2 = C: Biomass/Water
Actual Factor
B: Residential Time = 0.75
Energy Yield ((%))
50
40
30
20
10
0.14
0.13
0.12
0.11
0.1
0.09
C: Biomass/Water (%)
250
270
290
310
330
350
A: Temperature (oC)

(c)

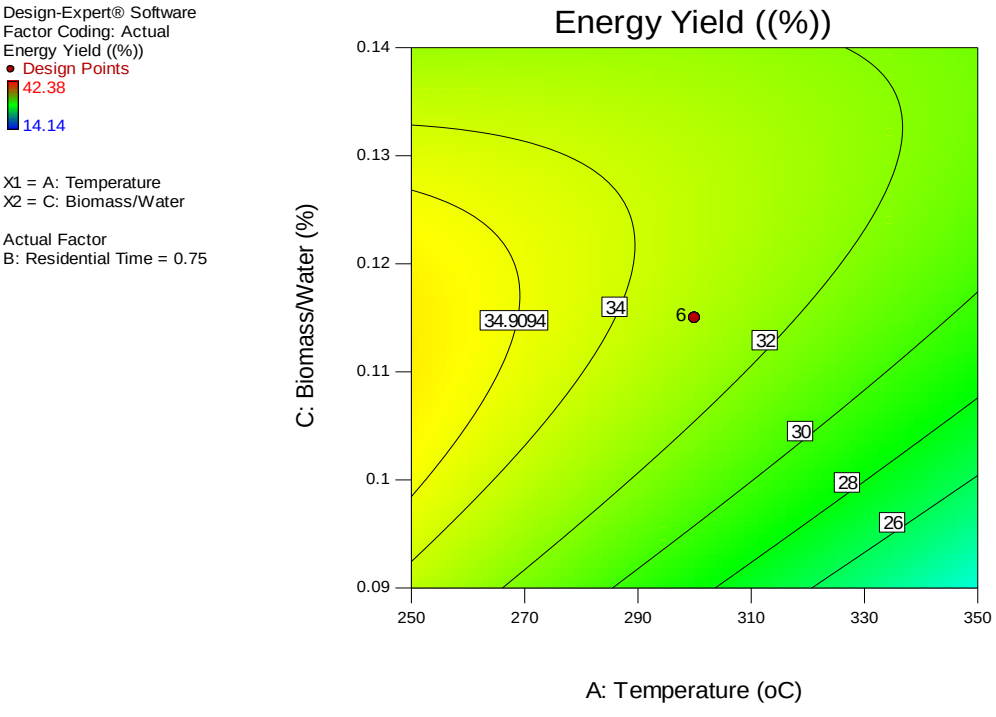
Design-Expert® Software
Factor Coding: Actual
Energy Yield ((%))
Design Points
42.38
14.14
X1 = A: Temperature
X2 = C: Biomass/Water
Actual Factor
B: Residential Time = 0.75
Energy Yield ((%))
0.14
0.13
0.12
0.11
0.1
0.09
C: Biomass/Water (%)
34.9094
34
32
30
28
26
6
250
270
290
310
330
350
A: Temperature (oC)

(d)

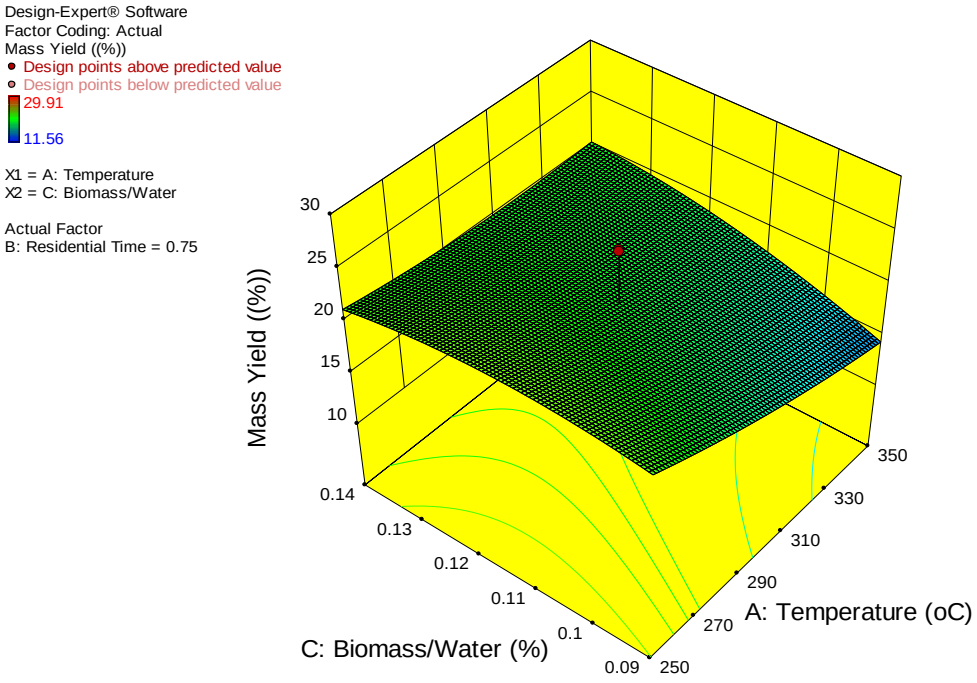

(e)

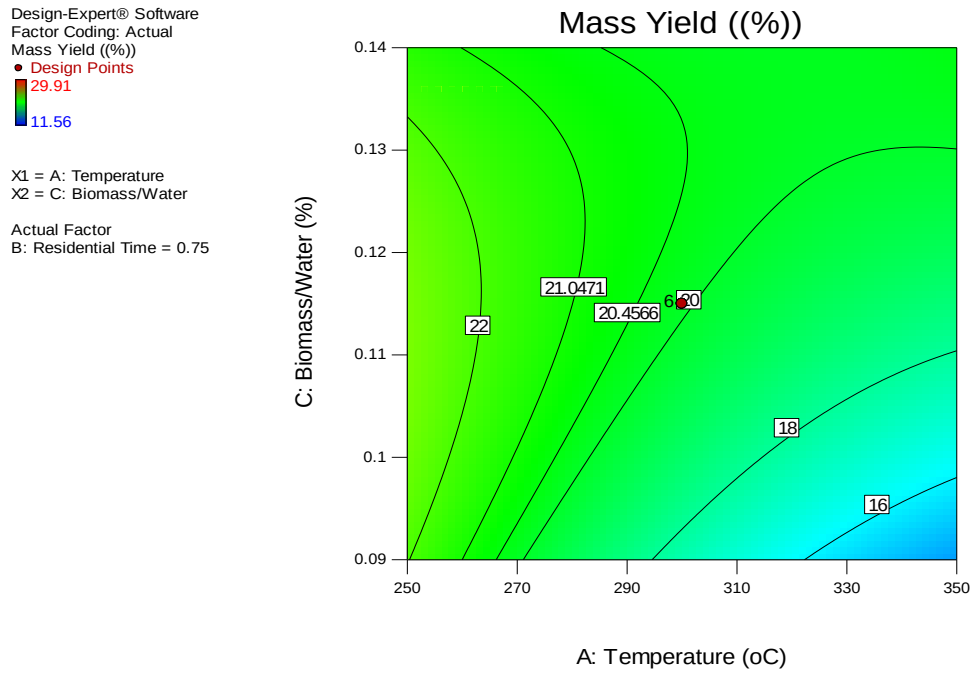

(f)

Figure 2.7.: Surface and Contour Plots of High Heating Value (**a**,**b**), Energy (**c**,**d**) and Mass (**e**,**f**) Yield.

The effects of interactions between the processing temperature and biomass/water ratio (at a constant residence time of 45 min) on the energy yield of the hydrochar are illustrated in Figure 2.7c, d. The response surface and contour plot show that as the temperature decreases from 384.09 to 215.9 °C, the energy yield increases from 29.88 wt.% to 42.38 wt.%, while at constant a temperature of 350 °C and residence time of 30 min, the energy yield increases from 14.14 wt.% to 26.40 wt.% with biomass/water ratios of 0.09 and 0.14, respectively. Both the processing temperature and biomass/water ratio display a strong influence on the hydrochar yield(Wang et al., 2018). Increased temperatures enable a comprehensive decomposition of the corn stover and aid the deposition of carbon in the solid fuel. Lower biomass/water ratios also promote total disintegration of the corn stover, yielding a small amount of solid fuel(He et al., 2013) Figure 2.7e,f depict the response surface and contour plots of the temperature and biomass/water ratio with respect to mass yield at a constant residence time of 45 min. Mass yield is a vital quantitative index that indicates how much the corn stover is transformed into solid fuel during HTC. The mass yield decreases as the temperature increases from 250 to 350 °C and biomass/water ratios change (0.09 to 0.14) because of the decomposition of the corn stover(Wang et al., 2018). The increased temperature (>200 °C) weakens intramolecular hydrogen bonding in cellulose, increases the polarity of the CH_2OH group and promotes the cleavage of polysaccharides that form hydrochar via a solid–solid reaction (Figure 2.6). The highest mass yield obtained in this study was 29.91% with a processing temperature of 215.9 °C, a 45 min residence time and a biomass/water ratio of 0.115. Our results suggest that it is possible to manipulate processing conditions to adjust the mass loss of corn stover converted into liquid and gas fractions.

2.9. Hydrothermal Process Modelling and Optimization of Corn Stover using RSM

The model for HHV detailed in Equation (2.7) was developed using RSM. The experimental data (Table 2.5) was used to fit the quadratic regression model of Equation (2.4), which describes the response of HHV to the independent experimental parameters of temperature, residence time and biomass/water ratios. The quadratic model was appraised by analysis of variances (ANOVA). The Fisher's test (F-value) and probability value (*p*-value) of the model are 3.32 and 0.02, respectively. Table 4 details the significances of the model at a 95% confident interval ($p < 0.05$). All quadratic, interaction and linear terms of the model equation were found to be significant. Performance assessments of the model were conducted using a statistical index (R^2 = 0.85 and adjusted R^2 = 0.80) that showed a good fit and correlation between the experimental and predicted data(Mohammed et al., 2019).

$$HHV\ \left[\frac{MJ}{kg}\right] = -52.849 + 0.302 * X_1 + 26.77 * X_2 + 316.06 * X_3 + 0.0198 * X_1X_2 - 0.2943 * X_1X_2 + 18.291 * X_2X_3 - 4.93x10^{-4} * X_1^2 - 17.905 * X_2^2 - 1087.89 * X_3^2 \quad \text{Eq (2.7)}$$

The optimization and validation results for the HHV of corn stover hydrochar are presented in Table 2.5. The predicted responses were formulated by employing a point prediction node beneath the optimization node in the CCD. Process variables included the temperature, residence time and biomass/water ratio in the ranges of 250–350 °C, 0.5–1 h and 0.09–0.114, respectively. HHV was maximized within the experimental range of 16.37–26.03 MJ/kg and the optimal conditions were suggested by the software at a desirability value of 0.937. Experimental validation of the optimal conditions was conducted in triplicate; a maximum HHV of 25.73 MJ/kg was obtained, which was 7.75% less than the predicted value. The experimental value was within the variance ranges of ±10 %. The difference between the experimental and predicted result may stem from the adjusted R^2 of 0.80 in the quadratic model.

Table 2.5: Response and Variables Condition of HTC Process Optimization Experiment, and Average Values of HHV, Energy Yield and Mass Yield.

Run	Temperature	Residence Time (h)	Biomass/ Water Ratio	Final pressure (Mpa)	HHV (MJ/kg)	Energy Yield (%)	Mass Yield (%)
1	300	0.75	0.157	14.95	20.73	28.48	20.23
2	300	0.75	0.115	15.95	25.85	31.45	17.91
3	300	0.75	0.115	14.99	23.70	31.26	19.42
4	350	1	0.09	22.45	21.95	19.21	12.89
5	300	0.75	0.115	15.75	24.49	41.46	24.93
6	300	0.75	0.073	12.25	23.23	31.03	19.66
7	384.09	0.75	0.115	26	21.75	29.88	20.23
8	300	0.33	0.115	15.95	16.37	28.36	25.51
9	250	0.5	0.09	10.35	19.85	31.19	23.13
10	250	1	0.14	10.50	23.08	30.16	19.24
11	300	0.75	0.115	15.75	24.05	27.94	17.10
12	215.91	0.75	0.115	8.85	20.86	42.38	29.91
13	300	0.75	0.115	15.25	24.19	24.67	15.01
14	300	0.75	0.115	16	23.91	40.76	25.10
15	250	1	0.09	10.40	23.20	22.88	14.52
16	300	1.170	0.115	16	26.03	40.90	23.13
17	350	1	0.14	23.2	23.93	32.97	20.29
18	250	0.5	0.14	20	19.82	26.40	19.61
19	250	0.5	0.14	10.50	21.44	29.68	20.38
20	350	0.5	0.09	23	18.01	14.14	11.56
Raw Samples					14.72		
HHV (Optimum)	305	1	0.14	16.34	25.42	-	-
HHV (Validated)	305	1	0.14	16.34	24.45	-	-
Standard deviation (%)					0.016	0.017	0.018

2.10 Conclusions

This study demonstrates that corn stover can be converted to solid fuel through HTC. The corn stover hydrochar has a high degree of coalification because of its high processing temperature and long residence time. CCD-RSM was used to optimize processing conditions. The effect of the temperature, residence time and biomass/water ratio on the properties of the hydrochar were also examined. The optimal processing parameters predicted using the model were a temperature of 305°C, residence time of 60 min, biomass/water ratio of 0.114 and a pressure of 16.25 MPa. These conditions were validated experimentally and found to be within 0.0097% of the predicted result. The ANOVA test revealed that temperature and residence time were the most significant variables that affect hydrochar yield.

SEM, TGA and DTG were used to reveal significant changes in the morphology, weight loss and thermal stability of corn stover hydrochar. Our results indicate that hydrochar produced at 300 °C contains the highest amount of fixed carbon.

HPLC analysis of the liquid fraction revealed that it contains high concentrations of acetic acid (up to 6.970 g/L). The hydrothermal liquid will be used in an anaerobic digestion in future work entailing process modeling, control, simulation and optimization of a biomethane production management system.

The yields of H_2, CO_2 and CH_4 in the gas fraction are higher at supercritical conditions than at subcritical conditions. The HHV of the hydrochar is higher at subcritical conditions (26.03 MJ/kg) than at supercritical conditions (21.75 MJ/kg). The highest mass and energy yields (29.91% and 42.38%, respectively) were obtained with the following processing parameters: a residence time of 45 min, biomass/water ratio of 0.115, processing temperature of 215.91 °C and pressure of 8.85 MPa.

CHAPTER 3

Modeling anaerobic digestion of lignocellulose biomass for sustainable biogas production

3.1 Introduction

As the consumption of energy increase globally, fossil fuel resources deteriorate because of overexploitation and likely to scare or extinct in future generation, therefore, developing renewable energy and alternative fuels is a promising solution to this situation (Wang et al., 2021; Wu & Xia, 2015). The emission of carbon and pollutant from burning of fossil fuel over the years as great impact to environment (Kambo & Dutta, 2014). To reduce the over dependence of fossil fuel consumption and pollutant emissions, exploitation of renewable energy resources like wind and solar power systems is required (Esen & Yuksel, 2013)Click or tap here to enter text.. Although environmental condition affects the amount of renewable energy produce by wind and solar power systems which are currently the main systems used to generate renewable energy around the world (Hamed & Alshare, 2021; Yoshida et al., 2020). These systems are terms as variables renewable resources. To increase the supply of renewable energy which are the key factors in the attainment of sustainable development goals, the used of lignocellulose biomass as a renewable and sustainable resources is needed which is not affected by environmental change (Yoshida et al., 2020). The production of lignocellulosic biomass is estimated to be 200 billion tons annually. Improper management of these lignocellulose biomass can cause pollution in both air and environment (Liang et al., 2020; Mohammed, Na, et al., 2020; Zhang et al., 2016). The conversion of lignocellulose biomass into biogas is a potential alternative for green energy to meet world demand and ensure an adequate future supply of clean energy and fuel (Mohammed, Aliyu, et al., 2020; Salman et al., 2017). A system in which energy is generated from lignocellulose biomass would be robust and could compensate for fluctuations in the outputs of other renewable energy

resources. AD can be applied to convert lignocellulose biomass to biogas, and it is also an important technique because it concurrently recovers energy and treat waste (Codignole Luz et al., 2018; Song et al., 2019). Additionally, the digestate which is a by-product of AD can be utilized as soil improver.

The numerical optimization of AD process has been extensively studied for bioenergy production and wastewater treatment due to its ability of converting energy crop or organic waste into biogas in the absence of oxygen (Kil et al., 2017). The anaerobic transformation of organic matter is a complex bio-chemical process involving numerous bacterial populations which make the process nonlinear and uncertain, therefore, difficult to predict and simulate. For this purpose, design, modelling, and simulation of AD process have attracted a considerable amount of attention over decades. As a basis for modeling and simulation of AD process, many mathematical models of AD process have been established and used to identify ways of decreasing operating costs and improving process stability. Méndez-Acosta et al. (2010) utilized a dynamic model to improve the process stability of AD by regulating the concentration of volatile fatty acid and total alkalinity which are inhibitors of the process. In addition, a feeding management strategy to compensate for variation between demand and supply of energy production is established by Mauky et al. (2016). Therefore, there have been few efforts to utilize the benefits of AD for energy demand and supply regulations, and the models facilitate exact prediction of biogas generation and offer flexibility and robustness in different operating conditions. Though, in terms of practicability, the development of a model for controlling biological variables such as substrate concentration, bacterial concentration, and product (biogas production) are still developing (Blumensaat & Keller, 2005; Hassam et al., 2015). This is because they consist of living organisms which behavior are dynamic, nonstationary, and nonlinear. There is also lack of cheap sensor that is efficient of

offering reliable online measurement of the bio-chemical parameter that is needed to execute high performance of computer control strategies. It is clumsy to ascertain all the parameters involve in ADM1 for each operating condition experientially when a simplified model for the prediction of biogas generation will be preferred. From the viewpoint of practicability at the commercial scale of biogas plant, a simplified model of biogas production and parametric study of the model constants were established by (Arzate et al., 2017; Bernard et al., 2001; Hassam et al., 2015; Kil et al., 2017; Lubenova et al., 2002; Mejdoub & Ksibi, 2015; Simeonov & Queinnec, 2006). Although, the kinetic parameters in these simplified models are varying drastically because of the abstract reaction dynamics, some parameters are obtained from literature while other are determined by conducting series of experiments (Martinez et al., 2012), these make it difficult in determining the values of the parameters effectively which hinders the use of this models in control process. Yoshida et al. (2020) established another simplified model for biogas production and developed an adaptive identifier system to estimate parameters from data acquired while a process is being performed. This adaptive identifier system has a control signal with polynomial functions of real and equal roots, meaning there is only one tuning parameter. This makes estimating the parameters, controlling the process, and predicting biogas production possible. In this study, the polynomial function of the control signal was modified to have real and unequal roots, meaning there are two tuning parameters which makes it flexible adjustment. However, to the best of authors knowledge, there is limited studies on modeling AD of lignocellulose biomass for sustainable biogas production.

It is possible to use AD to mitigate variations in the power outputs of other renewable energy sources because current practice is to run an AD system using the same amount of waste each day and to keep raw material input consistent. Quickly changing raw material inputs can excessively

affect the fermentation state and cause poor fermentation (Lauterböck et al., 2012). An improved model for predicting biogas production taking the fermentation state into account is required. A state–space model can describe an unobserved fermentation state, including substrate variables (corn stover hydrochar and food waste) and the bacteria concentration, from data from biogas analyses. It is important to estimate the variables used in the model. The aim of this study is to develop a state–space model appropriate for controlling biogas generation and an adaptive identifier that can automatically estimate the key parameters representing the input and output characteristics of the AD process from experimental data.

3.2 Materials and Methods

3.2.1 Flow during hydrothermal carbonization and anaerobic digestion

The HTC and AD process is shown as a flow diagram in Figure 3.1. The corn stover hydrochar used in the study was prepared as described in detail by Mohammed, Na, et al. (2020). The food waste used in the study was collected from a cafeteria at Hokkaido University. The food waste was ground using a food processor, then small portions were placed in bags and frozen. To prepare the feedstock, a portion of food waste (which had a high nitrogen content) was mixed with paper to achieve a C/N ratio of ~40 to decrease inhibition by ammonia that can be caused by AD of N-rich feedstock (Nakajima et al., 2016; Yoshida et al., 2020). Corn stover hydrochar was then mixed with the ground food waste at a mass ratio of 2:1. The prepared feedstock was then placed in a horizontal cylindrical bioreactor (effective volume 0.235 m^3) which was kept at ~52 °C and stirred frequently to allow degassing and to ensure that the feedstock was adequately mixed.

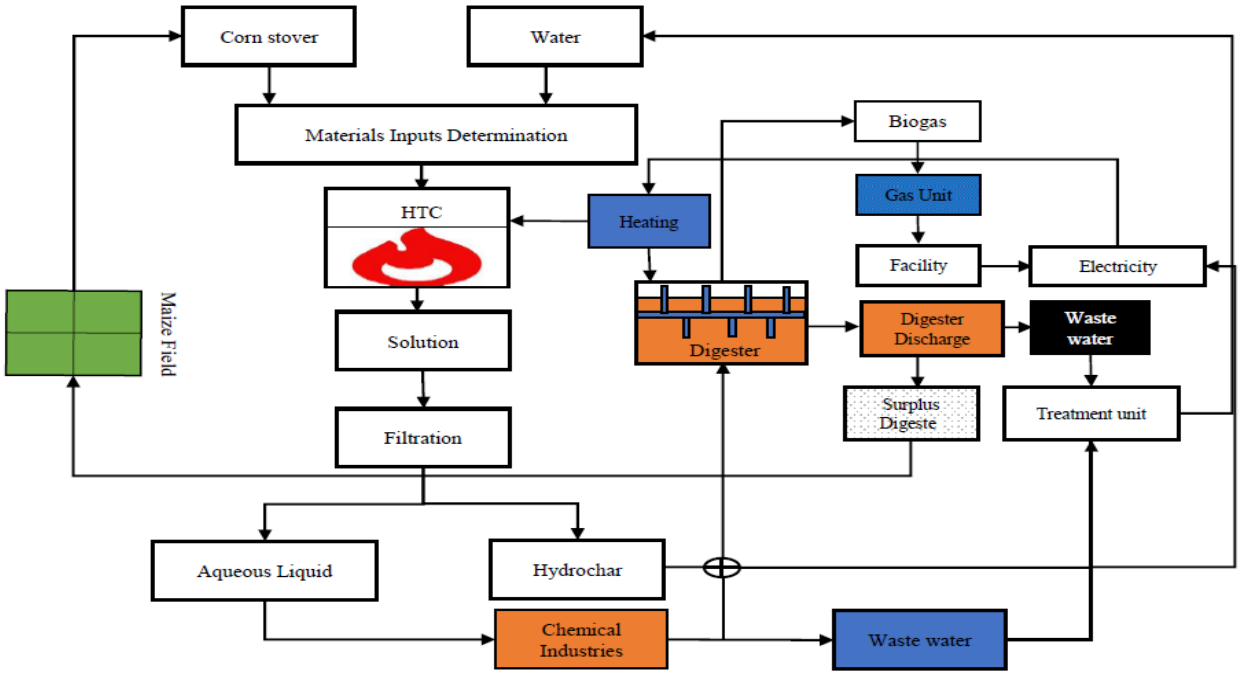

Figure 3.1: Hydrothermal carbonization and anaerobic digestion flow diagram. Corn stover feedstock was used to prepare hydrochar in the hydrothermal carbonization (HTC) unit, then the hydrochar was mixed with food waste and added to the anaerobic digester. Biogas was collected using a gas trap bag and the digestate from the biorefinery system was disposed of.

The biogas that was generated was stored in a gas trap bag. Some digestate was collected when the feedstock was added and the remaining digestate (excluding the returned digestate) was treated as surplus. The volatile compound and total solid contents of the feedstock were ~35% and ~40%, respectively. The sludge in the reactor remained at the thermophilic temperature of 52 °C. The HTC and AD processes were therefore classed as dry thermophilic techniques that would minimize digestate emissions because no water needed to be added (IEA, 2001).

3.3 State–Space Model of AD

Some assumptions about the AD process were made to simplify developing the model. The reactions that converted the input organic components (the substrate) to the output (biogas) were included in the model. A semi-batch bioreactor was used, and the sludge was completely mixed. The volume of sludge in the bioreactor was kept constant at 0.2 m^3. The substrate concentration $m(t)$ and bacteria concentration $z(t)$ were the state variables that characterized fermentation in the bioreactor. The substrate and bacteria concentrations in the feedstock were treated as manipulated variables $u_z(t)$ and $u_m(t)$, respectively, and the biogas concentration was treated as the controlled variable $Q(t)$. The simplified bioreactor using these variables is shown in Figure 3.2. The mathematical AD model was built based on mass balance theory.

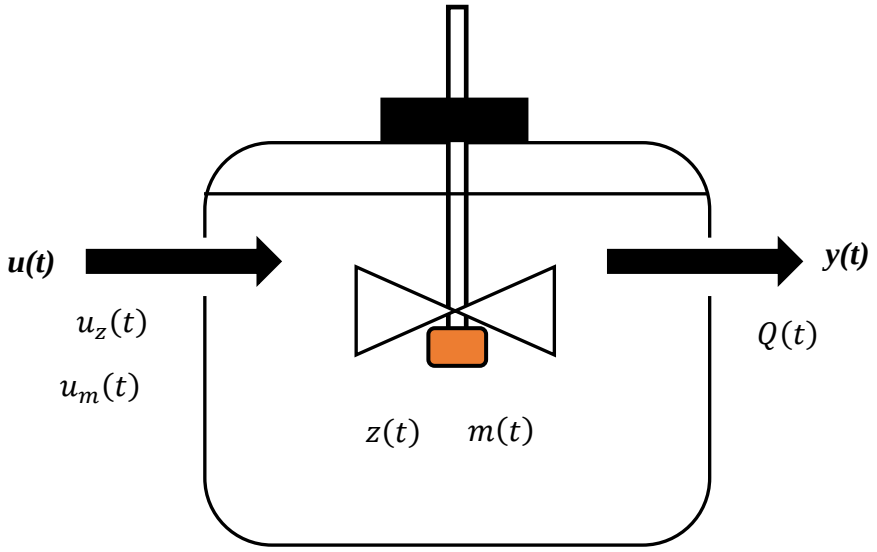

Figure. 3.2 Graphical representations of the semi-batch-type bioreactor used for anaerobic digestion ($u_z(t)$ = bacterial input (kg/ (m^3 h)), $u_m(t)$ = substrate input (kg/ (m^3 h)), $z(t)$ = bacteria concentration (kg/m^3), $m(t)$ = substrate concentration (kg/m^3), and $Q(t)$ = biogas flow rate (m^3/h))

The state equation consisted of two differential equations, one for bacterial growth and the other for substrate disintegration. A logistic difference equation was used to indicate bacterial growth

because it is an efficient equation that is used in population biology (Mejdoub & Ksibi, 2015). The substrate disintegration equation was used to indicate substrate degradation in line with bacterial growth. The output equation was used to describe the biogas flow rate caused by biogas production through substrate decay and bacterial growth (May, 1976). The growth rates used in these equations were given by a modified Monod equation (Bastin & Dochain, 1990). The mathematical model of AD was constructed by concatenating the two differential equations and one algebraic equation, as shown in Eq. (3.1).

$$\begin{cases} \dfrac{dz(t)}{dt}(\mu(m)-a)z(t)\left(1-\dfrac{z(t)}{z_{max}}\right)+u_z(t) \\ \dfrac{dm(t)}{dt}=-\dfrac{1}{w}\mu(m)z(t)+u_m(t) \\ y(t)=\left(Lq_1\ \dfrac{1}{w}\mu(m)+Lq_2a\right)vz(t) \end{cases} \qquad \text{Eq. (3.1)}$$

$$\mu(m)=\mu_{max}\frac{m(t)}{K_s+m(t)+bm^2(t)}$$

In Eq. (3.1), $z(t)$ is the bacteria concentration ($\mathrm{kg/m^3}$), $m(t)$ is the substrate concentration ($\mathrm{kg/m^3}$), y(t) is the gas generation rate ($\mathrm{m^3/h}$), $u_z(t)$ is bacterial input ($\mathrm{kg/(m^3\ h)}$, $u_m(t)$ is substrate input ($\mathrm{kg/(m^3\ h)}$, $\mu(m)$ is the specific growth rate ($\mathrm{h^{-1}}$), a is the autolysis rate ($\mathrm{h^{-1}}$), z_{max} is the bacteria-carrying capacity ($\mathrm{kg/m^3}$), w is the bacterial cell yield, Lq_1 and Lq_2 are gas generation coefficients, v is the sludge volume ($\mathrm{m^3}$), b is the inhibition coefficient, K_s is the dissociation constant ($\mathrm{kg/m^3}$), and μ_{max} is the maximum specific growth rate ($\mathrm{h^{-1}}$).

Perturbation theory was applied near the point at which equilibrium was reached using the nonlinear model by ignoring the second-order and higher-order terms after Taylor expansion of the two-variable functions, as shown in Eqs. (3.2)– (3.5), to give the linear-time state–space model shown in Eq. (3.6).

The method described next was used to derive Eq. (3.6). First, temporal changes in the state and the output variables of the AD system were considered using Eq. (3.2).

$$\frac{dX(t)}{dt} = F(X(t), U(t), t) \qquad \text{Eq. (3.2)}$$
$$y(t) = g(X(t), t)$$

Assuming that the reactions were near equilibrium, Eq. (3.2) was transformed into Eq. (3.3).

$$\frac{dX(t)}{dt} = F\big(X_{eq} + X'(t), U_{eq} + U'(t), t\big) \qquad \text{Eq. (3.3)}$$
$$y(t) = g\big(X_{eq} + X'(t), t\big)$$

In Eq. (3.3), (X_{eq}, U_{eq}) is the equilibrium point and $\big(X'(t), U'(t)\big)$ is the perturbation.

The right-hand side of Eq. (3.3) was rewritten by ignoring the second-order and higher-order terms after Taylor series expansion of the two variables to give Eq. (3.4).

$$F\big(X_{eq} + X'(t), U_{eq} + U'(t), t\big) \approx F\big(X_{eq}, U_{eq}, t\big) + \Big(X'(t)\frac{\partial}{\partial X(t)} + U'(t)\frac{\partial}{\partial U(t)}\Big) F(X(t), U(t), t)\Big|_{(X_{eq}, U_{eq}, t)} \qquad \text{Eq. (3.4)}$$
$$y(t) = g\big(X_{eq}\big) + X'(t)\frac{\partial g}{\partial X(t)}\Big|_{(X_{eq}, t)}$$

Finally, Eq. (3.6) was obtained by substituting the equilibrium point in Eq. (3.4) into Eq. (3.5).

$$\frac{dX(t)}{dt} = \frac{\partial F}{\partial X(t)}\Big|_{(X_{eq}, U_{eq}, t)} X(t) + \frac{\partial F}{\partial X(t)}\Big|_{(X_{eq}, U_{eq}, t)} U(t) \qquad \text{Eq. (3.5)}$$

$$y(t) = \frac{\partial g}{\partial X(t)}\Big|_{(X_{eq},t)} X(t)$$

The substitution above gave Eq. (3.6) in the form

$$\frac{dX(t)}{dt} = A_q X(t) + B_q U(t)$$
$$y(t) = C_q X(t)$$

$$A_q = \frac{\partial F}{\partial X(t)}\Big|_{(X_{eq},U_{eq},t)} = \begin{bmatrix} a_{11} & a_{12} \\ a_{21} & a_{22} \end{bmatrix}$$

$$B_q = \frac{\partial F}{\partial U(t)}\Big|_{(X_{eq},U_{eq},t)} = \begin{bmatrix} b_{11} & b_{12} \\ b_{21} & b_{22} \end{bmatrix}$$

$$C_q = \frac{\partial g}{\partial X(t)}\Big|_{(X_{eq},t)} = [c_{11} \quad c_{12}],$$

where $a_{11}, a_{12}, a_{21}, a_{22}, b_{11}, b_{12}, b_{21}, b_{22}, c_{11},$ and c_{12} are all Jacobian elements.

$$f_1(X(t), U(t), t);\ \frac{dz(t)}{dt} = (\mu(m) - a)z(t)\left(1 - \frac{z(t)}{z_{max}}\right) + u_z(t)$$
$$f_2(X(t), U(t), t);\ \frac{dm(t)}{dt} = -\frac{1}{w}\mu(m)z(t) + u_m(t)$$
$$g(X(t), t); Q(t) = \left(Lq_1\frac{1}{w}\mu(m) + Lq_2 a\right)vz(t)$$
$$F(X(t), U(t),\ t) = \begin{bmatrix} f_1(X(t), U(t), t) \\ f_2(X(t), U(t), t) \end{bmatrix} \qquad \text{Eq. (3.6)}$$

$X(t)$ therefore represents matrices containing coefficients of the vectors of the state variables and $U(t)$ represents the vectors of the manipulated variables that are partial derivative matrices for the

equilibrium point of the Jacobian matrix. These parameters provide information about the characteristics of the AD process under the relevant operating conditions.

3.3.1 Parameter Estimation System

A z-transformation was performed on the state–space model to give the discrete input and output relational expressions shown in Eq. (3.10) taking Eqs. (3.7)– (3.9) into consideration. This is equivalent to performing the Laplace transformation for discrete time but replacing the operator in the Laplace transformation with a delay operator. The z-transformation of Eq. (3.6) is shown in Eq. (3.7),

$$q^{-1}X(p) = A_q X(t) + B_q U(t)$$
$$y(p) = C_q X(p), \qquad \text{Eq. (3.7)}$$

where q^{-1} is the delay operator.

The coefficient of the variable on the left-hand side of Eq. (3.7) is a scalar variable, so Eq. (3.8) was derived from Eq. (3.7).

$$X(p) = \left(q^{-1}I - A_q\right)^{-1}\left(B_q U(t) + X(0)\right)$$
$$y(p) = C_q X(p) \qquad \text{Eq. (3.8)}$$

The initial value was therefore not considered in this study and Eq. (3.10) was obtained by combining the two expressions shown in Eq. (3.8) as shown below.

$$y(p) = C_q\left(q^{-1}I - A_q\right)^{-1}B_q U(t)$$

where

$$\left(q^{-1}I - A_q\right)^{-1} = \frac{adj\left(sI - A_q\right)}{\det\left(sI - A_q\right)}$$

$$= \frac{1}{q^{-2} + (-a_{11} - a_{22})q^{-1} + (a_{11}a_{22} - a_{12}a_{21})} \begin{bmatrix} q^{-1} - a_{22} & a_{12} \\ a_{12} & q^{-1} - a_{11} \end{bmatrix}$$

Eq. (3.9)

$$A(q)y(p) = B(q)U(p),$$

where

$$A(q) = q^{-2} + (-a_{11} - a_{22})q^{-1} + (a_{11}a_{22} - a_{12}a_{21}) = q^{-2} + a_1 q^{-1} + a_2$$

and

$$B(q) = [c_{11}(q^{-1} - a_{22}) + c_{12}a_{21} \quad c_{11}a_{12} + c_{12}(q^{-1} - a_{11})]$$
$$= [b_1 q^{-1} + b_2 \quad b_3 q^{-1} + b_4]. \qquad \text{Eq. (3.10)}$$

The original parameters of the model shown in Eq. (3.6) were changed to a_1, a_2 and b_1, b_2, b_3, b_4. Once the values had been estimated, biogas generation $y(p)$ could be predicted by inputting the bacteria and substrate concentrations in the feedstock $U(k)$ into Eq. (3.10). An adaptive identifier was developed using the adaptive identification theory to estimate the parameters from real operational data (Byrne & Abdallah, 1995; Yoshida et al., 2020). The adaptive identifier shown in Figure 3.3 was used as the control system. Input and output data were multiplied by the filter to produce the control signals $\zeta_{11}, \zeta_{12}, \zeta_{21}, \zeta_{22}, \zeta_3,$ and ζ_4 in the adaptive identifier. The control signals were multiplied by the operating parameters and then integrated, and the linear relationship between output and the parameters with the proportionality constant as the control signal was derived using Eq. (3.11).

$$y(p) = h(q)\varphi^T \psi(p)$$

$$\varphi^T = [b_1, \quad b_2, \quad b_3, \quad b_4, \quad \omega + \lambda - a_1, \quad \omega \times \lambda - a_2]^T$$
$$\psi(p) = [\zeta_{11}(p), \quad \zeta_{12}(p), \quad \zeta_{21}(p), \quad \zeta_{22}(p), \quad \zeta_3(p), \quad \zeta_4(p)]$$

Eq. (3.11)

The mechanism involved in the operation of the adaptive identifier shown in Figure 3 was verified using Eq. (3.11).

$$y(p) = h(q)\big(b_1\zeta_{11}(p) + b_3\zeta_{12}(p) + b_2\zeta_{21}(p) + b_4\zeta_{22}(p) + (\omega + \lambda - a_1)\zeta_3(p) + (\omega \times \lambda - a_2)\zeta_4(p)\big)$$

$$\begin{aligned} y(p) = h(q)\Bigg(& b_1 \frac{q^{-1}}{(q^{-1}+\lambda)(q^{-1}+\omega)} u_z(p) + b_3 \frac{1}{(q^{-1}+\lambda)(q^{-1}+\omega)} u_z(p) \\ & + b_2 \frac{q^{-1}}{(q^{-1}+\lambda)(q^{-1}+\omega)} u_m(p) + b_4 \frac{1}{(q^{-1}+\lambda)(q^{-1}+\omega)} u_m(p) \\ & + (\omega + \lambda - a_1) \frac{q^{-1}}{(q^{-1}+\lambda)(q^{-1}+\omega)} y(p) \\ & + (\omega \times \lambda - a_2) \frac{1}{(q^{-1}+\lambda)(q^{-1}+\omega)} y(p) \Bigg) \end{aligned}$$

$$\begin{aligned} = h(q)\Bigg(& \frac{b_1 q^{-1} + b_3}{(q^{-1}+\lambda)(q^{-1}+\omega)} u_z(p) + \frac{b_2 q^{-1} + b_4}{(q^{-1}+\lambda)(q^{-1}+\omega)} u_m(p) \\ & + \frac{(\omega + \lambda) q^{-1} - a_1 + (\omega \times \lambda) - a_2}{(q^{-1}+\lambda)(q^{-1}+\omega)} y(p) \Bigg) \end{aligned}$$

Eq. (3.12)

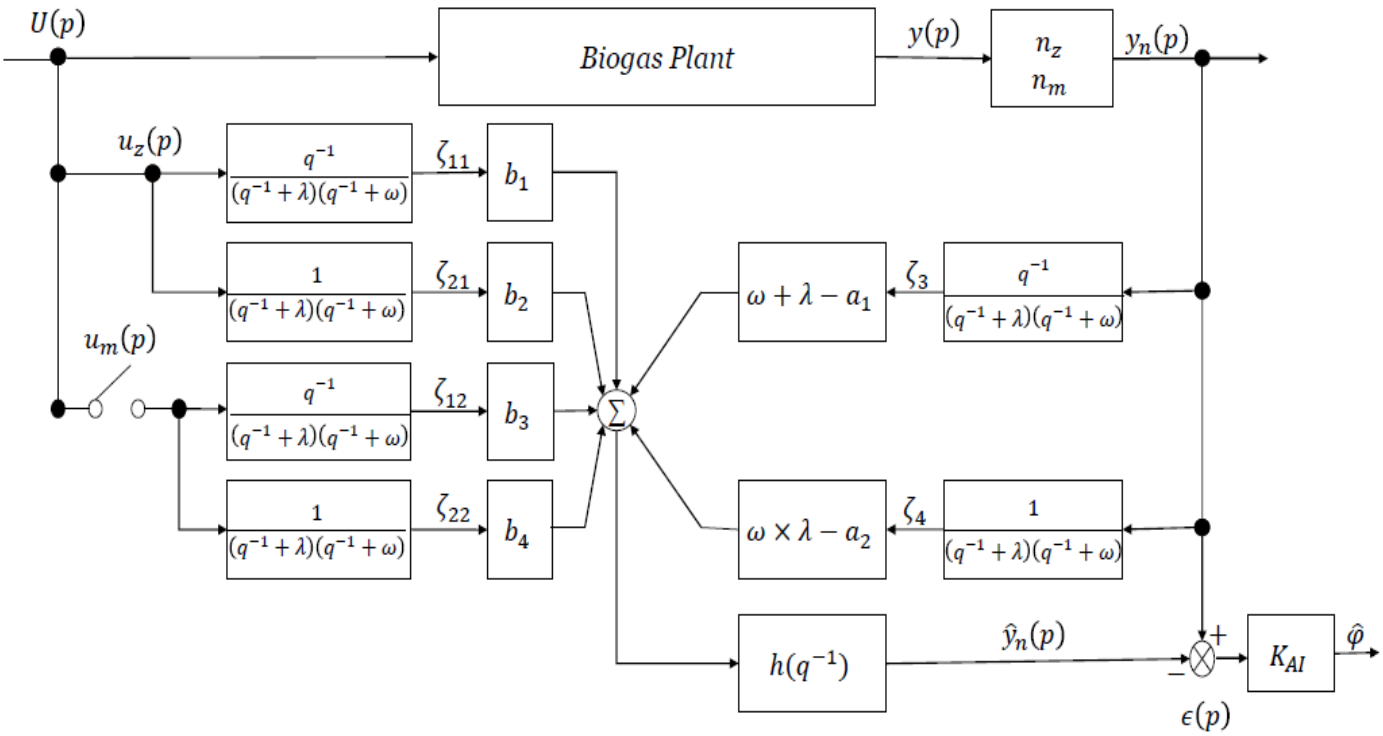

Figure 3.3. Adaptive identifier. $U(p)$ is the feedstock input (kg/(m^3 h)), $u_z(p)$ is the bacterial input (kg/(m^3 h)), $u_m(p)$ is the substrate input (kg/(m^3 h)), $y(p)$ is the biogas flow rate (m^3/h), $y_n(p)$ is the scaled biogas flow rate (L/h), $\zeta_{11}, \zeta_{12}, \zeta_{21}, \zeta_{22}, \zeta_3,$ and ζ_4 are control signals, a_1, a_2 and b_1, b_2, b_3, b_4 are parameters, $h(q^{-1})$ is the filter, n_z is a scaling coefficient related to the bacterial output, n_m is a scaling coefficient related to the substrate output, λ and ω are control system design constants, $\hat{y}_n(p)$ is the predicted scaled biogas flow rate (kg/(m^3 h)), $\epsilon(p)$ is the error (m^3/h), K_{AI} is the coefficient for the least-squares method, and $\hat{\varphi}$ is an estimated parameter.

The parameters used in Eq. (3.10) were integrated into φ using Eq. (3.11). If the matrix element values were obtained as described above, the amount of biogas generated could be predicted using Eq. (3.10) The difference between the measured output value and the value calculated using the estimated parameters was defined as the output error $\epsilon(p)$ and calculated using Eq. (3.13).

$$\epsilon(p) = y(p) - h(q)\varphi^T\psi(p)$$

Eq (3.13)

The recursive least-squares algorithm was applied to Eq. (3.13) with m datasets representing inputs and outputs assuming that the estimated parameters with minimized errors were valid. The least-squares estimates of the parameters were obtained using Eq. (3.14),

$$\hat{\varphi}_m = (\psi_m \psi_m^T)^{-1} \psi_m Y_m^T$$

where

$$Y_m = [y(1) \;\; y(2) \;\cdots\;\; y(m)]^T$$

and

$$\psi_m = [\psi(1) \;\; \psi(2) \;\cdots\;\; \psi(m)]^T. \qquad \text{Eq. (3.14)}$$

The parameters b_1, b_2, b_3, b_4, a_1 and a_2 were determined using the recursive least-squares algorithm, then the roots and coefficients of Eq. (3.10) for the system was estimated using the stepwise function shown in Eq. (3.15).

$$y(t) = \begin{cases} \left(Kz_1 e^{(\alpha(t-\tau))} + Kz_2 e^{(\beta(t-\tau))}\right)u_z + \left(Km_1 e^{(\alpha(t-\tau))} + Km_2 e^{(\beta(t-\tau))}\right)u_m, & if \;\; a_1^2 - 4a_2 > 0 \\ \left((Kz_1 + Kz_2)e^{(\alpha(t-\tau))}\right)u_z + \left((Km_1 + Km_2)e^{(\alpha(t-\tau))}\right)u_m, & if \; a_1^2 - 4a_2 = 0, \\ \left(Kz_1 e^{(-\alpha(t-\tau))} cos\big(\omega(t-\tau)\big) + Kz_2 e^{(-\beta(t-\tau))} sin\big(\omega(t-\tau)\big)\right)u_z + \cdots \\ \left(Km_1 e^{(-\alpha(t-\tau))} cos\big(\omega(t-\tau)\big) + Km_2 e^{(-\beta(t-\tau))} sin\big(\omega(t-\tau)\big)\right)u_m, & if \; a_1^2 - 4a_2 < 0 \end{cases}$$

Eq. (3.15)

For Eq. (3.15), if the discriminant function is $a_1^2 - 4a_2 > 0$, the α, β, Kz_1, and Kz_2 values can be calculated using the equations.

$$\alpha = \left(\frac{-a_1+\sqrt{a_1^2-4a_2}}{2}\right),\ \beta = \left(\frac{-a_1-\sqrt{a_1^2-4a_2}}{2}\right),\ Kz_1 = \left(\frac{b_1\alpha+b_2}{\alpha-\beta}\right),\ Kz_2 = \left(\frac{b_1\beta+b_2}{\beta-\alpha}\right),$$

$Km_1 = \left(\frac{b_3\alpha+b_4}{\alpha-\beta}\right)$, and $Km_2 = \left(\frac{b_3\beta+b_4}{\beta-\alpha}\right)$,

and if the discriminant function is $a_1^2 - 4a_2 < 0$, the α, ω, Kz_1, and Kz_2 values can be calculated using the equations

$\alpha = \frac{a_1}{2}$, $\omega = \sqrt{\frac{-a_1^2}{4} + a_2}$, $Kz_1 = b_1$, $Kz_2 = b_2$, $Km_1 = b_3$, and $Km_2 = \frac{-\alpha b_3+b_4}{\alpha}$,

where τ is a time constant, α, β are the roots of the function and Kz_1, Kz_2, Km_1, and Km_2 are coefficients related to the bacteria and substrate concentrations, Therefore, the bacterial and substrate solutions for the AD system were deduced, from Eq. (3.15), to be Eqs. (3.16) and (3.17), respectively.

$$y_{z-model} = \left(Kz_1 e^{(\alpha(t-\tau))} + Kz_2 e^{(\beta(t-\tau)}\right)u_z \qquad \text{Eq. (3.16)}$$

$$y_{m-model} = \left(Km_1 e^{(\alpha(t-\tau))} + Km_2 e^{(\beta(t-\tau))}\right)u_m \qquad \text{Eq. (3.17)}$$

In Eqs. (3.16) and (3.17), $y_{z-model}$ and $y_{m-model}$ are the amounts of biogas generated calculated from the bacterial and substrate concentrations, respectively.

The goodness-of-fit index (GFI) shown in Eq. (3.18) (Yoshida et al., 2020) was used to quantify the accuracy of the model predictions using the estimated parameters.

$$GFI\ [\%] = 100\left(1 - \frac{y(p) - \hat{y}(p)}{y(p) - mean(y)}\right) \quad \text{Eq. (3.18)}$$

The adaptive identifier included a switch relating to substrate inputs because the AD process had two inputs and one output. This allowed all the parameters to be estimated with or without substrate input data. The filter $h(q^{-1})$, scaling coefficients n_z and n_m, and control system design constants λ and ω were tuned to give the desired estimates.

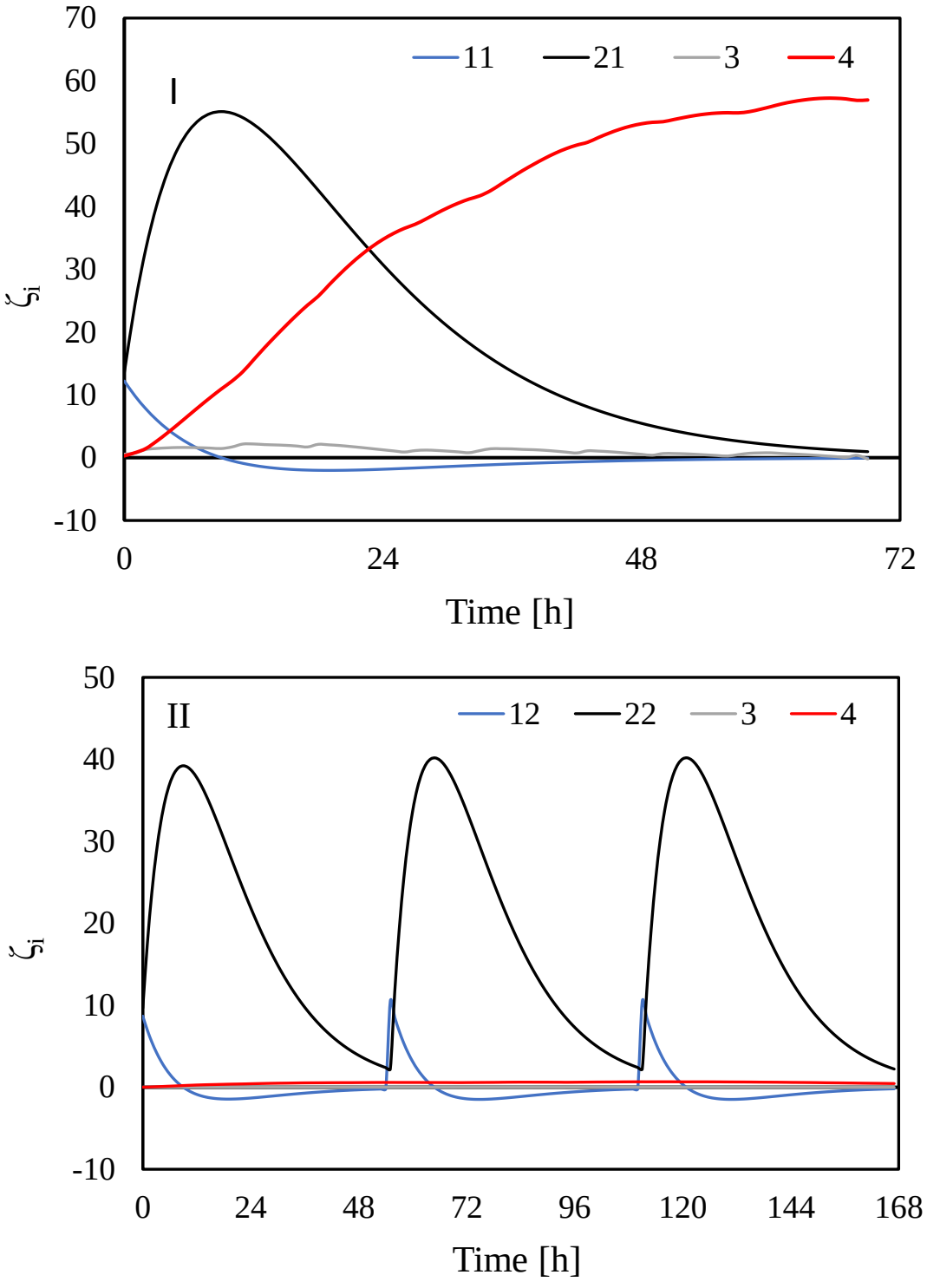

Figure 3.4: Control signals related to bacteria and substrate inputs **(I)** and outputs **(II).** ζ_i is the control signal and the numbers in the figure legends are the subscript i values for the control signals.

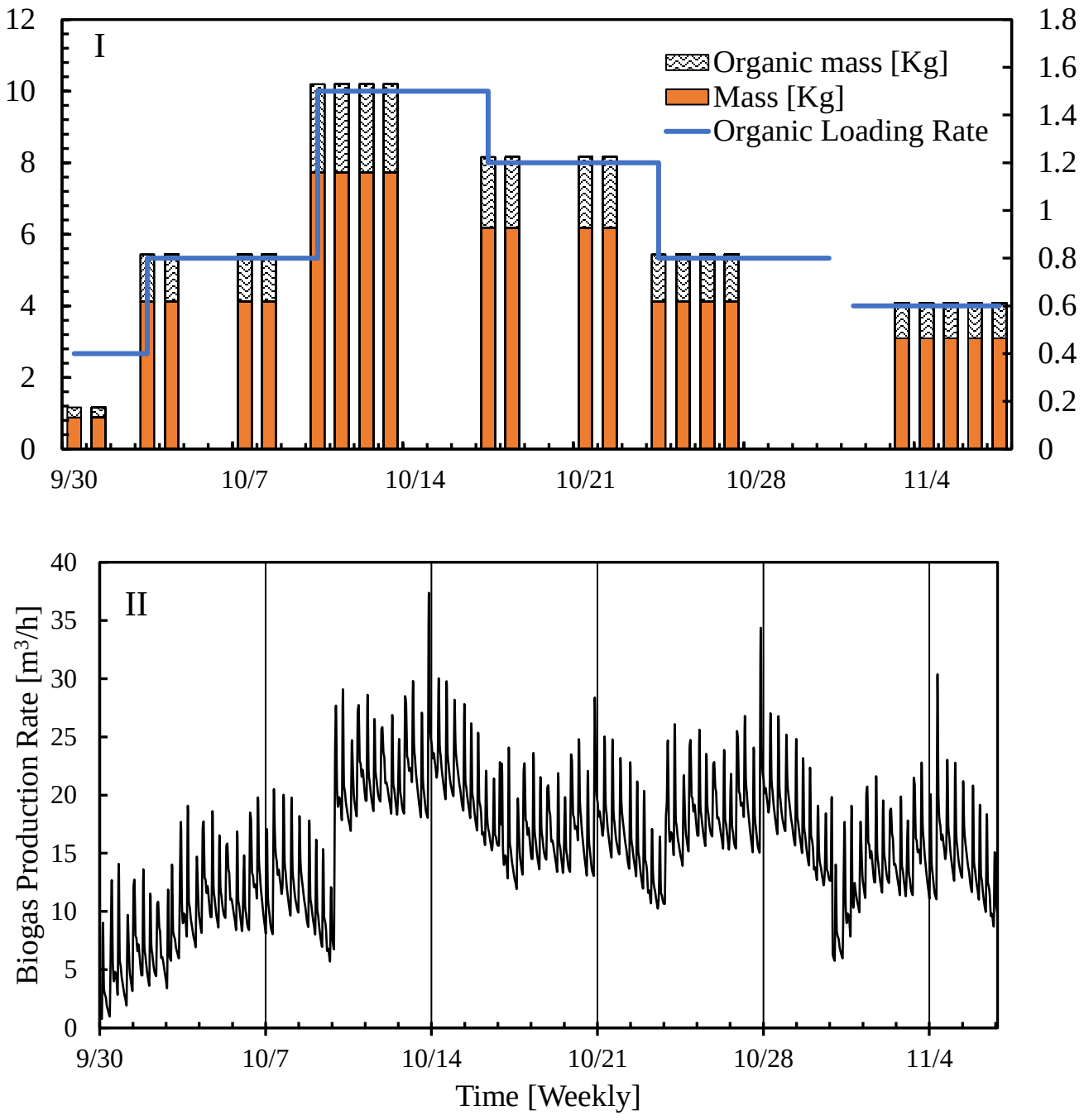

Figure 3.5: Experimental data used to construct the model and perform a simulation for the feedstocks **(I)** and for biogas generation **(II)**

Table 3.1: Tuned constants for the adaptive identifier

$h(q^{-1})$	n_z	n_m	λ	ω
1	0.025	0.0004	0.35	0.25

$h(q^{-1})$ is the filter, n_z and n_m are scaling coefficients related to the bacteria and substrate outputs, respectively, λ and ω are control system design constants.

3.4 Simulation Data

The substrate concentration was determined from the loss of mass when the feedstock was heated to 105 °C for 24 h and then 600 °C for 3 h. Biogas production was determined hourly using a wet gas meter (W-NKDa-0.5B; SHINAGAWA) and recorded using a data logger (Data mini LR 5000; HIOKI). The data used in the simulation were experimental data collected in the laboratory in 2018 (Figure 3.5). Bacterial input at 0 h was defined as the amount of substrate in the digestate at the beginning of the process(Shimizu & Yoshida, 2021). Feedstock input was determined at 0, 52, and 104 h. Data for 3 d (i.e., 72 h) from 30 September 2018 when no feedstock was added and for 7 d (i.e., 168 h) from 07 October 2018 when feedstock was added were used to estimate the parameters when developing the model.

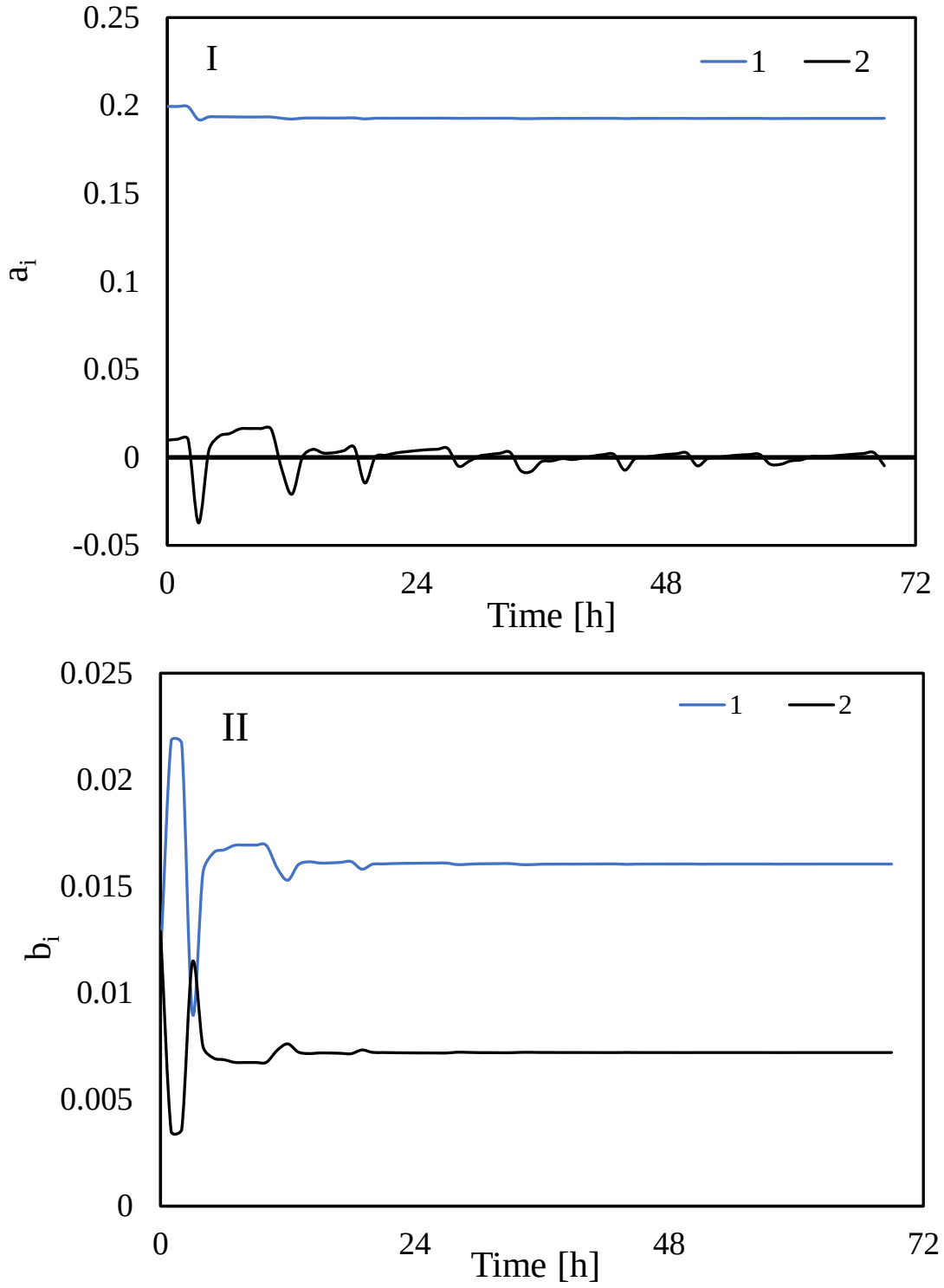

Figure 3.6: Estimated parameters related to bacterial input for the output side **(I)** and the input side **(II)** of Eq. (3.10). The numbers in the legend are the subscript i values. a_i is a parameter on the output side of Eq. (3.10) and b_i is a parameter on the input side of Eq. (3.10).

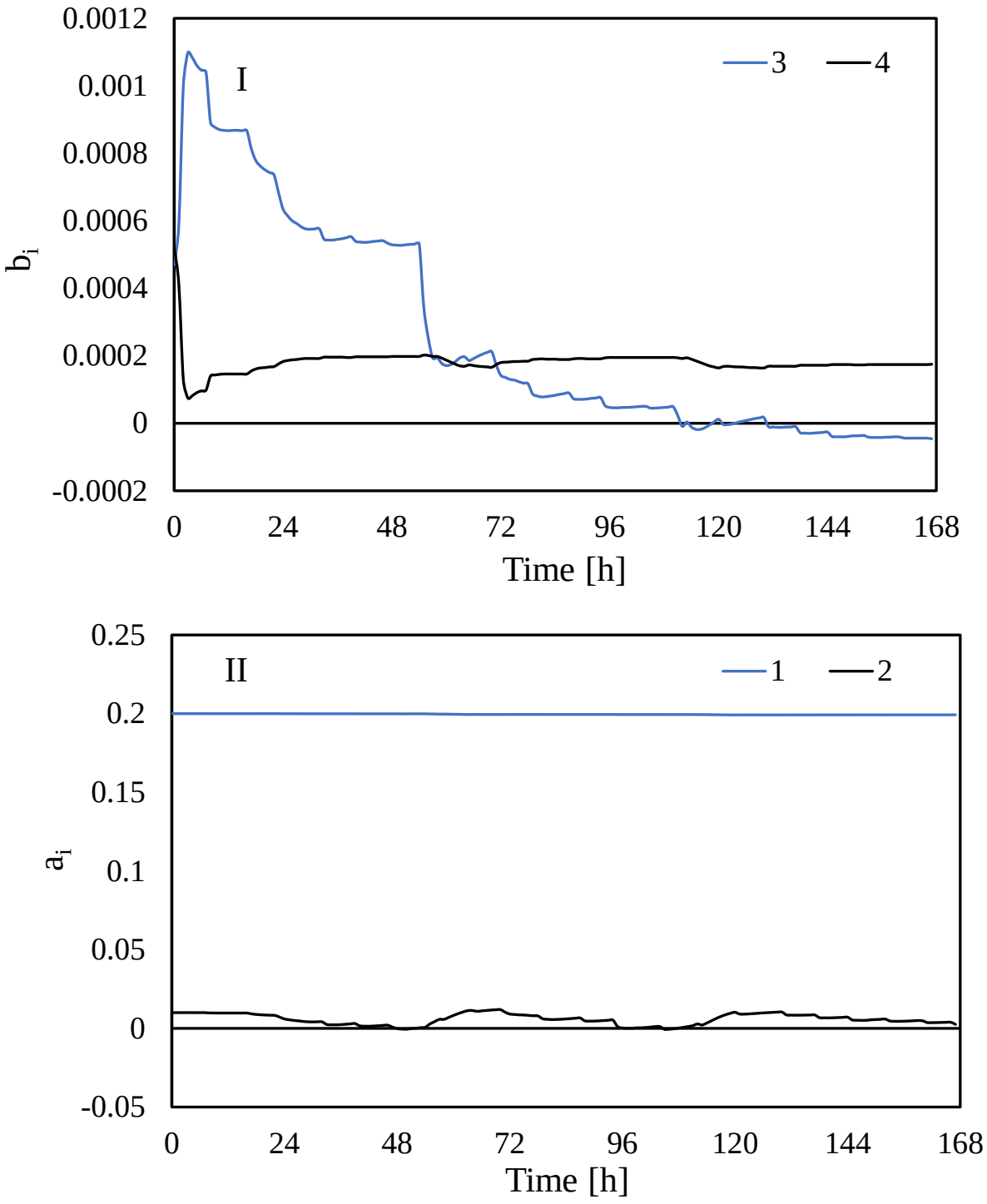

Figure 3.7: Estimated parameters relating to substrate input for the output side (**I**) and the input side (**II**) of Eq. (3.10). The numbers in the figure legend are the subscript i values. a_i is a parameter on the output side of Eq. (3.10) and b_i is a parameter on the input side of Eq. (3.10).

Data for 7 d (i.e., 168 h) from 21 October 2018 were used to validate the model. The organic loading rates for the model construction period and the model validation period were different, at 1.47 and 1.24 (kg- volatile solid)/ ((m^3 digester) d), respectively.

3.5 Results and discussion

The tuning constants for the control system when the adaptive identifier was used to generate the control signals (which are shown in Figure 3.4) are shown in Table 3.1. The bacterial and substrate inputs appeared as several pulse-wave signals because the AD flow used a semi-continuous system. As shown in Figure 3.5, the pulse-wave input signals were converted into a control signal that changed continually according to the input.

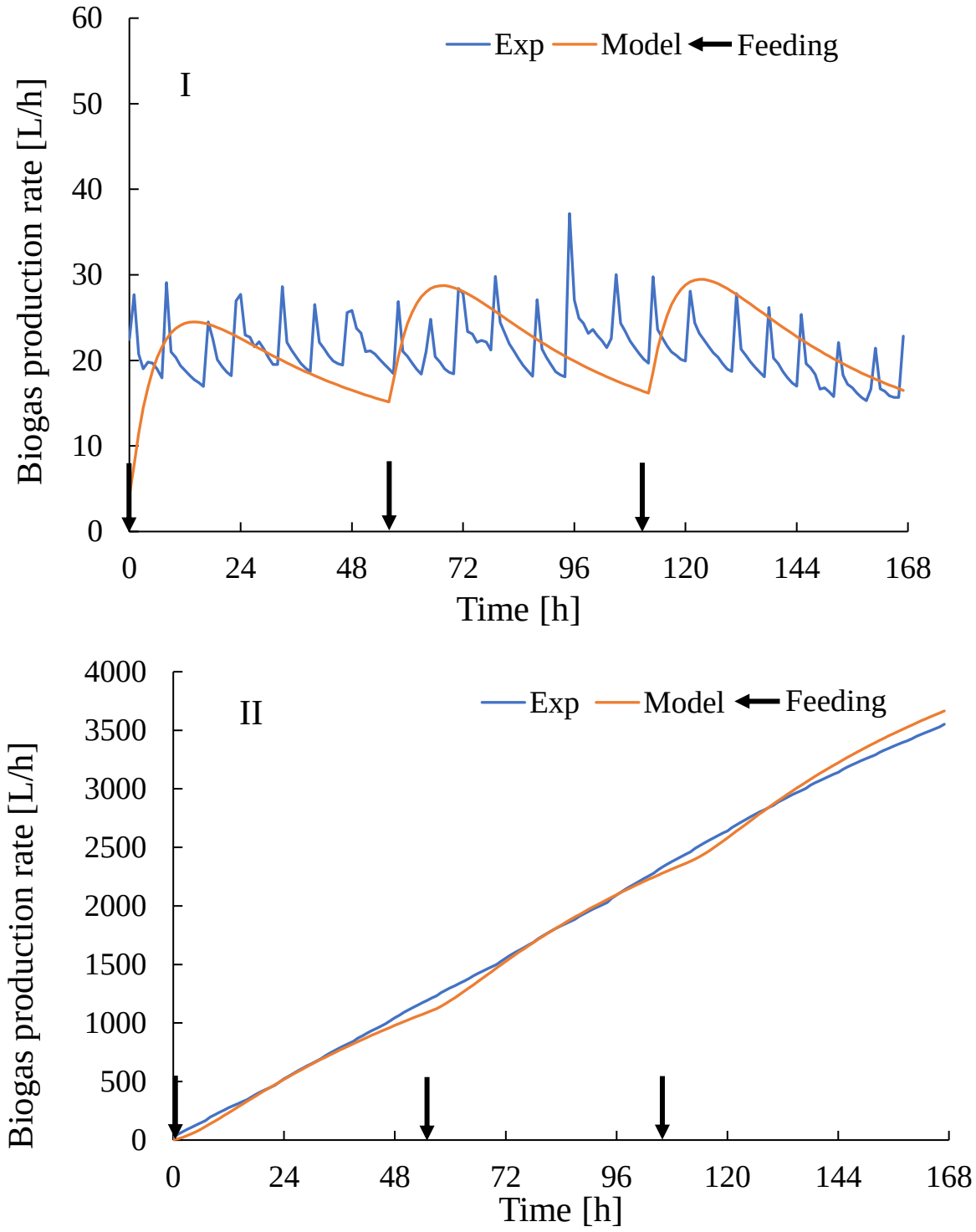

Figure 3.8: Data used to construct the model related to substrate models **(I)** and **(II)** for cumulative biogas generation determined using Eq. (3.17)

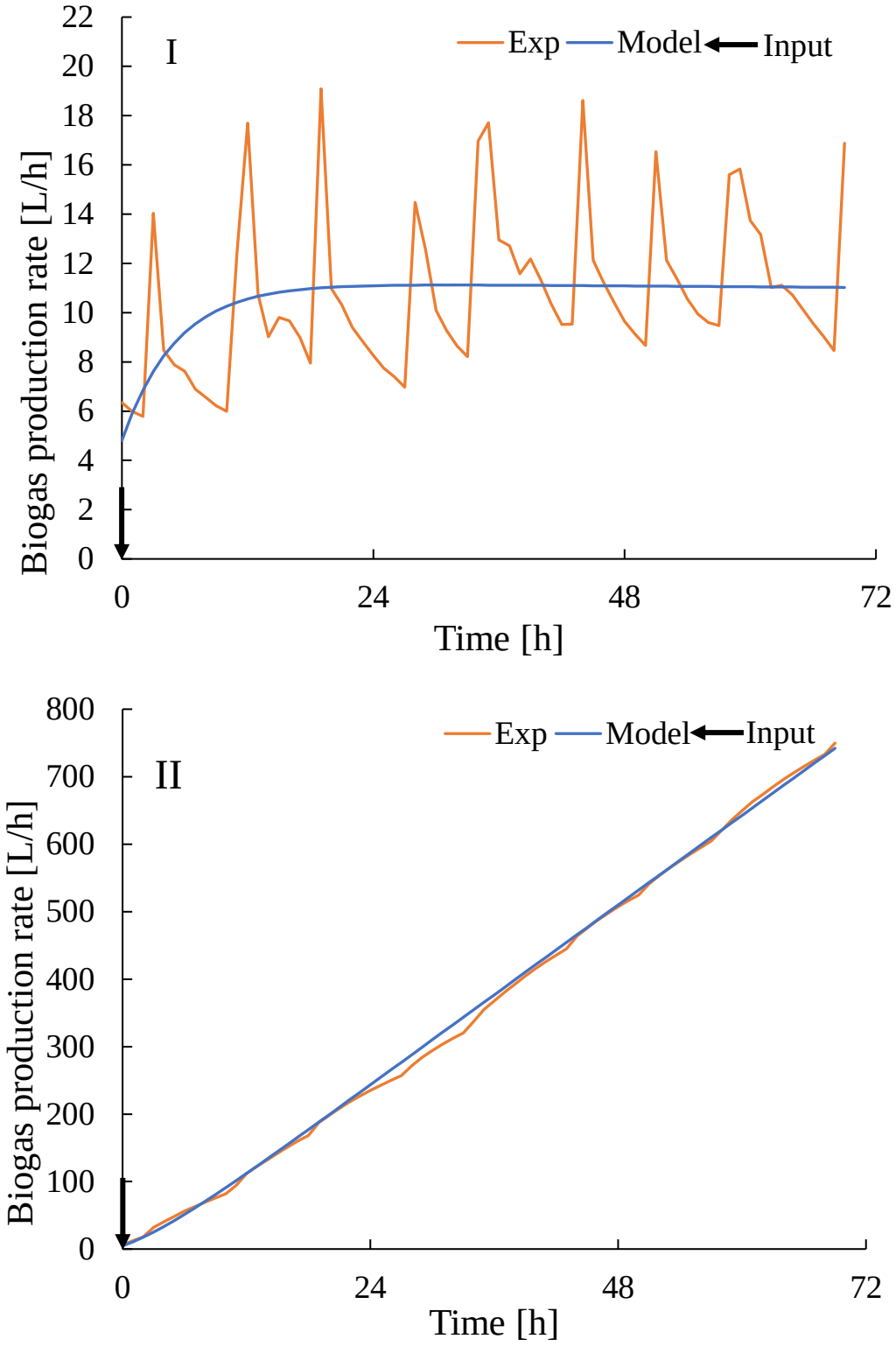

Figure 3.9: Data used to construct the model related to bacterial models **(I)** and **(II)** for cumulative biogas generation determined using Eq. (3.16)

The parameters estimated using data collected when feedstock had not been added are shown in Figure 3.6. The estimated parameters were very variable at first but slowly stabilized as the amount of data acquired increased and became stable at ~20 h (Yoshida et al., 2020). This indicates that data need to be collected for at least 20 h to estimate the parameters related to bacterial input. The parameters estimated from data collected when feedstock had been added (i.e., for identification of adaptation caused by 'turning on the switch' by adding substrate) are shown in Figure 3.7. The parameter estimates varied greatly at the beginning of the experiment but became stable at 140 h. Therefore, data needed to be collected for at least 140 h to estimate the parameters related to substrate input. This was slightly different from the time found by (Yoshida et al., 2020) after assessing the composition of the substrates in a bioreactor. Biogas generation predictions made using a model constructed with the estimated parameters for the substrate and bacteria are shown in Figures 3.8 and 3.9 made using models (I) and (II) cumulative biogas generation. The bacteria and substrate models did not effectively predict the amount of biogas inside the bioreactor because of the disturbance caused by agitation (stirring) and inhibition likely to slow down degradation of the substrate while the cumulative biogas generation by the models revealed high prediction accuracy. The results of the validation tests performed using different data to the data used to construct the model are shown in Figure 3.10. This was carried out to confirm the accuracy of the prediction model.

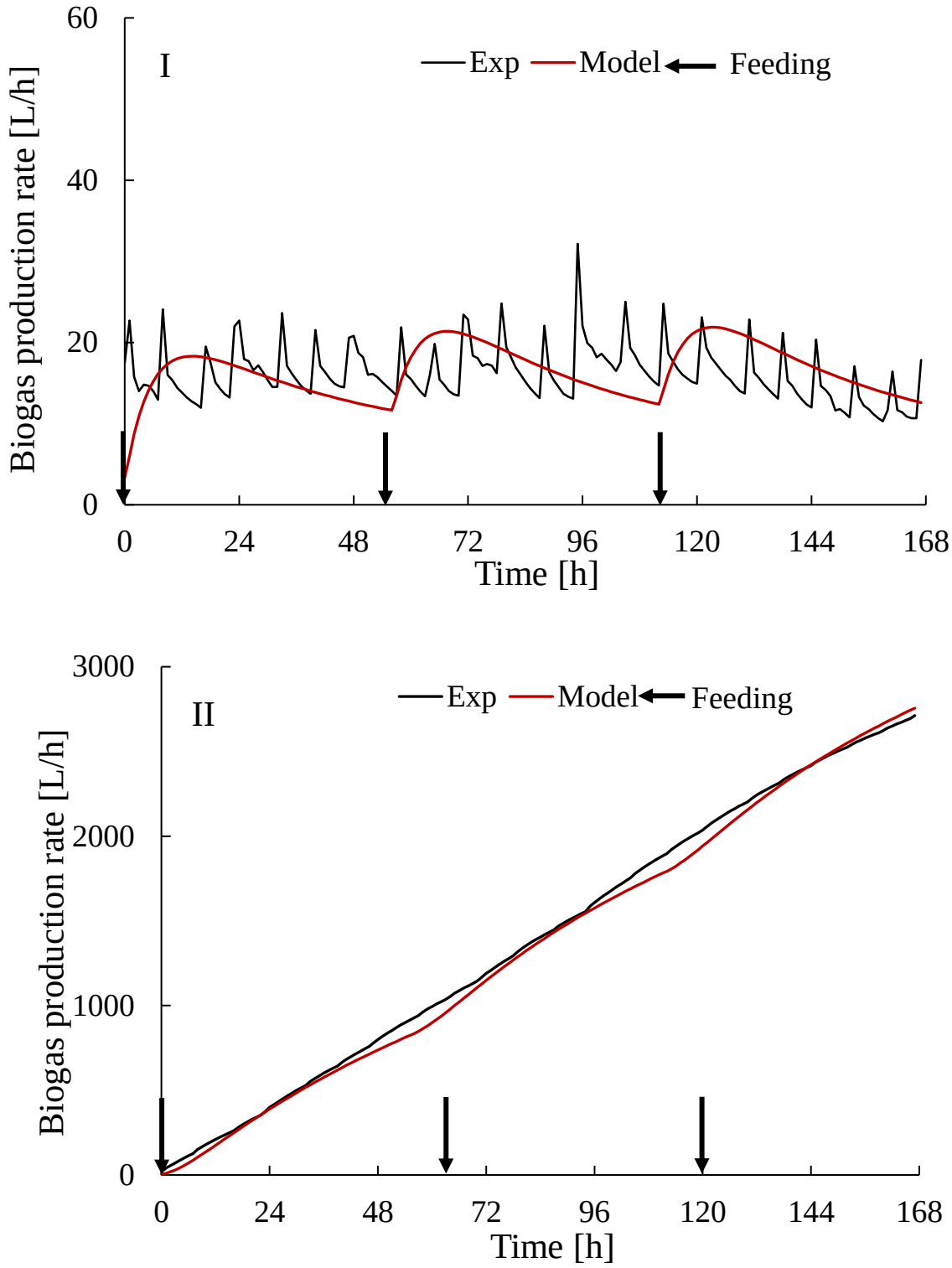

Figure 3.10: Amount of gas generated by anaerobic digestion predicted using models (**I**) and Cumulative (**II**) from data acquired from 14 October 2018 to 21 October 2018 using Eq. (3.15)

The initial bacteria concentrations for the period in which the data used to construct the model were acquired (30 September 2018 to 7 October 2018) and for the period in which the data used to validate the model were acquired (14 October 2018 to 21 October 2018) were different. The initial bacteria concentration for 30 September 2018 to 7 October 2018 was 28 kg/m^3 and the initial bacteria concentration for 14 October 2018 to 21 October 2018 was 25 kg/m^3. The amount of biogas generated predicted using the validation data had a low GFI (−81.91%) because degassing (caused by agitation) and heating strongly affected the hourly data. Cumulative biogas generation data are shown in Figure 3.10. This indicated that the predictions were good. The GFI for the dataset was 97.45%. The simulation results acquired using Eq. (3.12) are shown in Figure 3.11. The model correctly reproduced the dynamics of the system for the test periods, although there was some variability. At the beginning of the test period the amount of biogas generated was underestimated by the model because of destabilization, but the amount of biogas generated stabilized over time and the predictions became good. The GFI for the cumulative amount of biogas generated per day is shown in Figure 3.12. The predicted amount was >80% of the actual amount even at the lowest value except on day 4 of period 3, which started on 14 October 2018. This indicated that the parameter estimation system and model developed in this study gave very accurate predictions for periods of 1 d or more. The parameter estimation system and model could therefore be used to predict biogas generation during AD under various operating conditions. For a real plant it would, however, be necessary to continually consider variations in operating conditions such as the feedstock composition. This could be overcome by introducing an oblivion factor to limit input data for the parameter estimation system to, for example, only the last 72 h. Estimated parameters would therefore be adaptively controlled in response to changes in the operating conditions to allow the amount of biogas produced to be predicted accurately.

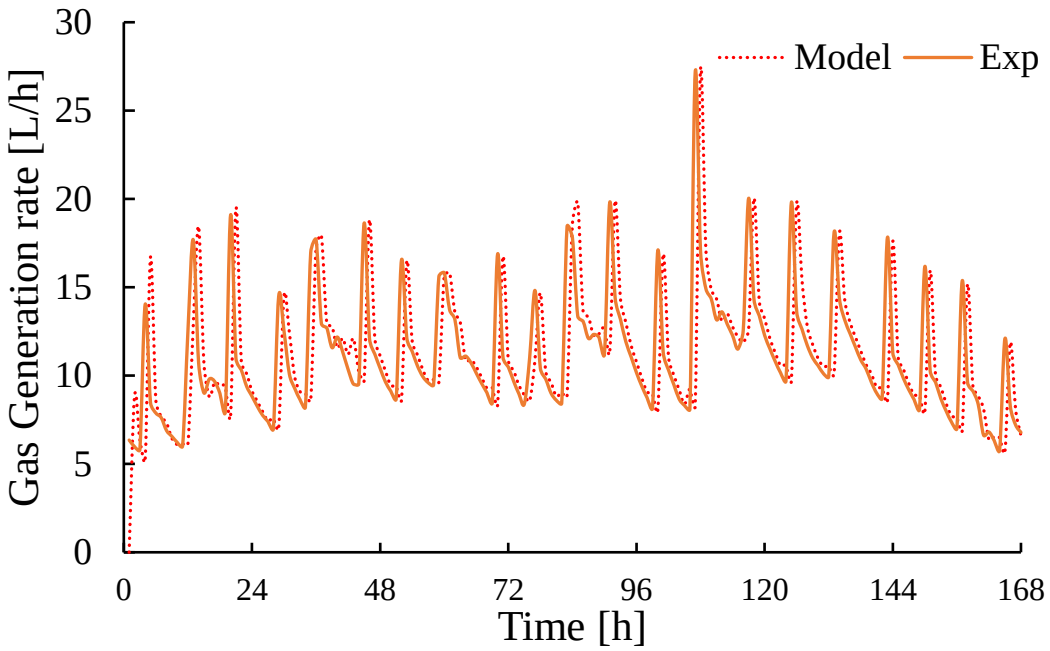

Figure 3.11: Experimental data and data predicted using Eq. (3.12) plotted against time

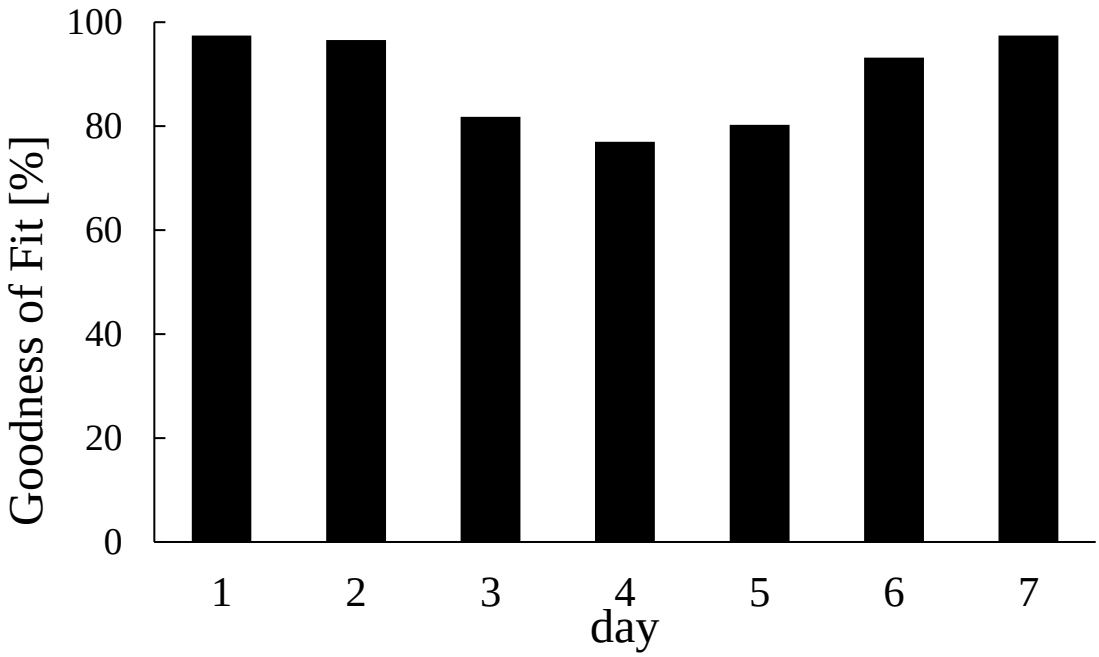

Figure 3.12: Goodness-of-fit values for the cumulative amount of biogas generated for each day in a 7 d period from 21 October 2018

3.6 Conclusions

The aim of this study was to develop an adaptive identifier system of anaerobic digestion process for sustainable biogas production to allow renewable energy supplies to be stabilized. A model and parameter estimation system were established for AD processes with various operating conditions. The adaptive identifier control system automatically estimates parameters from input and output data. Using the adaptive identifier indicated that data for at least 20 and 140 h were required to estimate stable parameters related to bacterial and substrate inputs, respectively. The model and estimated parameters made accurate predictions. Future work should be focused on constructing sustainable biogas production systems integrating predictive model biogas generation control. Such systems would allow renewable energy to be stabilized.

CHAPTER 4

4. General Discussion.

Corn stover hydrochar produced in HTC can be used as a substitution of coal. Here, pulverized coal was compared to hydrochar as a reference fuel. The hydrochar of close physicochemical properties of reference coal was considered as a useable hydrochar in this research.

The corn stover hydrochar carbon content increased and oxygen content decreased with increase in both HT temperature (215.9 ^{o}C and 300 ^{o}C) and residential time (45 min and 77 min) except for 350 ^{o}C and 384.09 ^{o}C and residential time (60 min and 45 min) hydrothermal process. In this process carbon content started to decrease and oxygen content started to increase compared to the hydrothermal process of 350 ^{o}C for 77 min. Here it can be noticed that cellulose is converted into glucose, the media became acidic, and a portion of glucose is further converted into HMF. Then for increasing temperature at 350 ^{o}C, HMF is rehydrated to produce levulinic acid and formic acid. On the other hand, the hydrothermal process water pH was decreased, and it worked as an acid catalyst to reduce the gasification temperature. This was another probable reason to reduce carbon content of hydrochar of 350 ^{o}C for 77 min residence time. The decomposed lignin monomers might have some bonding with alkali matter which produced ash.

Mass yield and energy yield of corn stover hydrochar samples were reduced for increase in both hydrothermal temperature and residential time. Similar result was found by Paul et al. (2018). A minor variation of mass yield and energy yield between residence times from 60 min to 30 min at 250 ^{o}C was observed; but this variation was increased for increase in hydrothermal process temperature. The mass yield at 250 ^{o}C in 30 min was 19.61 % and in 60 min it was 19.24 %.

The HHV increased as the temperature and residential time both increases, but it was observed more pronounced in temperature. The HHV of hydrochar produced at 250 ^{o}C for 60 min and 30

min residence time were 23.08 MJ/kg and 19.82 MJ/kg, respectively. But the HHV of hydrochar at 350 ^{o}C for 60 min and 30 min residence time were 21.95 MJ/kg and 18.01 MJ/kg, respectively. From Table 2.5, it can be observed that at 300 ^{o}C for 45 min residence time, produced hydrochar had HHV of 23.70 MJ/kg which is high when compared with hydrochar produced at 350 ^{o}C (21.95 – 18.01 MJ/kg).

Lignocellulose biomass in hydrothermal carbonization process reaction rate is exponentially proportional to its process temperature but directly proportional to the residence time. For this reason, hydrothermal process temperature is more important than its residence time. On the other hand, in subcritical stage water's physicochemical properties are significantly affected by reaction temperature (Kruse et al., 2013). Lignin portion of lignocellulose biomass contains the highest HHV among its three components such as lignin, cellulose, and hemicellulose. Lignin has 23.3 to 26.6 MJ/kg HHV whereas cellulose and hemicellulose have 17.6 to 17.9 MJ/kg HHV. Hence, for the thermal stability of lignocellulose biomass components from most to least, the order is Lignin > Cellulose > Hemicellulose. Hemicellulose is degraded at 180 ^{o}C to 200 ^{o}C and cellulose is degraded at 200 ^{o}C to 220 ^{o}C and both are called polysaccharide (hemicellulose and cellulose). In the hydrothermal carbonization process, the polysaccharide portion of biomass is degraded into the water-soluble organics at the maximum amounts at 45 min residence time within the maximum temperature of 300 ^{o}C and above this temperature it is further degraded into HMF and other organic acids such as levulinic acid and formic acid (Weingarten et al., 2012).

The main aim of producing hydrochar in hydrothermal carbonization process is to use it as the substitute of coal, especially the pulverized coal or coal dust. As corn stover is a lignocellulosic biomass, which is completely broken down in plant cell and it is immediately converted into a lignite-like product named hydrochar . The HHV of pulverized coal (Australian subbituminous

coal) is 26.86 MJ/kg (Paul et al., 2018)and the coal (lignite- Anthracite) is 15 - 27 MJ/kg. Hence, hydrochar with the highest mass yield and closest HHV of the pulverized coal was criterion to choose the hydrothermal carbonization process conditions.

HPLC-RI analysis indicated that the major components of the liquid fraction were acetic acid, glycolic acid, and ethanol. The highest concentrations of acetic acid, glycolic acid and ethanol were achieved with a processing temperature of 250 or 350 °C, a constant biomass/water ratio of 0.14 and a residence time of 60 min. The acetic acid concentration increased with higher processing temperatures, while the glycolic acid concentration increased with longer residence times, likely because of the oxidation of glycoladehyde. Hemicellulose and cellulose are hydrolyzed into monosaccharides via the hydrothermal process(Abdullah et al., 2014). These monosaccharides are unstable, and some of them are converted into other products such glycoladehyde, furfural and acetaldehyde, which in turn are converted to acetic acid (at high temperatures) and glycolic acid (at a longer residence time).

Gas yields from the HTC of corn stover was analyzed by Gas chromatography, As the processing temperature was increased from subcritical water conditions to supercritical water conditions (215.91–384.09 °C), H_2 yield increased from 0.02 *v/v*% to 0.25 *v/v*%. The highest concentrations of CH_4 (0.135 *v/v*%) and CO_2 (3.5 *v/v*%) were also obtained with a processing temperature of 384.09 °C, residence time of 45 min and biomass/water ratio of 0.115, while the yield of CO yields was maximized at 250 °C, 60 min and 0.14 (0.085 *v/v*%). This is a result of CO reacting with water vapor in the water–gas shift reaction to liberate CO_2 and H_2 (Kruse, 2008). The water–gas shift reactions are favorable at high temperatures, mainly in supercritical water, and contribute to major yields of H_2 and CO_2(Reddy et al., 2014).

The amount of biogas generated predicted using the validation data had a low GFI (−81.91%) because degassing (caused by agitation) and heating strongly affected the hourly data. Cumulative biogas generation data are shown in Figure 3.10. This indicated that the predictions were good. The GFI for the dataset was 97.45%. The simulation results acquired using the adaptive identifier model are shown in Figure 3.11. The model correctly reproduced the dynamics of the system for the test periods, although there was some variability. At the beginning of the test period the amount of biogas generated was underestimated by the model because of destabilization, but the amount of biogas generated stabilized over time and the predictions became good. The GFI for the cumulative amount of biogas generated per day is shown in Figure 3.12. The predicted amount was >80% of the actual amount even at the lowest value except on day 4 of period 3. This indicated that the parameter estimation system and model developed in this study gave very accurate predictions for periods of 1 d or more. The parameter estimation system and model could therefore be used to predict biogas generation during AD under various operating conditions.

CHAPTER 5

5. General Conclusion and Recommendation

Chemical components of corn stover hydrochar and hydrothermal process water varies with its process temperature and residence time.

Useable corn stover hydrochar were produced at all processing temperature and residence time in this study because their HHV were comparable with coal except corn stover hydrochar produced at processing temperature of 215.9 ^{o}C and residence time 45 min. Energy yield of corn stover hydrochar produced at 215.9 ^{o}C for 45 min was the highest (16.16 MJ/kg of raw dry corn stover) among the whole processes. It is recommended that freshly harvested corn stover from the field should be used to produces hydrochar.

Anaerobic digestion of corn stover hydrochar produced at processing temperature of 215.9 ^{o}C and residence time of 45 min, is a better feed stock of biogas production but it is recommended that inhibitory chemicals such as phenolic compound and furfural should be below the inhibition limit. From my preliminary investigation among three selected residence times (30, 45 and 60 min) for a given temperatures of 215.9 ^{o}C, 300 ^{o}C and 350 ^{o}C respectively, 30 min residence time was the lowest producer of these two inhibitory chemicals. These two inhibitory chemicals were produced low amount at 215.9 ^{o}C for 30 min hydrothermal condition and the hydrochar produced at same condition was not considered as a useable energy source (substitution of coal). The biogas that was produced at the three selected condition were 300 ^{o}C for 60 min (377 L/kg Vs), 350 ^{o}C for 45 min (362 L/kg Vs) and 215.9 ^{o}C for 30 min (447 L/kg Vs). Thus, corn stover hydrochar produced at low temperature resulted in an increased in biogas production due to increased hydrolysis of the hemicellulose fraction of the corn stover while the HTC of the corn stover produced at high

temperature led to inhibition and thus limit the amount of biogas production due to the production of phenol and furfural which are known to be methanogenesis inhibitors.

The corn stover hydrochar AD digestate would be nutrient enriched liquid fertilizer available to apply into the maize field. It could improve about one third of corn stover containing nitrogen and other nutrients.

The possibility of more nutrient's retrieval will reduce the chemical fertilizer use in maize field, which will improve maximum resources and reduce greenhouse gas emission. It is also noticeable that the liquid hydrothermal process uses water at the subcritical phase. Therefore, the pressure inside reactor stays at a very high level. For commercial application of this operation, it is recommended that the high-pressure hydrothermal equipment with proper safety should be considered. The facility of producing sustainable bioenergy system and biofertilizer should also be available near the maize field.

The adaptive identifier control system automatically estimates parameters from input and output data. Using the adaptive identifier indicated that data for at least 20 and 140 h were required to estimate stable parameters related to bacterial and substrate inputs, respectively. it is recommended that Kalman filter algorithm should be employed in parameter estimation of bacteria and substrate concentration for optimum production of biogas.

Reference

Abdullah, R., Ueda, K., & Saka, S. (2014). Hydrothermal decomposition of various crystalline celluloses as treated by semi-flow hot-compressed water. *Journal of Wood Science 2014 60:4*, *60*(4), 278–286. https://doi.org/10.1007/S10086-014-1401-7

A. Cantero, D., Celia Martínez, D. Bermejo, M., & J. Cocero, M. (2014). Simultaneous and selective recovery of cellulose and hemicellulose fractions from wheat bran by supercritical water hydrolysis. *Green Chemistry*, *17*(1), 610–618. https://doi.org/10.1039/C4GC01359J

Ahring, B. K., Biswas, R., Ahamed, A., Teller, P. J., & Uellendahl, H. (2015). Making lignin accessible for anaerobic digestion by wet-explosion pretreatment. *Bioresource Technology*, *175*, 182–188. https://doi.org/10.1016/J.BIORTECH.2014.10.082

Akhtar, J., & Amin, N. A. S. (2011). A review on process conditions for optimum bio-oil yield in hydrothermal liquefaction of biomass. *Renewable and Sustainable Energy Reviews*, *15*(3), 1615–1624. https://doi.org/10.1016/J.RSER.2010.11.054

Anca-Couce, A. (2016). Reaction mechanisms and multi-scale modelling of lignocellulosic biomass pyrolysis. *Progress in Energy and Combustion Science*, *53*, 41–79. https://doi.org/10.1016/J.PECS.2015.10.002

Arzate, J. A., Kirstein, M., Ertem, F. C., Kielhorn, E., Ramirez Malule, H., Neubauer, P., Cruz-Bournazou, M. N., & Junne, S. (2017). Anaerobic Digestion Model (AM2) for the Description of Biogas Processes at Dynamic Feedstock Loading Rates. *Chemie-Ingenieur-Technik*, *89*(5), 686–695. https://doi.org/10.1002/CITE.201600176

Athika Chuntanapum, Tau Len-Kelly Yong, †, Shigeru Miyake, and, & Matsumura*, Y. (2008). Behavior of 5-HMF in Subcritical and Supercritical Water. *Industrial and Engineering Chemistry Research*, *47*(9), 2956–2962. https://doi.org/10.1021/IE0715658

Bastin, G., & Dochain, D. (1990). *On-line estimation and adaptive control of bioreactors*. Elsevier.

Bernard, O., Hadj-Sadok, Z., Dochain, D., Genovesi, A., & Steyer, J.-P. (2001). Dynamical model development and parameter identification for an anaerobic wastewater treatment process. *Biotechnology and Bioengineering*, *75*(4), 424–438. https://doi.org/10.1002/BIT.10036

Blumensaat, F., & Keller, J. (2005). Modelling of two-stage anaerobic digestion using the IWA Anaerobic Digestion Model No. 1 (ADM1). *Water Research*, *39*(1), 171–183. https://doi.org/10.1016/j.watres.2004.07.024

Bonawitz, N. D., & Chapple, C. (2010). The Genetics of Lignin Biosynthesis: Connecting Genotype to Phenotype. *Http://Dx.Doi.Org/10.1146/Annurev-Genet-102209-163508*, *44*, 337–363. https://doi.org/10.1146/ANNUREV-GENET-102209-163508

Byrne, R. H., & Abdallah, C. T. (1995). Design of a Model Reference Adaptive Controller for Vehicle Road Following. In *Mathl. Comput. Modelling* (Vol. 22, Issue 7).

Cai, J., Li, B., Chen, C., Wang, J., Zhao, M., & Zhang, K. (2016). Hydrothermal carbonization of tobacco stalk for fuel application. *Bioresource Technology*, *220*, 305–311. https://doi.org/10.1016/J.BIORTECH.2016.08.098

Camillo Falco, Niki Baccile, & Maria-Magdalena Titirici. (2011). Morphological and structural differences between glucose , cellulose and lignocellulosic biomass derived hydrothermal carbons. *Green Chemistry*, *13*(11), 3273–3281. https://doi.org/10.1039/C1GC15742F

Chen, X. yan, Huang, Y. han, Zhao, Y., Mo, B., Mi, H. xing, & Huang, C. hua. (2017). Analytical method for determining rill detachment rate of purple soil as compared with that of loess soil. *Journal of Hydrology*, *549*, 236–243. https://doi.org/10.1016/J.JHYDROL.2017.03.065

Chew, J. J., & Doshi, V. (2011). Recent advances in biomass pretreatment – Torrefaction fundamentals and technology. *Renewable and Sustainable Energy Reviews*, *15*(8), 4212–4222. https://doi.org/10.1016/j.rser.2011.09.017

Codignole Luz, F., Volpe, M., Fiori, L., Manni, A., Cordiner, S., Mulone, V., & Rocco, V. (2018). Spent coffee enhanced biomethane potential via an integrated hydrothermal carbonization-anaerobic digestion process. *Bioresource Technology*, *256*, 102–109. https://doi.org/10.1016/j.biortech.2018.02.021

de Vlieger, D. J. M., Chakinala, A. G., Lefferts, L., Kersten, S. R. A., Seshan, K., & Brilman, D. W. F. (2012). Hydrogen from ethylene glycol by supercritical water reforming using noble and base metal catalysts. *Applied Catalysis B: Environmental*, *111–112*, 536–544. https://doi.org/10.1016/J.APCATB.2011.11.005

Deng, J., Li, M., & Wang, Y. (2016). Biomass-derived carbon: synthesis and applications in energy storage and conversion. *Green Chemistry*, *18*(18), 4824–4854. https://doi.org/10.1039/C6GC01172A

Ding, L., Cheng, J., Lin, R., Deng, C., Zhou, J., & Murphy, J. D. (2020). Improving biohydrogen and biomethane co-production via two-stage dark fermentation and anaerobic digestion of the pretreated seaweed Laminaria digitata. *Journal of Cleaner Production*, *251*, 119666. https://doi.org/10.1016/J.JCLEPRO.2019.119666

Ding, L., Cheng, J., Qiao, D., Yue, L., Li, Y. Y., Zhou, J., & Cen, K. (2017). Investigating hydrothermal pretreatment of food waste for two-stage fermentative hydrogen and methane co-production. *Bioresource Technology*, *241*, 491–499. https://doi.org/10.1016/J.BIORTECH.2017.05.114

Effendi, A., Gerhauser, H., & Bridgwater, A. v. (2008). Production of renewable phenolic resins by thermochemical conversion of biomass: A review. *Renewable and Sustainable Energy Reviews*, *12*(8), 2092–2116. https://doi.org/10.1016/J.RSER.2007.04.008

Elaigwu, S. E., & Greenway, G. M. (2016). Microwave-assisted and conventional hydrothermal carbonization of lignocellulosic waste material: Comparison of the chemical and structural properties of the hydrochars. *Journal of Analytical and Applied Pyrolysis*, *118*, 1–8. https://doi.org/10.1016/J.JAAP.2015.12.013

Erdogan, E., Atila, B., Mumme, J., Reza, M. T., Toptas, A., Elibol, M., & Yanik, J. (2015). Characterization of products from hydrothermal carbonization of orange pomace including anaerobic digestibility of process liquor. *Bioresource Technology*, *196*, 35–42. https://doi.org/10.1016/J.BIORTECH.2015.06.115

Erlach, B., Harder, B., & Tsatsaronis, G. (2012). Combined hydrothermal carbonization and gasification of biomass with carbon capture. *Energy*, *45*(1), 329–338. https://doi.org/10.1016/J.ENERGY.2012.01.057

Esen, M., & Yuksel, T. (2013). Experimental evaluation of using various renewable energy sources for heating a greenhouse. *Energy and Buildings*, *65*, 340–351. https://doi.org/10.1016/j.enbuild.2013.06.018

Fan, J., bruyn, M. de, Budarin, V. L., Gronnow, M. J., Shuttleworth, P. S., Breeden, S., Macquarrie, D. J., & Clark, J. H. (2013). Direct Microwave-Assisted Hydrothermal Depolymerization of Cellulose. *Journal of the American Chemical Society*, *135*(32), 12728–12731. https://doi.org/10.1021/JA4056273

Fang, Z., Sato, T., Smith, R. L., Inomata, H., Arai, K., & Kozinski, J. A. (2008). Reaction chemistry and phase behavior of lignin in high-temperature and supercritical water. *Bioresource Technology*, *99*(9), 3424–3430. https://doi.org/10.1016/J.BIORTECH.2007.08.008

Fengel, D. (1992). *Characterization of Cellulose by Deconvoluting the OH Valency Range in FTIR Spectra*. *46*(4), 283–288. https://doi.org/10.1515/HFSG.1992.46.4.283

Fuertes, A. B., Arbestain, M. C., Sevilla, M., Maciá-Agulló, J. A., Fiol, S., López, R., Smernik, R. J., Aitkenhead, W. P., Arce, F., & Macías, F. (2010). Chemical and structural properties of carbonaceous products obtained by pyrolysis and hydrothermal carbonisation of corn stover. *Soil Research*, *48*(7), 618. https://doi.org/10.1071/SR10010

Funke, A., & Ziegler, F. (2010). Hydrothermal carbonization of biomass: A summary and discussion of chemical mechanisms for process engineering. *Biofuels, Bioproducts and Biorefining*, *4*(2), 160–177. https://doi.org/10.1002/bbb.198

Gao, P., Zhou, Y., Meng, F., Zhang, Y., Liu, Z., Zhang, W., & Xue, G. (2016). Preparation and characterization of hydrochar from waste eucalyptus bark by hydrothermal carbonization. *Energy*, *97*, 238–245. https://doi.org/10.1016/J.ENERGY.2015.12.123

Gao, Y., Wang, X. H., Yang, H. P., & Chen, H. P. (2012). Characterization of products from hydrothermal treatments of cellulose. *Energy*, *42*(1), 457–465. https://doi.org/10.1016/J.ENERGY.2012.03.023

Hamed, T. A., & Alshare, A. (2021). Environmental Impact of Solar and Wind energy- A Review. *Journal of Sustainable Development of Energy, Water and Environment Systems*, *N/A*(N/A), 0–0. https://doi.org/10.13044/j.sdewes.d9.0387

Hassam, S., Ficara, E., Leva, A., & Harmand, J. (2015). A generic and systematic procedure to derive a simplified model from the anaerobic digestion model No. 1 (ADM1). *Biochemical Engineering Journal*, *99*, 193–203. https://doi.org/10.1016/j.bej.2015.03.007

Hastings, A., Clifton-Brown, J., Wattenbach, M., Mitchell, C. P., Stampfl, P., & Smith, P. (2009). Future energy potential of *Miscanthus* in Europe. *GCB Bioenergy*, *1*(2), 180–196. https://doi.org/10.1111/j.1757-1707.2009.01012.x

He, C., Giannis, A., & Wang, J. Y. (2013). Conversion of sewage sludge to clean solid fuel using hydrothermal carbonization: Hydrochar fuel characteristics and combustion behavior. *Applied Energy*, *111*, 257–266. https://doi.org/10.1016/J.APENERGY.2013.04.084

Heidari, M., Salaudeen, S., Norouzi, O., Acharya, B., & Dutta, A. (2020). Numerical Comparison of a Combined Hydrothermal Carbonization and Anaerobic Digestion System with Direct Combustion of Biomass for Power Production. *Processes*, *8*(1), 43. https://doi.org/10.3390/pr8010043

Himmel, M. E., Ding, S. Y., Johnson, D. K., Adney, W. S., Nimlos, M. R., Brady, J. W., & Foust, T. D. (2007). Biomass recalcitrance: Engineering plants and enzymes for biofuels production. *Science*, *315*(5813), 804–807. https://doi.org/10.1126/SCIENCE.1137016

Hoekman, S. K., Broch, A., & Robbins, C. (2011). Hydrothermal Carbonization (HTC) of Lignocellulosic Biomass. *Energy and Fuels*, *25*(4), 1802–1810. https://doi.org/10.1021/EF101745N

Hu, B., Wang, K., Wu, L., Yu, S.-H., Antonietti, M., & Titirici, M.-M. (2010). Engineering Carbon Materials from the Hydrothermal Carbonization Process of Biomass. *Advanced Materials*, *22*(7), 813–828. https://doi.org/10.1002/adma.200902812

IEA. (2001). *Biogas and More! Systems and Markets Overview of Anaerobic digestion Biogas and More!*

In-Gu Lee, †,‡, Mi-Sun Kim, ‡ and, & Son-Ki Ihm*, †. (2002). Gasification of Glucose in Supercritical Water. *Industrial and Engineering Chemistry Research*, *41*(5), 1182–1188. https://doi.org/10.1021/IE010066I

Kabadayi Catalkopru, A., Kantarli, I. C., & Yanik, J. (2017). Effects of spent liquor recirculation in hydrothermal carbonization. *Bioresource Technology*, *226*, 89–93. https://doi.org/10.1016/J.BIORTECH.2016.12.015

Kambo, H. S., & Dutta, A. (2014). Strength, storage, and combustion characteristics of densified lignocellulosic biomass produced via torrefaction and hydrothermal carbonization. *Applied Energy*, *135*, 182–191. https://doi.org/10.1016/j.apenergy.2014.08.094

Kambo, H. S., & Dutta, A. (2015). Comparative evaluation of torrefaction and hydrothermal carbonization of lignocellulosic biomass for the production of solid biofuel. *Energy Conversion and Management*, *105*, 746–755. https://doi.org/10.1016/J.ENCONMAN.2015.08.031

Kang, K., Nanda, S., Sun, G., Qiu, L., Gu, Y., Zhang, T., Zhu, M., & Sun, R. (2019). Microwave-assisted hydrothermal carbonization of corn stalk for solid biofuel production: Optimization of process parameters and characterization of hydrochar. *Energy*, *186*, 115795. https://doi.org/10.1016/J.ENERGY.2019.07.125

Kang, S., Ye, J., Zhang, Y., & Chang, J. (2013). Preparation of biomass hydrochar derived sulfonated catalysts and their catalytic effects for 5-hydroxymethylfurfural production. *RSC Advances*, *3*(20), 7360. https://doi.org/10.1039/c3ra23314f

Karimi, K., & Taherzadeh, M. J. (2016). A critical review of analytical methods in pretreatment of lignocelluloses: Composition, imaging, and crystallinity. *Bioresource Technology*, *200*, 1008–1018. https://doi.org/10.1016/J.BIORTECH.2015.11.022

Kil, H., Li, D., Xi, Y., & Li, J. (2017). Model predictive control with on-line model identification for anaerobic digestion processes. *Biochemical Engineering Journal*, *128*, 63–75. https://doi.org/10.1016/j.bej.2017.08.004

Kruse, A. (2008). Supercritical water gasification. In *Biofuels, Bioproducts and Biorefining* (Vol. 2, Issue 5, pp. 415–437). https://doi.org/10.1002/bbb.93

Kruse, A., Funke, A., & Titirici, M. M. (2013). Hydrothermal conversion of biomass to fuels and energetic materials. *Current Opinion in Chemical Biology*, *17*(3), 515–521. https://doi.org/10.1016/J.CBPA.2013.05.004

Kumar, S. (2013). Sub- and Supercritical Water Technology for Biofuels. *Advanced Biofuels and Bioproducts*, *9781461433484*, 147–183. https://doi.org/10.1007/978-1-4614-3348-4_11

Lauterböck, B., Ortner, M., Haider, R., & Fuchs, W. (2012). Counteracting ammonia inhibition in anaerobic digestion by removal with a hollow fiber membrane contactor. *Water Research*, *46*(15), 4861–4869. https://doi.org/10.1016/j.watres.2012.05.022

Li, Y., Zhang, R., Liu, G., Chen, C., He, Y., & Liu, X. (2013). Comparison of methane production potential, biodegradability, and kinetics of different organic substrates. *Bioresource Technology*, *149*, 565–569. https://doi.org/10.1016/J.BIORTECH.2013.09.063

Liang, J., Nabi, M., Zhang, P., Zhang, G., Cai, Y., Wang, Q., Zhou, Z., & Ding, Y. (2020). Promising biological conversion of lignocellulosic biomass to renewable energy with rumen microorganisms: A comprehensive review. In *Renewable and Sustainable Energy Reviews* (Vol. 134). Elsevier Ltd. https://doi.org/10.1016/j.rser.2020.110335

Lin, R., Deng, C., Ding, L., Bose, A., & Murphy, J. D. (2019). Improving gaseous biofuel production from seaweed Saccharina latissima: The effect of hydrothermal pretreatment on energy efficiency. *Energy Conversion and Management*, *196*, 1385–1394. https://doi.org/10.1016/J.ENCONMAN.2019.06.044

Liu, Z., Quek, A., Kent Hoekman, S., & Balasubramanian, R. (2013). Production of solid biochar fuel from waste biomass by hydrothermal carbonization. *Fuel*, *103*, 943–949. https://doi.org/10.1016/J.FUEL.2012.07.069

Lubenova, V., Simeonov, I., & Queinnec, I. (2002). Two-Step Parameter and State Estimation of the Anaerobic Digestion. *IFAC Proceedings Volumes*, *35*(1), 455–460. https://doi.org/10.3182/20020721-6-ES-1901.01385

Machado, N. T., de Castro, D. A. R., Santos, M. C., Araújo, M. E., Lüder, U., Herklotz, L., Werner, M., Mumme, J., & Hoffmann, T. (2018). Process analysis of hydrothermal carbonization of corn Stover with subcritical H2O. *The Journal of Supercritical Fluids*, *136*, 110–122. https://doi.org/10.1016/J.SUPFLU.2018.01.012

Marin-Batista, J. D., Villamil, J. A., Rodriguez, J. J., Mohedano, A. F., & de la Rubia, M. A. (2019). Valorization of microalgal biomass by hydrothermal carbonization and anaerobic digestion. *Bioresource Technology*, *274*, 395–402. https://doi.org/10.1016/J.BIORTECH.2018.11.103

Martinez, E., Marcos, A., Al-Kassir, A., Jaramillo, M. A., & Mohamad, A. A. (2012). Mathematical model of a laboratory-scale plant for slaughterhouse effluents biodigestion for biogas production. *Applied Energy*, *95*, 210–219. https://doi.org/10.1016/j.apenergy.2012.02.028

Mauky, E., Weinrich, S., Nägele, H. J., Jacobi, H. F., Liebetrau, J., & Nelles, M. (2016). Model Predictive Control for Demand-Driven Biogas Production in Full Scale. *Chemical Engineering and Technology*, *39*(4), 652–664. https://doi.org/10.1002/ceat.201500412

May, R. M. (1976). *Simple mathematical models with very complicated dynamics* (Vol. 261, Issue 5560).

Mejdoub, H., & Ksibi, H. (2015). Regulation of Biogas Production Through Waste Water Anaerobic Digestion Process: Modeling and Parameters Optimization. *Waste and Biomass Valorization*, *6*(1), 29–35. https://doi.org/10.1007/s12649-014-9324-5

Méndez-Acosta, H. O., Palacios-Ruiz, B., Alcaraz-González, V., González-Álvarez, V., & García-Sandoval, J. P. (2010). A robust control scheme to improve the stability of anaerobic digestion processes. *Journal of Process Control*, *20*(4), 375–383. https://doi.org/10.1016/j.jprocont.2010.01.006

Mohammed, I. S., Aliyu, M., Abdullahi N.A., & Alhaji, I. A. (2020). Production of Bioenergy from Rice-Melon Husk Co-Digested with Cow Dung as Innoculant. *Agricultural Engineering International: CIGR Journal*, *22*(1), 108–117. https://cigrjournal.org/index.php/Ejounral/article/view/4795

Mohammed, I. S., Aliyu, M., Dauda, S. M., Balami, A. A., & Yunusa, B. K. (2019). Synthesis and Optimization Process of Ethylene Glycol-Based Bio-lubricant from Palm Kernel Oil (PKO). *JREE*, *5*(2), 1–9. http://repository.futminna.edu.ng:8080/jspui/handle/123456789/11950

Mohammed, I. S., Na, R., Kushima, K., & Shimizu, N. (2020). Investigating the Effect of Processing Parameters on the Products of Hydrothermal Carbonization of Corn Stover. *Sustainability*, *12*(12), 5100. https://doi.org/10.3390/su12125100

Monlau, F., Barakat, A., Trably, E., Dumas, C., Steyer, J.-P., & Carrère, H. (2013). Lignocellulosic Materials Into Biohydrogen and Biomethane: Impact of Structural Features and Pretreatment. *Http://Dx.Doi.Org/10.1080/10643389.2011.604258*, *43*(3), 260–322. https://doi.org/10.1080/10643389.2011.604258

Mosier, N., Hendrickson, R., Ho, N., Sedlak, M., & Ladisch, M. R. (2005). Optimization of pH controlled liquid hot water pretreatment of corn stover. *Bioresource Technology*, *96*(18), 1986–1993. https://doi.org/10.1016/J.BIORTECH.2005.01.013

Nakajima, S., Shimizu, N., Ishiwata, H., & Ito, T. (2016). *The Start-up of Thermophilic Anaerobic Digestion of Municipal Solid Waste*. http://www.enecho.

Nakason, K., Panyapinyopol, B., Kanokkantapong, V., Viriya-empikul, N., Kraithong, W., & Pavasant, P. (2018a). Characteristics of hydrochar and liquid fraction from hydrothermal carbonization of cassava rhizome. *Journal of the Energy Institute*, *91*(2), 184–193. https://doi.org/10.1016/J.JOEI.2017.01.002

Nakason, K., Panyapinyopol, B., Kanokkantapong, V., Viriya-empikul, N., Kraithong, W., & Pavasant, P. (2018b). Hydrothermal carbonization of unwanted biomass materials: Effect of process temperature and retention time on hydrochar and liquid fraction. *Journal of the Energy Institute*, *91*(5), 786–796. https://doi.org/10.1016/J.JOEI.2017.05.002

Pala, M., Kantarli, I. C., Buyukisik, H. B., & Yanik, J. (2014). Hydrothermal carbonization and torrefaction of grape pomace: A comparative evaluation. *Bioresource Technology*, *161*, 255–262. https://doi.org/10.1016/J.BIORTECH.2014.03.052

Paul, S., Dutta, A., & Defersha, F. (2018). Biocarbon, biomethane and biofertilizer from corn residue: A hybrid thermo-chemical and biochemical approach. *Energy*, *165*, 370–384. https://doi.org/10.1016/J.ENERGY.2018.09.182

Pavlovič, I., Knez, Ž., & Škerget, M. (2013). Hydrothermal Reactions of Agricultural and Food Processing Wastes in Sub- and Supercritical Water: A Review of Fundamentals, Mechanisms, and State of Research. *Journal of Agricultural and Food Chemistry*, *61*(34), 8003–8025. https://doi.org/10.1021/JF401008A

Qian EW. (2013). *Pretreatment and saccharification of lignocellulosic biomass. In: Tojo S, Hirasawa T, editors. Research approaches to sustainable biomass systems*. Academic Press.

Reddy, S. N., Nanda, S., Dalai, A. K., & Kozinski, J. A. (2014). Supercritical water gasification of biomass for hydrogen production. *International Journal of Hydrogen Energy*, *39*(13), 6912–6926. https://doi.org/10.1016/J.IJHYDENE.2014.02.125

Renard, P., Dochain, D., Bastin, G., Naveau, H., & Nyns, E.-J. (1988). Adaptive control of anaerobic digestion processes?a pilot-scale application. *Biotechnology and Bioengineering*, *31*(4), 287–294. https://doi.org/10.1002/bit.260310402

Reza, M. T., Rottler, E., Herklotz, L., & Wirth, B. (2015). Hydrothermal carbonization (HTC) of wheat straw: Influence of feedwater pH prepared by acetic acid and potassium hydroxide. *Bioresource Technology*, *182*, 336–344. https://doi.org/10.1016/J.BIORTECH.2015.02.024

Rowel RM. (2005). Handbook of Wood Chemistry and Wood Composites. *CRC Press*. https://doi.org/10.1201/9780203492437

Salman, C. A., Schwede, S., Thorin, E., & Yan, J. (2017). Enhancing biomethane production by integrating pyrolysis and anaerobic digestion processes. *Applied Energy*, *204*, 1074–1083. https://doi.org/10.1016/j.apenergy.2017.05.006

Sevilla, M., & Fuertes, A. B. (2009). The production of carbon materials by hydrothermal carbonization of cellulose. *Carbon*, *47*(9), 2281–2289. https://doi.org/10.1016/J.CARBON.2009.04.026

Shimizu, N., Abea, A., Ushiyama, T., & Öner, E. T. (2020). Effect of temperature on the hydrolysis of levan treated with compressed hot water fluids. *Food Science & Nutrition*, *8*(4), 2004–2014. https://doi.org/10.1002/FSN3.1488

Shimizu, N. & Yoshida Kazuto. (2021). Development of an Efficient Anaerobic Co-digestion Process for Biogas from Food Waste and Paper. *Environ. Control Biol., 59*(4), 1–7.

Simeonov, I., & Queinnec, I. (2006). Linearizing control of the anaerobic digestion with addition of acetate (control of the anaerobic digestion). *Control Engineering Practice*, *14*(7), 799–810. https://doi.org/10.1016/j.conengprac.2005.04.011

Sinechal, X. J., Installe, M. J., & Nyns, E. J. (1979). Differentiation between acetate and higher volatile acids in the modeling of the anaerobic biomethanation process. *Biotechnology Letters*, *1*(8), 309–314. https://doi.org/10.1007/BF01388184

Smith, A. M., & Ross, A. B. (2016). Production of bio-coal, bio-methane and fertilizer from seaweed via hydrothermal carbonisation. *Algal Research*, *16*, 1–11. https://doi.org/10.1016/J.ALGAL.2016.02.026

Soccol, C. R., Faraco, V., Karp, S. G., Vandenberghe, L. P. S., Thomaz-Soccol, V., Woiciechowski, A. L., & Pandey, A. (2019). Lignocellulosic Bioethanol: Current Status and Future Perspectives. *Biomass, Biofuels, Biochemicals: Biofuels: Alternative Feedstocks and Conversion Processes for the Production of Liquid and Gaseous Biofuels*, 331–354. https://doi.org/10.1016/B978-0-12-816856-1.00014-2

Song, X., Wachemo, A. C., Zhang, L., Bai, T., Li, X., Zuo, X., & Yuan, H. (2019). Effect of hydrothermal pretreatment severity on the pretreatment characteristics and anaerobic digestion performance of corn stover. *Bioresource Technology*, *289*. https://doi.org/10.1016/j.biortech.2019.121646

Steinbeiss, S., Gleixner, G., & Antonietti, M. (2009). Effect of biochar amendment on soil carbon balance and soil microbial activity. *Soil Biology and Biochemistry*, *41*(6), 1301–1310. https://doi.org/10.1016/J.SOILBIO.2009.03.016

Taherzadeh, M. J., & Karimi, K. (2008). Pretreatment of Lignocellulosic Wastes to Improve Ethanol and Biogas Production: A Review. *International Journal of Molecular Sciences 2008, Vol. 9, Pages 1621-1651*, *9*(9), 1621–1651. https://doi.org/10.3390/IJMS9091621

Tekin, K., Karagöz, S., & Bektaş, S. (2014). A review of hydrothermal biomass processing. *Renewable and Sustainable Energy Reviews*, *40*, 673–687. https://doi.org/10.1016/J.RSER.2014.07.216

Theander, O. (1985). Cellulose, Hemicellulose and Extractives. *Fundamentals of Thermochemical Biomass Conversion*, 35–60. https://doi.org/10.1007/978-94-009-4932-4_2

Theegala, C. S., & Midgett, J. S. (2012). Hydrothermal liquefaction of separated dairy manure for production of bio-oils with simultaneous waste treatment. *Bioresource Technology*, *107*, 456–463. https://doi.org/10.1016/J.BIORTECH.2011.12.061

Ushiyama, T., & Shimizu, N. (2018). Microencapsulation using Spray-drying: The Use of Fine Starch Solution for the Wall Material. *Food Science and Technology Research*, *24*(4), 653–659. https://doi.org/10.3136/fstr.24.653

Volpe, M., & Fiori, L. (2017). From olive waste to solid biofuel through hydrothermal carbonisation: The role of temperature and solid load on secondary char formation and hydrochar energy properties. *Journal of Analytical and Applied Pyrolysis*, *124*, 63–72. https://doi.org/10.1016/J.JAAP.2017.02.022

Volpe, M., Goldfarb, J. L., & Fiori, L. (2018). Hydrothermal carbonization of Opuntia ficus-indica cladodes: Role of process parameters on hydrochar properties. *Bioresource Technology*, *247*, 310–318. https://doi.org/10.1016/J.BIORTECH.2017.09.072

Wang, F., Ouyang, D., Zhou, Z., Page, S. J., Liu, D., & Zhao, X. (2021). Lignocellulosic biomass as sustainable feedstock and materials for power generation and energy storage. *Journal of Energy Chemistry*, *57*, 247–280. https://doi.org/10.1016/j.jechem.2020.08.060

Wang, F., Wang, J., Gu, C., Han, Y., Zan, S., & Wu, S. (2019). Effects of process water recirculation on solid and liquid products from hydrothermal carbonization of Laminaria. *Bioresource Technology*, *292*, 121996. https://doi.org/10.1016/J.BIORTECH.2019.121996

Wang, T., Zhai, Y., Zhu, Y., Li, C., & Zeng, G. (2018). A review of the hydrothermal carbonization of biomass waste for hydrochar formation: Process conditions, fundamentals, and physicochemical properties. *Renewable and Sustainable Energy Reviews*, *90*, 223–247. https://doi.org/10.1016/J.RSER.2018.03.071

Weingarten, R., Conner, Wm. C., & Huber, G. W. (2012). Production of levulinic acid from cellulose by hydrothermal decomposition combined with aqueous phase dehydration with a solid acid catalyst. *Energy & Environmental Science*, *5*(6), 7559. https://doi.org/10.1039/c2ee21593d

Weng, J.-K., & Chapple, C. (2010). The origin and evolution of lignin biosynthesis. *New Phytologist*, *187*(2), 273–285. https://doi.org/10.1111/J.1469-8137.2010.03327.X

Wörmeyer, K., Ingram, T., Saake, B., Brunner, G., & Smirnova, I. (2011). Comparison of different pretreatment methods for lignocellulosic materials. Part II: Influence of pretreatment on the properties of rye straw lignin. *Bioresource Technology*, *102*(5), 4157–4164. https://doi.org/10.1016/J.BIORTECH.2010.11.063

Wu, Z., & Xia, X. (2015). Optimal switching renewable energy system for demand side management. *Solar Energy*, *114*, 278–288. https://doi.org/10.1016/j.solener.2015.02.001

Xiao, L. P., Shi, Z. J., Xu, F., & Sun, R. C. (2012). Hydrothermal carbonization of lignocellulosic biomass. *Bioresource Technology*, *118*, 619–623. https://doi.org/10.1016/J.BIORTECH.2012.05.060

Yoshida, K., Kametani, K., & Shimizu, N. (2020). Adaptive identification of anaerobic digestion process for biogas production management systems. *Bioprocess and Biosystems Engineering*, *43*(1), 45–54. https://doi.org/10.1007/s00449-019-02203-9

Yoshida, M., Liu, Y., Uchida, S., Kawarada, K., Ukagami, Y., Ichinose, H., Kaneko, S., & Fukuda, K. (2008). Effects of Cellulose Crystallinity, Hemicellulose, and Lignin on the Enzymatic Hydrolysis of Miscanthus sinensis to Monosaccharides. *Bioscience, Biotechnology, and Biochemistry*, *72*(3), 805–810. https://doi.org/10.1271/BBB.70689

Zhang, H., Zhang, P., Ye, J., Wu, Y., Fang, W., Gou, X., & Zeng, G. (2016). Improvement of methane production from rice straw with rumen fluid pretreatment: A feasibility study. *International Biodeterioration and Biodegradation*, *113*, 9–16. https://doi.org/10.1016/j.ibiod.2016.03.022

Zhao, K., Li, Y., Zhou, Y., Guo, W., Jiang, H., & Xu, Q. (2018). Characterization of hydrothermal carbonization products (hydrochars and spent liquor) and their biomethane production performance. *Bioresource Technology*, *267*, 9–16. https://doi.org/10.1016/J.BIORTECH.2018.07.006

Zhao, P., Shen, Y., Ge, S., & Yoshikawa, K. (2014). Energy recycling from sewage sludge by producing solid biofuel with hydrothermal carbonization. *Energy Conversion and Management*, *78*, 815–821. https://doi.org/10.1016/J.ENCONMAN.2013.11.026

Zhu, Z., Liu, Z., Zhang, Y., Li, B., Lu, H., Duan, N., Si, B., Shen, R., & Lu, J. (2016). Recovery of reducing sugars and volatile fatty acids from cornstalk at different hydrothermal treatment severity. *Bioresource Technology*, *199*, 220–227. https://doi.org/10.1016/J.BIORTECH.2015.08.043